YEAST CHORISMATE MUTASE:

MOLECULAR EVOLUTION OF AN ALLOSTERIC ENZYME

Kerstin Helmstaedt

YEAST CHORISMATE MUTASE:

MOLECULAR EVOLUTION OF AN ALLOSTERIC ENZYME

Dissertation
zur Erlangung des Doktorgrades
der Mathematisch-Naturwissenschaftlichen Fakultäten
der Georg-August-Universität zu Göttingen

vorgelegt von
Kerstin Helmstaedt
geb. Probst
aus Bad Harzburg

Göttingen 2002

Die vorliegende Arbeit wurde in der Arbeitsgruppe von Prof. Dr. Gerhard H. Braus in der Abteilung Molekulare Mikrobiologie und Genetik des Instituts für Mikrobiologie und Genetik der Georg-August-Universität Göttingen angefertigt.

Veröffentlichungen:

Krappmann, S., Helmstaedt, K., Gerstberger, T., Eckert, S., Hoffmann, B., Hoppert, M., Schnappauf, G., and G. H. Braus (1999) The *aroC* Gene of *Aspergillus nidulans* Codes for a Monofunctional, Allosterically Regulated Chorismate Mutase. *J Biol Chem* 274:22275-22282.

Helmstaedt, K., Krappmann, S., and G. H. Braus (2001) Allosteric Regulation of Catalytic Activity: *Escherichia coli* Aspartate Transcarbamoylase versus Yeast Chorismate Mutase. *Microbiol Mol Biol Rev* 65:404-421.

Helmstaedt, K., Heinrich, G., Lipscomb, W. N., and G. H. Braus (2002) Refined molecular hinge between allosteric and catalytic domain determines allosteric regulation and stability of fungal chorismate mutase. *Proc Natl Acad Sci USA* 99:6631-6636.

D7

Referent: Prof. Dr. G. H. Braus

Korreferent: Prof. Dr. B. Bowien

Tag der mündlichen Prüfung: 31. Oktober 2002

Für Andreas

DANKSAGUNGEN

Mein besonderer Dank gilt Gerhard Braus für die Betreuung dieser Arbeit, die optimalen Arbeitsbedingungen und das grosse Interesse an meinem Thema.

Herrn Prof. Bowien danke ich für die Übernahme des Korreferats.

Ganz herzlich bedanke ich mich bei Gaby Heinrich, ohne deren unermüdliches Schaffen und Spaß an der Arbeit sicher Manches im Rahmen dieser Doktorarbeit nicht hätte untersucht werden können. Durch die gute Zusammenarbeit hat die zweite Hälfte meiner Arbeit besonders viel Spaß gemacht.

Mein Dank geht auch an Sven Krappmann für die gute Einführung in das Arbeiten mit Proteinen, die wertvollen Ratschläge in festgefahrenen Situationen und seinen großen Anteil am Schreiben des Reviews. Gleiches gilt für Hans-Ueli Mösch, der auch zu denen gehört, die gern ihr Wissen weitergeben.

Hervorzuheben ist auch Olav Grundmann, der der beste Ansprechpartner für plötzlich auftretende Probleme war und von dem ich mir einige Tricks des Laboralltags abschauen konnte.

Auch nicht vergessen werde ich das lustige Team aus Labor 102: Silke Busch, Olli Draht, Verena Große, Katja Anttonen, Elke Schwier, Sabine Eckert und Eric Kübler. Vielen Dank für die nette Arbeitsathmospäre! Vielen Dank auch an Katja für die gute Zusammenarbeit während ihrer Diplomarbeit!

Für das gute Klima in der Abteilung danke ich den ehemaligen und derzeitigen Mitgliedern der AG Braus wie Andrea Pfeil, Ralph Pries, Tim Köhler, Naimeh Taheri, Axel Strittmatter, Maria Mayer, Ole Valerius, Melanie Bolte, Pattrick Dieckmann, Stefan Irniger, Heidi Northemann, Claudia Wagner, Katrin Bömecke, Malte Kleinschmidt, Helge Woldt, Matthias Bäumer, Katrin Düvel, und Markus Hartmann.

TABLE OF CONTENTS

Summary 1

Zusammenfassung 3

Introduction 5
  References 6

Aim of this work 7

Allosteric regulation of catalytic activity: *E.coli* ATCase versus yeast chorismate mutase 9
  Abstract 9
  Introduction 10
  ATCase activities 12
  Struture of *E. coli* ATCase 13
  Catalytic center of *E. coli* ATCase 14
  Allosteric site of *E. coli* ATCase 15
  Conformations of *E. coli* ATCase 16
  CM activities 17
  Structures of CM enzymes 19
  Catalytic center of ScCM 23
  Allosteric site of ScCM 25
  Conformations of ScCM 27
  Intramolecular signal transduction in ScCM and *E. coli* ATCase 28
    ScCM 28
    ATCase 32
  Separation of activation and inhibition 35
    ScCM 35
    ATCase 36
  Separation of homotropic and heterotropic effects 38
    ATCase 38
    ScCM 39
  Models for the allosteric mechanisms 39
  Lessons learned from the model systems and the dawn of a new paradigm of allostery 42
  References 45

Chapter 1:

A refined molecular hinge between allosteric and catalytic domain determines allosteric regulation and stability of fungal chorismate mutase 59
Abstract........ 59
Introduction 60
Materials & Methods 61
Results........ 65
Discussion 74
References 76

Chapter 2:

***aro7* mutant *S. cerevisiae* strains show an osmophenotype like the wild-type**........ 81
Abstract........ 81
Introduction 82
Materials & Methods 84
Results........ 87
Discussion 95
References 96

Chaper 3:

The chorismate mutase of *Thermus thermophilus* is a monofunctional AroH class enzyme inhibited by tyrosine 103
Abstract........ 103
Introduction 104
Materials & Methods 106
Results........ 111
Discussion 121
References 125

Conclusions 131
The two folding motifs of chorismate mutases........ 131
Evolution of AroQ chorismate mutases........ 132
Oligomerization and regulation 133
Thermostability of chorismate mutases........ 134

Chorismate mutase and osmoregulation 135
References 136

Curriculum Vitae 141

Abbreviations

ATCase	aspartate transcarbamoylase from *Escherichia coli*
ATP	adenosine triphosphate
b, bp	base (pair)
BsCM	chorismate mutase from *Bacillus subtilis*
CA	chorismic acid
CM	chorismate mutase
C-terminus	carboxyterminus
CTP	cytidine triphosphate
DTT	*DL*-dithiothreitol
EcCM	chorismate mutase from *Escherichia coli*
EDTA	ethylendiaminetetraacetate
HEPES	N-[2-hydroxyethyl]piperazine-N‘-[2-ethanesulfonic acid]
k	rate constant
K_m	Michaelis-Menten constant
μ	growth rate
MV	minimal vitamins
N-terminus	aminoterminus
OD	optical density
ORF	open reading frame
PALA	N-(phosphonoacetyl-*L*-aspartate
PCR	polymerase chain reaction
PMSF	phenylmethylsulfonyl fluoride
R state	relaxed state
$S_{0.5}$	substrate concentration at half-maximal velocity
ScCM	chorismate mutase from *Saccharomyces cerevisiae*
SDS	sodium dodecyl sulfate
$t_{1/2}$	half life
T state	tense state
Tris	tris(hydroxymethyl)amino methane
TtCM	chorismate mutase from *Thermus thermophilus*
UTP	uridine triphosphate
UV	ultraviolet
V_{max}	maximal velocity
wt	wild type
YEPD	yeast extract peptone dextrose
YNB	yeast nitrogen base
Zn	zinc

Summary

Chorismate mutase (CM, EC 5.4.99.5), encoded by *ARO7*, catalyzes the Claisen rearrangement of chorismate to prephenate in the biosynthesis of the amino acids tyrosine and phenylalanine. The small, dimeric enzyme of the yeast *Saccharomyces cerevisiae* is allosterically activated by tryptophan and allosterically inhibited by tyrosine.

In this work, earlier data in the literature which suggested that chorismate mutase functions in osmoregulation and vacuole biogenesis were disproven. The analysis of several strains containing *aro7* point mutations or deletions did not show any other function for CM but its role in amino acid biosynthesis. By fusion to the green fluorescent protein, this protein was localized in the cytoplasm as well as in the nucleus.

On the protein level, the intramolecular signal transduction from the allosteric to the active sites occuring upon effector binding was investigated in more detail. Chimeric enzymes were constructed, in which the molecular hinge loop L220s connecting the allosteric and catalytic domain in the dimer interface, were subtituted by the corresponding loops from homologous fungal enzymes. Kinetic analysis verified that this structural component is critical for protein stability and distinguishes between the activation and inhibition signal. This hinge is also involved in dimerization of the protein.

Substitution of hydrophobic amino acids in and near this loop by charged residues produced a stable monomeric enzyme variant. This chorismate mutase showed reduced activity and lost allosteric regulation, but the encoding gene complemented phenylalanine and tyrosine auxotrophy of an *aro7* mutant strain.

These results supported the theory that yeast CM originated from a monomeric, unregulated ancestral protein similar to the *Escherichia coli* CM by coevolution of regulatory and stabilizing elements.

In order to gain further insight into the principles of protein stabilization, the chorismate mutase from *Thermus thermophilus* was purified and analyzed after cloning of the structural gene *aroG*. This enzyme was similar to the structurally unique CM from *Bacillus subtilis*, but in contrast to the latter CM was inhibited by tyrosine. Computer modeling studies revealed that like in other proteins enhanced hydrophilicity on the protein surface, increased hydrophobicity of residues within the tertiary structure as well as the tightening of active site loops stabilized the protein fold.

Zusammenfassung

Die Chorismatmutase (CM, EC 5.4.99.5), kodiert durch *ARO7*, katalysiert die Claisen-Umlagerung von Chorismat zu Prephenat in der Biosynthese von Tyrosin und Phenylalanin. Das relativ kleine, dimere Enzym der Hefe *Saccharomyces cerevisia*e wird allosterisch durch Tryptophan aktiviert und allosterisch durch Tyrosin inhibiert.

In der vorliegenden Arbeit wurde die Theorie widerlegt, dass die Chorismatemutase an der Osmoregulation und Vakuolenentstehung beteiligt ist. Die Analyse einiger Stämme mit punktmutiertem oder deletiertem *ARO7*-Gen zeigte ausschließlich eine Funktion in der Aminosäure-Biosynthese. Die Fusion an das grün-fluoreszierende Protein ermöglichte die Lokalisierung der CM in Cytoplasma und Kern der Hefezelle.

Auf Proteinebene wurde der intramolekulare Signalübertragungsweg von den allosterischen zu den aktiven Zentren näher untersucht. Es wurden Chimären-Enzyme hergestellt, in denen das molekulare Scharnier L220s zwischen der katalytischen und allosterischen Domäne ausgetauscht wurde gegen den entsprechenden Bestandteil homologer Pilzenzyme. Die kinetische Analyse zeigte, dass dieser Proteinteil essentiell ist für die Unterscheidung zwischen dem Signal Aktivierung bzw. Inhibierung. Diese Region ist auch für die Dimerisierung der CM von Bedeutung.

Durch Austausch hydrophober Aminosäuren gegen geladene Reste in und in der Nähe dieses Scharniers wurde eine stabile, monomere Enzymvariante hergestellt. Diese CM zeigte reduzierte Aktivität und keine Regulation, aber das kodierende Gen komplementierte die Tyrosin- und Phenylalanin-Auxotrophie der Zellen. Diese Ergebnisse unterstützen die Theorie, dass das Hefeenzym durch gleichzeitige Evolution von Regulations- und Stabilisierungsmechanismen aus einem monomeren, unregulierten Vorläuferprotein entstanden ist, welches dem der *Escherichia coli* CM ähnlich war.

Um weitere Erkenntnisse über die Prinzipien der Proteinstabilisierung zu erhalten, wurde auch die Chorismatmutase von *Thermus thermophilus* charakterisiert, nachdem das kodierende Gen kloniert war. Dieses Enzym ist ähnlich zu der strukturell einzigartigen Chorismatmutae aus *Bacillus subtilis*, wird aber, im Gegensatz zu letzterem durch Tyrosin in seiner Aktivität gehemmt. Modellierungsstudien zeigten, dass wie auch bei anderen Proteinen verstärkte Hydrophilität von Oberflächen, erhöhte Hydrophobizität innerhalb der Struktur wie auch die Versteifung von Loops in der Nähe des aktiven Zentrums zur Stabilisierung dieser Proteinfaltung beitragen.

Introduction

Yeast chorismate mutase (CM, EC 5.4.99.5) catalyzes the intramolecular 3,3-sigmatropic rearrangement of the *enol*pyruvyl side chain of chorismate to prephenate in the biosynthesis of aromatic amino acids (Andrews *et al*., 1973). CM is a key regulatory enzyme catalyzing an important reaction in the highly branched metabolism of aromatic compounds.

Multiple pathways are known which start from chorismate, while only one pathway of six conserved reactions yields chorismate in fungi and plants (Bentley, 1990; Dosselaere & Vanderleyden, 2001). Three other branches lead to the formation of ubiquinone, *para*-aminobenzoate, and tryptophan, while CM catalyzes the last common reaction in phenylalanine and tyrosine biosynthesis. The biosynthesis of the aromatic amino acids attracted much attention as a model pathway for the regulation of gene expression and catalytic activities (Braus, 1991).

In yeast and other fungi, a detailed regulatory pattern for these biosyntheses has evolved. In the so-called *general control*, the binding of the yeast activator Gcn4p to promoter elements causes the transcriptional derepression of several biosynthetic genes which leads to increased enzyme levels upon starvation of any single amino acid (Hinnebusch, 1992). This system seems to be conserved in numerous fungi and is also known as cross-pathway control in filamentous fungi (Piotrowska, 1980). In addition, the catalytic activities of the fungal branch point enzymes anthranilate synthase and chorismate mutase as well as the DAHP synthase isozymes which catalyze the first reaction of the shikimate pathway, are precisely regulated (Braus, 1991). The end product tryptophan allosterically inhibits anthranilate synthase and activates chorismate mutase directing the metabolic flux towards tyrosine and phenylalanine. These amino acids, in return, inhibit the DAHP synthase isozymes while tyrosine also allosterically inhibits chorismate mutase.

The catalytic and regulatory properties of yeast CM were characterized in great detail by the solution of the three-dimensional structure and site-directed mutagenesis of the allosteric and active sites (Schnappauf *et al*., 1998; Schnappauf *et al*., 1997; Sträter *et al*., 1997). The structural and regulatory features of this model enzyme like the existence of several allosteric states as well as a sophisticated intramolecular signaling pathway for allosteric inhibition can probably contribute to the understanding of other important metabolic enzymes.

References

Andrews, P. R., Smith, G. D. & Young, I. G. (1973). Transition-state stabilization and enzymic catalysis. Kinetic and molecular orbital studies of the rearrangement of chorismate to prephenate. *Biochemistry* **12**, 3492-3498.

Bentley, R. (1990). The shikimate pathway - a metabolic tree with many branches. *Crit Rev Biochem Mol Biol* **25**, 307-384.

Braus, G. H. (1991). Aromatic amino acid biosynthesis in the yeast *Saccharomyces cerevisiae*: a model system for the regulation of a eukaryotic biosynthetic pathway. *Microbiol Rev* **55**, 349-370.

Dosselaere, F. & Vanderleyden, J. (2001). A metabolic node in action: chorismate-utilizing enzymes in microorganisms. *Crit Rev Microbiol* **27**, 75-131.

Hinnebusch, A. (1992). General and pathway-specific regulatory mechanisms controlling the synthesis of amino acid biosynthesis in *Saccharomyces cerevisiae*. In *The molecular and cellular biology of the yeast* Saccharomyces, pp. 319-414. Edited by E. W. Jones, J. R. Pringle & J. R. Broach. Cold Spring Harbor, New York: Cold Spring Harbor Laboratory Press.

Piotrowska, M. (1980). Cross-pathway regulation of ornithine carbamoyltransferase synthesis in *Aspergillus nidulans*. *J Gen Microbiol* **116**, 336-339.

Schnappauf, G., Krappmann, S. & Braus, G. H. (1998). Tyrosine and tryptophan act through the same binding site at the dimer interface of yeast chorismate mutase. *J Biol Chem* **273**, 17012-17017.

Schnappauf, G., Sträter, N., Lipscomb, W. N. & Braus, G. H. (1997). A glutamate residue in the catalytic center of the yeast chorismate mutase restricts enzyme activity to acidic conditions. *Proc Natl Acad Sci USA* **94**, 8491-8496.

Sträter, N., Schnappauf, G., Braus, G. & Lipscomb, W. N. (1997). Mechanisms of catalysis and allosteric regulation of yeast chorismate mutase from crystal structures. *Structure* **5**, 1437-1452.

Aim of this work

In the last decade, detailed knowledge was accumulated about activity and regulation of yeast chorismate mutase. Crystal structure of different allosteric states were analyzed regarding allosteric regulation. Therefore, the first objective of this work was to summerize the information gained on the structure-function relationship in this chorismate mutase. The comparison with the allosteric model enzyme aspartate transcarbamoylase (ATCase) from *Escherichia coli* should give further insights into the principles of allostery.

By the construction of chimeric enzymes generated from yeast chorismate mutase and the homologous enzymes from the fungi *Hansenula polymorpha* and *Aspergillus nidulans*, the function of these‘ enzymes molecular hinge, the loop L220s, in recognition and transduction of the allosteric signal should be further investigated. In addition, a monomeric yeast chorismate mutase was to be generated by disruption of the hydrophobic dimer interface in the vicinity of loop L220s.

ARO7, encoding yeast CM, was described to be identical to *OSM2*, a gene necessary for growth in hypertonic medium, and was linked to a salt-sensitive vacuolar mutant phenotype. Therefore, the putative function of chorismate mutase for osmoregulation and vacuole biogenesis was addressed by the construction and examination of yeast strains with mutant *aro7* alleles including a complete deletion. Furthermore, yeast chorismate mutase was to be localized in the cell by fusion to the green fluorescent protein.

As thermostability of enzymes attracts more and more attention, the *aroG* gene from the extreme thermophile *Thermus thermophilus* should be cloned and the encoded enzyme characterized with respect to its stabilizing features and regulatory properties in comparison to mesophilic chorismate mutases.

Allosteric regulation of catalytic activity: *E. coli* ATCase versus yeast chorismate mutase

Abstract

Allosteric regulation of key metabolic enzymes is a fascinating field to study the structure-function relationship of induced conformational changes of proteins. Here, we compare the principles of allosteric transitions of the complex classical model aspartate transcarbamoylase (ATCase) from *E. coli* consisting of 12 polypeptides and the less complicated chorismate mutase derived from the baker's yeast which functions as a homodimer. Chorismate mutase presumably represents the minimal oligomerization state of a cooperative enzyme which still can be either activated or inhibited by different heterotropic effectors. The detailed knowledge of the number of possible quaternary states and the description of molecular triggers for conformational changes of model enzymes as ATCase and chorismate mutase sheds more and more light on allostery as important regulatory mechanisms of any living cell. The comparison of wild-type with engineered mutant enzymes reveals that current textbook models for regulation do not cover the entire picture to describe the function of these enzymes in detail.

In 1965, Monod, Wyman and Changeux summarised the properties of two dozen allosteric enzyme systems, resulting in their ‘plausible model on the nature of allosteric transition’ (MWC) (Monod *et al.*, 1965). Since then, the description of a plethora of allosteric enzymes and systems has led to the concept that allostery is a common theme in regulating the activity of various proteins (for review see Perutz, 1989). Direct control of protein function via allosteric regulation is usually achieved through conformational changes of a given protein structure induced by effectors. In contrast to intrasteric regulation (Kobe & Kemp, 1999), effectors bind to regulatory sites distinct from the active site (Greek, *allos* = other, *stereos* = rigid, solid or space). One term tightly linked to allostery is ‘cooperativity‘. This describes the interaction of binding processes of ligands to proteins with multiple binding sites (Ricard & Cornish-Bowden, 1987). Ligand binding plots of positively cooperative systems generally display sigmoidicity, resulting in an S-shaped curve of fractional saturation or rate against concentration. Allosteric behaviour itself was often observed for regulatory or control enzymes of metabolic pathways and forms the basis for feedback inhibition and activation. The so-called homotropic effects originate from identical (e. g., substrate) molecules which bind to an allosteric protein and influence each other’s affinity. In the case of different ligands (e. g., effector molecules and substrate molecules), the interactions are called heterotropic (Monod *et al.*, 1965). For both effects, cooperativity and allostery, positive as well as negative effects can be observed, resulting in an increase or decrease, respectively, of affinity and activity.

In the established model of global allosteric transition, binding of an effector induces a concerted shift in the equilibrium between two quaternary conformations of the oligomeric protein. The activated conformation, termed the R (relaxed) state, is assumed to have higher catalytic activity in comparison to the T (tense) state (Monod *et al.*, 1963). This model was later challenged by the sequential model established by Koshland, Némethy, and Filmer (KNF) (Koshland *et al.*, 1966), finally leading to the general model by Eigen (Eigen, 1967) which combines both the MWC and KNF extremes. In most allosteric proteins, homotropic effects seem to be best accounted for by the concerted model, while the sequential model better describes the heterotropic effects (Stryer, 1988).

The exact mechanisms by which allosteric control of protein function can be achieved are extremely varied. Among the multitude of allosteric proteins, a few prototypes have been established in basic research (for review see Perutz, 1989). The most prominent example is hemoglobin, with which the initial attempts to explain the mechanisms of cooperativity have been carried out.

Hemoglobins are generally composed of two pairs of polypeptide chains arranged in a symmetrical tetrahedral manner. While oxyhemoglobin displays a high affinity for oxygen, desoxyhemoglobin has a low affinity for the molecule. On oxygen binding, changes in quaternary and tertiary structure account for the shift in the allosteric T-R equilibrium. As a result, oxygen acts as homotropic ligand on hemoglobin. A variety of heterotropic ligands lowering the oxygen affinity have been described, with protons and 2,3-diphosphoglycerate being the most important. An interesting feature is displayed by the lamprey hemoglobin, in which cooperativity is mediated by the reversible dissociation of dimers or tetramers into monomers with high oxygen affinity (Dohi *et al*., 1973).

The majority of allosteric proteins are presumably metabolic enzymes which act as control devices for flux alterations in metabolic pathways. Enzymes are regulated predominantly by heterotropic effector molecules modulating the catalytic turnover rates in a positive and/or negative fashion. Positive effectors often abolish cooperativity resulting in Michaelis-Menten-like kinetics in substrate saturation assays, whereas negatively acting ligands decrease catalytic efficiency either by decreasing substrate affinity (K systems) or by altering the intrinsic k_{cat} values (V systems) (Segel, 1993). Prominent examples for allosteric enzymes in metabolic pathways are for instance glycogen phosphorylase (Johnson *et al*., 1989), phosphofructokinase (Blangy *et al*., 1968; Schirmer & Evans, 1990), glutamine synthetase (Stadtman & Ginsburg, 1974), and aspartate transcarbamoylase (ATCase) (Weber, 1968). In particular, ATCase, which catalyzes the first step of pyrimidine biosynthesis, has been established as a prototype for allostery (Kantrowitz & Lipscomb, 1988; Lipscomb, 1994; Macol *et al*., 2001; Schachman, 1988). For this allosteric enzyme paradigm, the homotropic and heterotropic effects of its ligands as well as cooperativity have been investigated in great detail. The models of allosteric behavior developed from experimental data exceed previous theories and can be very helpful for the more accurate description of the characterisitics of other allosteric proteins.

In recent years, the chorismate mutase (CM) of the baker's yeast *Saccharomyces cerevisiae* (ScCM) has become a suitable and well characterised model for allosteric regulation of enzyme activity. CM is necessary for the biosynthesis of tyrosine and phenylalanine and catalyzes one reaction at the first branch point of aromatic amino acid biosynthesis. Structural analyses combined with classic kinetic studies performed on this enzyme, as well as molecular modeling studies, have led to detailed insights into the catalytic mechanism of this enzyme. Furthermore, the allosteric response to effector binding was intensively studied. The monofunctional, dimeric yeast enzyme is strictly regulated in its activity by allosteric effectors. The substrate chorismate serves as homotropic effector as indicated by the sigmoid curvature of substrate saturation kinetics, whereas tyrosine and tryptophan act as negative and positive heterotropic ligands, respectively (Kradolfer *et al*., 1977).

The purpose of the following review is to sum up major investigations into yeast chorismate mutase made in the last decade. The main focus is the comparison of the established ATCase model system with the knowledge which has been accumulated during recent years on the catalytic and regulatory features of yeast chorismate mutase. Despite its small size, chorismate mutase exhibits multisubunit allostery and cooperativity and has many similarities to the ATCase system. Thus, yeast chorismate mutase is well suited to be a model system to improve our understanding of the allostery of small enzymes consisting of only two subunits as presumably the minimal structure which is required for this kind of regulation.

ATCase activities

Aspartate transcarbamoylase (ATCase, Carbamoylphosphate: *L*-aspartate carbamoyltransferase, EC 2.1.3.2.) catalyzes the carbamoylation of the amino group of aspartate by carbamoylphosphate leading to phosphate and *N*-carbamoyl-*L*-aspartate (Cunin *et al*., 1985). ATCase is the first enzyme unique to pyrimidine biosynthesis and a key enzyme for regulating purine, pyrimidine, and arginine biosynthesis in *Escherichia coli*. The enzymes from enterobacteria are dodecameric holoenzymes composed of two different polypeptides which are inhibited by CTP and UTP and activated by ATP. The same architecture was found for other bacterial ATCases, like that from *Methanococcus janaschii* though it exhibited few regulatory properties (Hack *et al*., 2000). Some bacterial and eukaryotic ATCases are part of a multifunctional enzyme containing carbamoylphosphate synthetase and/or dihydroorotase activity, among them the enzyme of *S. cerevisiae*, which is inhibited by UTP (Serre *et al*., 1999). However, plant ATCases seem to be simple homotrimers which can be regulated by UMP (Williamson & Slocum, 1994).

For the two-substrate reaction carbamoylphosphate binds before aspartate and subsequently induces a conformational change in the enzyme, resulting in a higher affinity for aspartate (Griffin *et al*., 1972; Hsuanyu & Wedler, 1987). On aspartate binding, a larger conformational change is exerted on the active site and the whole enzyme, leading to T-R transition. Accordingly, phosphate dissociates from the active site after carbamoylaspartate (Hsuanyu & Wedler, 1988). ATCase exhibits positive cooperativity for aspartate (Bethell *et al*., 1968; Gerhart & Pardee, 1962). The apparent cooperativity for carbamoylphosphate only reflects cooperativity for aspartate (England *et al*., 1994). During catalysis, the amino group of aspartate is involved in a nucleophilic attack on the carbonyl carbon of carbamoylphosphate to form a tetrahedral intermediate. The transition state is processed to the products by transfer of a proton from the amino group of aspartate to the closest oxygen of the leaving phosphate group derived from carbamoylphosphate (Gouaux *et al*., 1987).

Structure of *E. coli* ATCase

The ATCase holoenzyme, composed of 12 polypeptide chains of two types (Fig. 1A) (Allewell, 1989; Wiley & Lipscomb, 1968), has a molecular weight of 310,000. Six larger chains (33,000 each, encoded by *pyrB*) are the catalytic (C) chains, which are insensitive to the allosteric effectors, while the smaller regulatory (R) chains (17,000 each, encoded by *pyrI*) are devoid of catalytic activity but bind the effectors ATP, CTP, and/or UTP. The catalytic chains are packed in two catalytic trimers, one subunit containing chains C1, C2, C3, the other containing chains C4, C5, and C6. Chain C4 is located below C1, while C5 and C6 are below chains C2 and C3, respectively. Each catalytic subunit has a threefold axis. The regulatory chains are organized in dimers which bridge the two catalytic trimers noncovalently. Each polypeptide chain folds into two domains. The N-terminal and C-terminal domains of the C chains are termed carbamoylphosphate (or polar) domain and aspartate (or equatorial) domain, respectively, according to the substrates bound to them. Each R chain harbors the allosteric domain including the allosteric site in the N terminus. A C-terminal Zinc domain contains a Zn(II) ion. The metal is coordinated by four sulfhydryl groups and mediates R-C interactions. Thus, on treatment with heat or mercurials, the holoenzyme dissociates into the catalytic and regulatory subunits. The active sites are composed of residues from adjacent C chains within a trimer: from both the aspartate and carbamoylphosphate (cp) domains of one chain and the cp domain of the adjacent chain. The allosteric sites are located at the distal ends of the R chains, 60 Å away from the nearest active site, and bind each effector. Assembly into the holoenzyme yields extensive interfaces between C chains within a catalytic trimer (for example, C1-C2) and in opposed trimers (C1-C4), between R chains within a regulatory dimer (R1-R6) and C and R chains (C1-R1 and C1-R4). The C1-C4 and symmetry-related interfaces are present in the T state, but not in the R state (Fig. 1A).

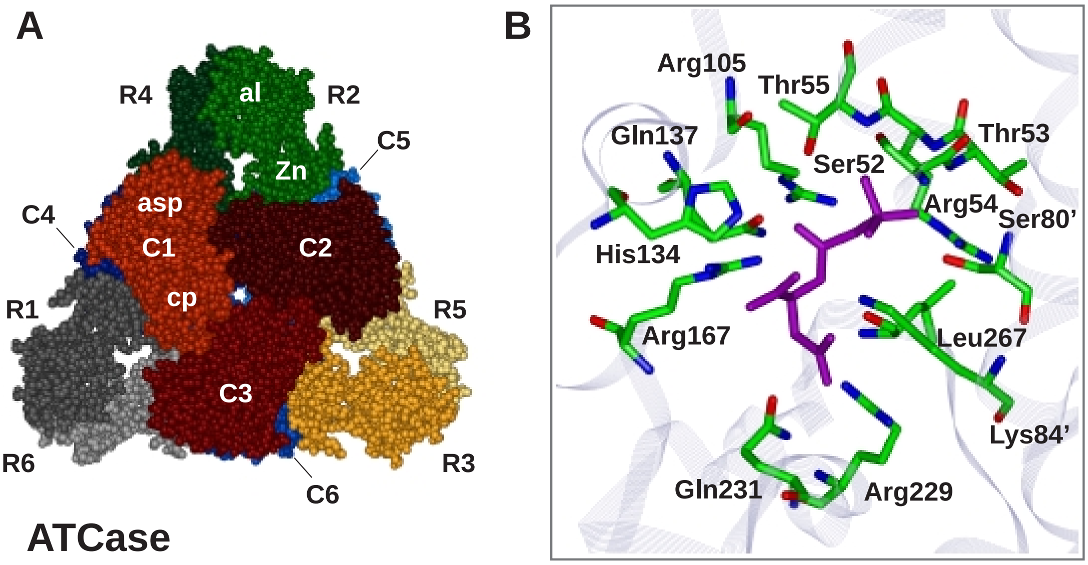

Fig. 1: Quaternary structure of *E. coli* ATCase. **A**, Holoenzyme viewed along the threefold axis. Catalytic chains are numbered C1 to C6, regulatory chains R1 to R6. The different catalytic and regulatory subunits are indicated by different colours. The aspartate domain of the catalytic chain is designated asp, the carbamoylphosphate domain cp. The domains of the regulatory chain are named Zn for zinc domain and al for allosteric domain. **B**, Binding mode of the bisubstrate analogue PALA (purple) to the active site of ATCase. Side chains are shown as sticks with atoms labelled by colour (green: carbon, blue: nitrogen, red: oxygen). Apostrophes after residue numbers indicate the residue’s position in an adjacent polypeptide chain. The figures are based on the data for the CTP-liganded structure and the bisubstrate analogue PALA-liganded structure, respectively (Honzatko & Lipscomb, 1982; Krause *et al*., 1987).

Catalytic center of *E. coli* ATCase

Insight into the binding mode of the substrates to the catalytic center of *E. coli* ATCase required analysis of the binding of a bisubstrate analogue, *N*-(phosphonoacetyl)-*L*-aspartate (PALA). In addition, the binding of carbamoylphosphate and succinate was studied; the study resulted in computer models which were verified by amino acid substitutions achieved by site-directed mutagenesis of corresponding codons in the open reading frames. Several residues have been identified as crucial for catalysis: Ser52, Thr53, Arg54, Thr55, Arg105, His134, Gln137, Arg167, Arg229, Glu231, and Ser80 and Lys84 from an adjacent catalytic chain (Macol *et al*., 1999) (Fig. 1B). Thus, the active site is a highly positively charged pocket. The most critical side chain originates from Arg54 (Stebbins *et al*., 1992). It interacts with a terminal oxygen and the anhydride oxygen of carbamoylphosphate and thereby stabilizes the negative charge of the leaving phosphate group. Arg105, His134, and Thr55 help to increase the electrophilicity of the carbonyl carbon by interacting with the carbonyl oxygen (Jin *et al*., 1999). Rate enhancement is achieved by orientation and stabilization of substrates, intermediates, and products rather than by involvement of residues in the catalytic mechanism. Instead of Lys84 acting as base which captures the proton from the amino group of aspartate, the recent model suggests that the fully ionized phosphate group is capable to accept a proton during catalysis (Gouaux *et al*., 1987; Jin *et al.*, 1999).

Allosteric site of *E. coli* ATCase

The allosteric site in the allosteric domain of the R chains of the *E. coli* ATCase complex binds ATP, CTP and/or UTP (Wild *et al*., 1989). There is one site with high affinity for ATP and CTP and one with 10- to 20-fold lower affinity for these nucleotides in each regulatory dimer (Dutta & Kantrowitz, 1998; Lipscomb, 1994). ATP binds predominantly to the high-affinity sites and subsequently activates the enzyme. UTP and CTP binding leads to inhibition of activity. UTP can bind to the allosteric site, but inhibition of ATCase by UTP is possible only in combination with CTP. With CTP present, UTP binding is enhanced and preferentially directed to the low-affinity sites. Conversely, UTP binding leads to enhanced affinity for CTP at the high-affinity sites and inhibits enzyme activity by up to 95% while CTP binding alone inhibits activity to 50-70% (Dutta & Kantrowitz, 1998; Wild *et al*., 1988; Zhang & Kantrowitz, 1991). ATP and CTP bind in anti-conformation with negative cooperativity with respect to themselves (Stevens *et al*., 1991). ATP strongly reduces cooperativity of substrate binding, while CTP enhances it (Stevens *et al*., 1991). The purine and pyrimidine rings, as well as the ribose rings, bind at similar locations. However, when CTP is bound, base and triphosphate moieties are closer together than when ATP is bound (Stevens & Lipscomb, 1992). In addition, the ribose moiety of ATP protrudes deeper into the binding sites than that of CTP (Stevens & Lipscomb, 1992). The triphosphate is necessary for high affinity and full nucleotide effects (Thiry & Hervé, 1978). Groups interacting with CTP are Val91r, Lys94r, Arg96r, Asp19r, His20r, Val9r, Lys56r, Lys60r, Val17r, Ala11r, Ile12r, and Tyr89r (r refers to the residues which are part of a regulatory chain) (Allewell, 1989; Stevens *et al.*, 1991). UTP differs from CTP in the carbonyl group in position 4 and the protonation of the nitrogen at position 3 of the pyrimidine ring. Discrimination between these two nucleotides seems to be based on the subtle differences in the interaction of the amino group and the nitrogen at position three with Ile12r (Dutta & Kantrowitz, 1998). ATP, on the other hand, is hydrogen bonded to side-chain or main-chain atoms of residues Asn84r, Val91r, Lys94r, Leu58r, Asp19r, Val9r, Lys60r, Glu10r, Ala11r, Ile12r, and Tyr84r (Stevens *et al.*, 1991). ATP induces an expansion of the site with the R1 and R6 allosteric domains pushed apart. This induces an overall increase of the allosteric domains. CTP, however, decreases the size of the allosteric site, with the result that the L50s loop moves closer to the nucleotide (Stevens & Lipscomb, 1992) (the letter s indicates the plural according to the term 'the fifties loop' that comprises residues around position 50). Both cavities are larger than the binding site in the unliganded enzyme (Stevens *et al*., 1991).

Conformations of *E. coli* ATCase

According to the MWC model, the ATCase has (at least) two conformational states: a low-activity T state with low affinity for the substrates and a high-activity, high-affinity R state. Both states are in an equilibrium which is shifted to the side of the T state with a value of about 250 for the allosteric equilibrium constant (L) (Eisenstein *et al*., 1990). The substrates, as well as the bisubstrate analogue PALA, produce a significant change in tertiary and quaternary structure of both catalytic and regulatory chains. Some authors conclude that the PALA-bound structure does not represent the R state since the isolated C-trimer structure and the catalytic trimer of *B. subtilis* ATCase resemble more the T state than the R state (Beernink *et al*., 1999; Endrizzi *et al*., 2000; Stevens *et al*., 1991). However, the PALA-bound structure allows the identification of the active site, a description of the more active form and a model for homotropic transition of ATCase (Krause *et al*., 1987), and strong similarities were found to R-like structures with single substrate or product analogues like phosphate and citrate (Lipscomb, 1994). PALA binding promotes a closure of the hinge between the C chain domains by 8°, while the gap between allosteric and Zn domain expands. Domain closure in the C chain is required for cooperativity and fully creates the aspartate binding site. Through these changes, interchain contacts of side chains of the 80s loop and 240s loop and active-site residues become reoriented (Jin *et al.*, 1999). On the quaternary conformational level, the holoenzyme undergoes a screw motion with a shift of 11 Å along and a rotation of 7° about the threefold axis and a 15° rotation of the regulatory chains about the three twofold axes. While the affinity of the R state for substrates is higher than that of the T state, there are only slight differences for the affinity to the allosteric ligands. Thus, ATP or CTP binding causes only minor changes in the quaternary structure (Schachman, 1988). The structure with CTP bound is termed T state. This conformation was also found for the unliganded enzyme or when ATP is bound (Stevens & Lipscomb, 1990). On ATP or UTP binding, only small changes in enzyme structure are observed. ATP causes an elongation (Stevens & Lipscomb, 1992) along the threefold axis of the T form by only 0.4 Å and so does not promote a T-R transition by itself (Van Vliet *et al*., 1991). Whereas ATP has nearly no effect on the distance between the C trimers in the R state, CTP decreases it by 0.5 Å toward the T state (Stevens & Lipscomb, 1992). Accordingly, CTP has no effect on C trimer separation in the T state (Stevens & Lipscomb, 1992).

In summary, the *E.coli* ATCase complex represents a highly sophisticated interplay between numerous polypeptides. Several effector molecules predominantly act on more than one polypeptide chain, resulting in different effects on the complicated overall enzyme. In contrast, the regulation of yeast chorismate mutase is based only on the interplay of two identical polypeptides. This allows a detailed study of very subtle effects even within a single polypeptide chain.

CM activities

CM activities (chorismate pyruvate mutase, EC 5.4.99.5) catalyse the intramolecular rearrangement of (-)chorismic acid to prephenic acid (Fig. 2) (Andrews *et al*., 1973). This Claisen rearrangement is a key step in the biosynthetic pathway of archea, bacteria, fungi, and plants resulting in the aromatic amino acids L-phenylalanine or L-tyrosine. Additionally, it represents a rare example of a pericyclic reaction in primary metabolism (Weiss & Edwards, 1980). Prephenate itself is transformed either into phenylpyruvate, the precursor of phenylalanine, or into 4-hydroxyphenylpyruvate, the last intermediate in tyrosine biosynthesis. A third, alternative route is utilized most commonly in plants, where prephenate is converted to arogenate before tyrosine and phenylalanine are formed.

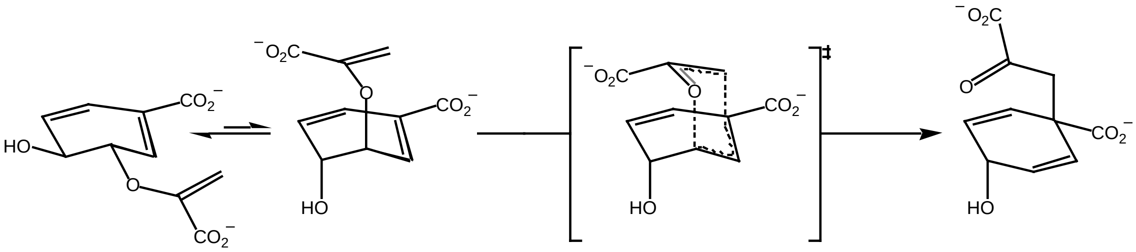

Fig. 2: The Claisen rearrangement of chorismic acid resulting in prephenic acid. The two conformers of chorismate as well as the proposed transition state finally leading to prephenate are shown.

In comparison to the uncatalysed, thermal [3,3] sigmatropic rearrangement, CMs can enhance the conversion of chorismate to prephenate by a factor of up to 10^6. A variety of CM enzymes have been described and characterised during the past three decades, and catalytic antibodies (‘abzymes’) accelerating the chorismate-to-prephenate rearrangement have been generated (Haynes *et al*., 1994; Jackson *et al*., 1992). Prokaryotic CM activities can be part of a bifunctional enzyme in which the CM domain is fused to a prephenate dehydratase (P-protein), a prephenate dehydrogenase (T-protein), or a 3-deoxy-D-arabinoheptulosonate-7-phosphate synthase moiety (Romero *et al*., 1995) (the letters P and T indicate the biosynthetic pathway that is initiated by the CM catalytic activity to yield phenylalanine and tyrosine, respectively). In contrast, all eukaryotic CMs characterized to date, as well as the CM from the archaeon *Methanococcus jannaschii* (MacBeath *et al*., 1998), are described to be monofunctional.

In most organisms analyzed, CM activities are strictly regulated. Whereas both enzyme activities of bifunctional T-proteins are inhibited by tyrosine, phenylalanine inhibits the two activities of P-proteins. In Gram-negative bacteria, including the cyanobacteria, as well as in Gram-positive *Bacillus subtilis* and *Streptomyces aureofaciens*, monofunctional CMs were found that lack regulatory properties. Eukaryotic CM enzymes are generally monofunctional and subject to allosteric inhibition and activation. Tyrosine and/or phenylalanine are negative effectors, whereas tryptophan serves as positive regulator of enzyme activity. In plants, different isoenzymes are often present which differ in their regulatory behaviour. Furthermore, some of them are regulated in their activities not only by end products of aromatic amino acid biosynthesis but also by secondary metabolites; for example, the CM isoenzymes of alfalfa can be inhibited by coumarate, caffeate, or ferulate and activated by 3,4-dimethoxycinnamate (Romero *et al.*, 1995).

In addition to this enzymatic regulation, the amount of enzymes at metabolic branch points is important for distribution of intermediates. For a balanced biosynthesis of the amino acids in yeast, a sophisticated, strictly regulated network composed of allosteric enzymes and ‘the general control of amino acid biosynthesis‘ has evolved (Krappmann *et al*., 2000). While anthranilate synthase, the competing enzyme complex at the branch point of aromatic amino acid biosynthesis, is feedback-inhibited by tryptophan, the expression of the encoding genes is induced by a transcriptional activator under amino acid starvation. However, the total amount of chorismate mutase is not regulated by the general control due to the fact that its activity is modulated more strongly by two different allosteric effectors.

Structures of CM enzymes

The crystal structures of three natural CM enzymes have been determined so far. Based on these structural insights and on primary sequence information of the encoding genes cloned to date, it has become evident that two different structural folds have evolved to contrive the enzymatic isomerization of chorismate to prephenate.

One structural class, AroH, is represented by the monofunctional, homotrimeric enzyme of *Bacillus subtilis.* The X-ray structure of this enzyme was determined at 1.9 Å resolution (Fig. 3A, B) (Chook *et al*., 1993) and more recently at 1.3 Å resolution (Ladner *et al*., 2000). The *aroH* gene product is a non-allosteric CM of 127 amino acids per monomer. Each monomer consists of a five-stranded mixed β-sheet packed against an 18-residue α-helix and a two-turn 3_{10} helix. The interfaces between adjacent subunits form three equivalent clefts open and accessible to solvent. These clefts harbor the active sites.

Sequences of all CM domains from bifunctional enzymes characterised to date, as well as most prokaryotic and eukaryotic monofunctional CMs, are consistant with the AroQ class of CM enzymes. These enzymes are, in contrast to the three-dimensional pseudo-α/β-barrel structure established by the AroH class, all-helical polypeptides and show similarity in sequence to the monofunctional CM of *Erwinia herbicola* encoded by the *aroQ* gene (Xia *et al*., 1993). In contrast to the situation in prokaryotes, primary sequences of eukaryotic CM proteins are rare. Only a few encoding sequences have been determined so far like the genes from the yeasts *S. cerevisiae*, *Schizosaccharomyces pombe*, and *Hansenula polymorpha*, from the filamentous fungus *Aspergillus nidulans*, and those coding for three isoenzymes in *Arabidopsis thaliana* (Eberhard *et al*., 1993; Krappmann *et al*., 1999; Krappmann *et al*., 2000; Mobley *et al*., 1999; Oliver & Harris, 1995; Schmidheini *et al*., 1989). On the basis of the solved structure of ScCM and on conserved primary structures among cloned eukaryotic CM-encoding genes, these CM enzymes are included into the AroQ class. They constitute the separate subclass of AroQ$_r$ enzymes (formerly AroR) due to their additional regulatory domains (MacBeath *et al.*, 1998).

The structural prototype of the AroQ class is the CM domain of the bifunctional, homodimeric *Escherichia coli* CM-prephenate dehydratase, the so-called P-protein which is inhibitable by phenylalanine. The N-terminal 109 residues of this P-protein constitute a functional CM, and its X-ray structure was solved at 2.2 Å resolution (Fig. 3A, B) (Lee *et al*., 1995). In the monomer, the polypeptide chain resembles the numeral 4 by its unusual fold of three α-helices, two longer (H1 and H3) and one short (H2), connected by two loops. Two equivalent active sites with contributions from each monomer are present in the quaternary structure of this engineered CM from *E. coli*.

The only solved crystal structure of a eukaryotic CM enzyme, the 256 amino acid *ARO7* gene product of the baker's yeast *S. cerevisiae*, also is an all-helical polypeptide (Fig. 3A, B). X-ray data have been determined for three conformational structures of this enzyme resembling different allosteric states. The conformation of the wild-type (wt) enzyme with tyrosine bound to the allosteric site was determined at 2.8-Å resolution and this structure yielded detailed insights into the global structure of the T state (Sträter *et al*., 1996).

Fig. 3 (opposite page): Structural prototypes of chorismate mutase enzymes and binding mode of a stable transition state analogue. **A**, Schematic presentations of the structural folds displayed by chorismate mutases from *B. subtillis* (BsCM, left), *E. coli* (EcCM, middle) or *S. cerevisiae* (ScCM, right). The helix numbers in brackets indicate the corresponding helices in the yeast enzyme. The polypeptide backbone is displayed in ribbon style, and secondary elements are labelled with red cylinders (α-helices) and yellow bars (β-sheets). N and C termini are indicated as well as structural elements of ScCM (see text for details). **B**, Oligomeric structure of BsCM (left), EcCM (middle), and ScCM (right) in complex with a stable transition state analogue. Monomeric subunits are indicated by different shades of grey. For ScCM, the binding position of the positive effector tryptophan is also shown. **C**, Section views of the catalytic sites of EcCM (left) and ScCM (right) with the transition state analogue (purple) bound. Side chains are shown as sticks with atoms labelled by colour (green: carbon, blue: nitrogen, red: oxygen). Apostrophes indicate the respective residue's position in an adjacent polypeptide chain.

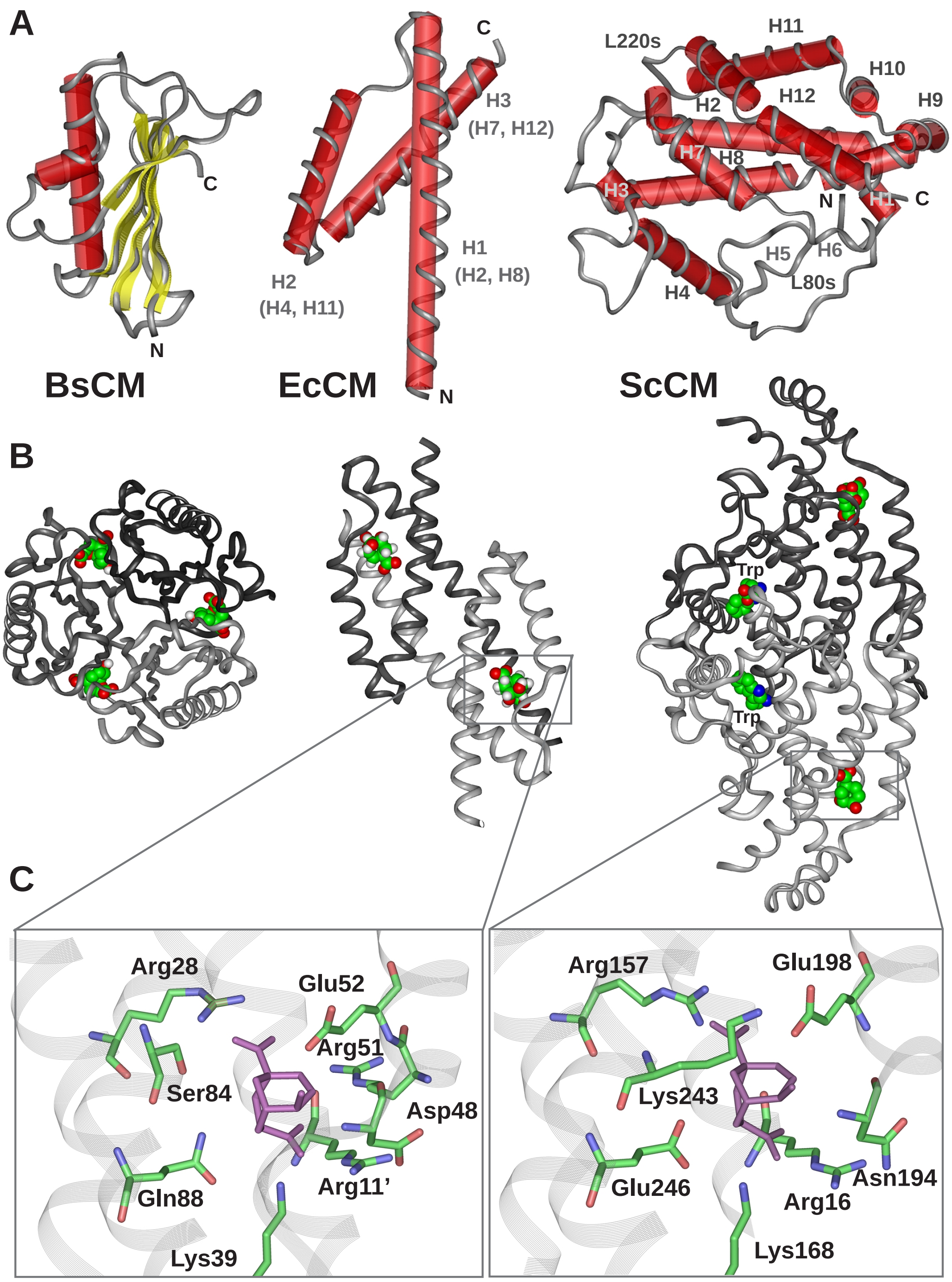
A
L220s
H11
C
H10
H3
(H7, H12)
H2
H12
H9
C
H7
H8
H3
N
H1
C
H1
(H2, H8)
H5
H6
H2
(H4, H11)
L80s
H4
N
BsCM
EcCM
ScCM
N
B
Trp
Trp
C
Arg28
Glu52
Arg51
Ser84
Asp48
Gln88
Arg11'
Lys39
Arg157
Glu198
Lys243
Asn194
Glu246
Arg16
Lys168

In contrast, a Thr226Ile mutant enzyme is locked in the R state and its structure was determined at 2.2-Å resolution with tryptophan at the effector binding site (Xue *et al*., 1994). The enzyme in complex with the stable transition state analogue displays a super R state and identifies the probable binding mode of the transition state (Sträter *et al*., 1997).

The basic topology of one monomeric subunit is that of a Greek key motif forming a four-helix bundle with essentially no β-strand elements. The 12 helices of the polypeptide chain are arranged in a twisted two-layer structure with a packing angle between the helical axes from each layer of about 60°. The dimer has the shape of a bipyramid, with four helices (H2, H4, H8, and H11) forming the hydrophobic interface between the protomers. The active site is part of the four-helix bundle set up by the helices H2, H8, H11, and H12 separately in each monomer. The binding site for both heterotropic effectors is a cleft in the dimer interface between the subunits. This regulatory site is formed by two helices (H4 and H5) of one monomer and the L80s loop and helix H8 of the other. The latter is the longest helix in the molecule as it consists of 32 residues and spans the overall structure from the regulatory site to the catalytic domain.

The fact that the three-dimensional structure of the *E. coli* CM domain and its eukaryotic counterpart are both AroQ class enzymes and resemble similar folds has led to the speculation that the yeast CM fold might have evolved from an ancestral protein similar to the bacterial CM by a gene duplication event followed by dimerization (Lee *et al.*, 1995; Sträter *et al*., 1997; Xue & Lipscomb, 1995). In fact, the *E. coli* CM dimer can be superimposed onto a monomer of yeast CM. The topology of a four-helix bundle forming the active site is conserved in the two enzymes, and also the binding mode of the *endo*-oxabicyclic inhibitor is similar. Helices H2, H4, H7, H8, H11, and H12 of the yeast enzyme correspond to H1, H2, H3, H1‘, H2‘, and H3‘ in EcCM. Modelling two *E. coli* CM dimers onto the *S. cerevisiae* dimer has led to further insights: two bacterial CM monomers superimpose well on the catalytic domains of the yeast CM whereas the other monomers and the other halves of the yeast monomers are more diverse due to the evolution of regulatory domains in this region of the molecules (Sträter *et al*., 1997).

Catalytic center of ScCM

The chorismate-to-prephenate rearrangement is a unimolecular one substrate–one product reaction. Generally, this Claisen rearrangement is thought to proceed in a nearly concerted but not necessarily synchronous way (Lowry & Richardson, 1987). A variety of interdisciplinary studies have gained detailed insight into the catalytic mechanism to achieve the >10^6-fold rate enhancement performed by chorismate mutases compared to the uncatalyzed reaction (for review see Ganem, 1996).

In solution, 10-20% of the substrate occupy the less stable pseudodiaxial conformation of the enolpyruvate side chain. Binding of this energetically less favoured conformer is proposed to be the first essential step in catalytic turnover. Subsequently, two alternative mechanistic ways follow: concerted but perhaps asynchronous bond cleavage and formation, as in the uncatalysed reaction, or catalysis via an intermediate after attack of an active site nucleophile at C-5.

Further insight into the catalytic mechanism has been obtained by structural and computational data of CMs in complex with an *endo*-oxabicyclic inhibitor resembling a stable transition state analogue (Lin *et al*., 1997). Binding of this so-called Bartlett's inhibitor (Bartlett & Johnson, 1985) to the yeast active site cavity is achieved by a series of electrostatic interactions and hydrogen bonding (Sträter *et al*., 1997) (Fig. 4). Interestingly, the active site structures are nearly identical upon inhibitor binding with no respect to the different effectors, either tyrosine or tryptophan, bound to the allosteric site. Therefore, this structural state was referred to as 'super R' state. Whether chorismic acid alone is able to promote the transition to the super R state remains to be shown. Two guanidinium groups of arginine residues (Arg16/Arg157) bind the inhibitor's carboxylate groups via salt bridges and its hydroxyl group is complexed by the carboxyl side chain of Glu198 and the backbone NH group of Arg194. Arg157 is of special importance for binding, because it is the molecular switch for allosteric transition to the T state. This residue is not in an appropriate position for interaction with the substrate in the T state, but only in the R or super R state. Additionally, hydrophobic interactions contribute to inhibitor binding. The most interesting contacts focus on the inhibitor's ether oxygen O-7. In the crystal structures the two side chain groups of Lys168 and protonated Glu246 are within hydrogen-bonding distance of this atom.

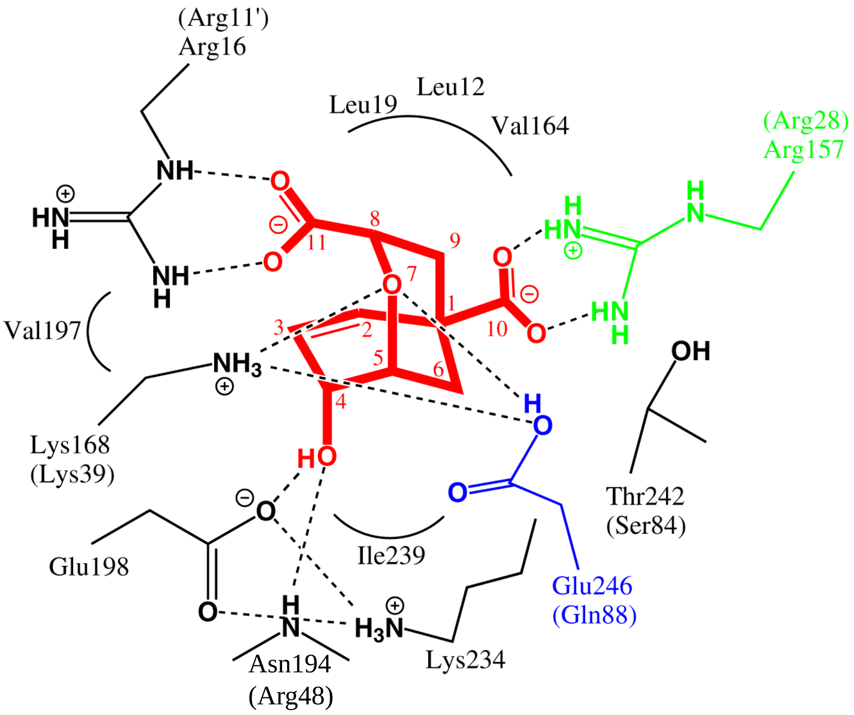
(Arg11')
Arg16
Leu19
Leu12
Val164
(Arg28)
Arg157
NH
HN
H
NH
H
O
O
11
8
9
7
O
HN
H
H
N
O
O
1
10
HN
H
Val197
NH$_3$
3
2
5
6
4
H
O
OH
Lys168
(Lys39)
HO
O
O
Thr242
(Ser84)
Glu198
Ile239
Glu246
(Gln88)
O
H
N
H$_3$N
Asn194
(Arg48)
Lys234

Fig. 4: Binding mode of the *endo*-oxabicyclic inhibitor to the active site of ScCM. The stable transition analogue is highlighted in red, and residues Arg157 and Glu246 are shown in green and blue, respectively. Hydrogen bond interactions are indicated by dotted lines. Corresponding residues of EcCM are indicated in parentheses. Apostrophes indicate the respective residue's position in an adjacent polypeptide chain.

Despite of low sequence similarities in primary structures, both the yeast CM and *E. coli* P-protein CM active site cavities display significant similarities upon binding the stable transition state analogue as deduced from X-ray crystal structures (Fig. 3C). However, a particular difference between the organisms is also reflected in their chorismate mutases. The activity of the yeast enzyme is adapted to acidic pH in accordance with the fungi's ability to grow at relatively low pH. In contrast, the bacterial enzyme which is active in a broader pH range reflects the ability of *E.coli* to live under more alkaline conditions as well. Thus, the binding modes for the *endo*-oxabicyclic structure of the enzymes are very similar, with one significant exception. Whereas in the bacterial structure a glutamine residue (Gln88) is hydrogen-bonded to the ether oxygen O-7, the active site residue Glu246 is displayed at the corresponding position in the yeast enzyme (Fig. 4). Molecular modelling studies imply this key residue is protonated well above neutral pH with an effective pK_a of 8.1 (Sträter *et al*., 1997). Whereas for the wild-type (wt) CM a bell-shaped profile was determined with an optimal acidic pH, in a Glu246Gln mutant enzyme catalytic activity is detectable over a broad pH range without a particular optimum (Schnappauf *et al*., 1997). In conclusion, this active site mutant mimics the situation as it is found for the bacterial CM where catalytic turnover rates are similar at both acidic and neutral pH. Consistent with this observation is the fact that mutation of the Gln88 codon to a glutamate codon in the *E. coli* gene leads to strong pH dependency of the resulting CM activity with an optimal pH at acidic conditions (Galopin *et al*., 1996). Nevertheless, for both enzymes similar effects contribute to rate acceleration: conversion of the less stable pseudodiaxial conformer, specific electrostatic stabilisation of the ether oxygen by hydrogen bonding via Lys168 and Glu246 or Lys39 and Gln88 in yeast and *E. coli*, respectively, and charge separation probably aided by Glu198 or Glu52, respectively.

Allosteric site of ScCM

Whereas the enzyme from *B. subtilis* is unregulated, the *E. coli* CM is inhibited by binding of an end product, tyrosine or phenylalanine, to a distinct domain of the bifunctional protein. The yeast chorismate mutase shows an additional level of regulation. It is feedback-inhibited by the end-product tyrosine, but can also be activated by tryptophan, the end product of the other biosynthetic branch of aromatic amino acid biosynthesis. The effectors for this dual regulation bind to the same allosteric sites in the regulatory domains. Using equilibrium dialysis, binding of tryptophan and tyrosine could be measured and two binding sites per CM dimer for each amino acid were found (Schmidheini *et al*., 1990; Schmidheini *et al.*, 1989). Their location was determined when the crystal structures of a Thr226Ile mutant, which is locked in the activated state, and of wt chorismate mutase with the ligand tyrosine were solved (Sträter *et al.*, 1996; Xue *et al*., 1994). It was found that the two allosteric effectors bind to the same binding sites in an mutually exclusive manner (Fig. 5). These allosteric sites are located in a distance of 20 and 30 Å, respectively, from the active sites of each monomer (Xue & Lipscomb, 1995). They reside at the dimer interface in a cleft between helix H8 and loop L130s of monomer A and helices H4 and H5 of monomer B.

Although both amino acids are oriented into the same direction, there are differences in the contacts of the effector amino acids to neighbouring protein residues of the enzyme. Only the hydrogen bonds between the amino group and one carboxyl oxygen are found identical for both effectors. The amino nitrogen of tyrosine and tryptophan, respectively, is hydrogen bonded to side chains from residues Asn139^{A} and Ser142^{A}, which are located at the N terminus and inside helix H8 of monomer A, respectively. The carboxyl oxygen of the effector amino acids interacts with the amide nitrogens from Gly141^{A} and Ser142^{A} of helix H8 of the same monomer. When tryptophan is bound, further hydrogen bonds exist between its second carboxyl oxygen and three water molecules and between the ring nitrogen and another water molecule. In addition, van der Waals interactions between the ring atoms and residues of both monomers are observed.

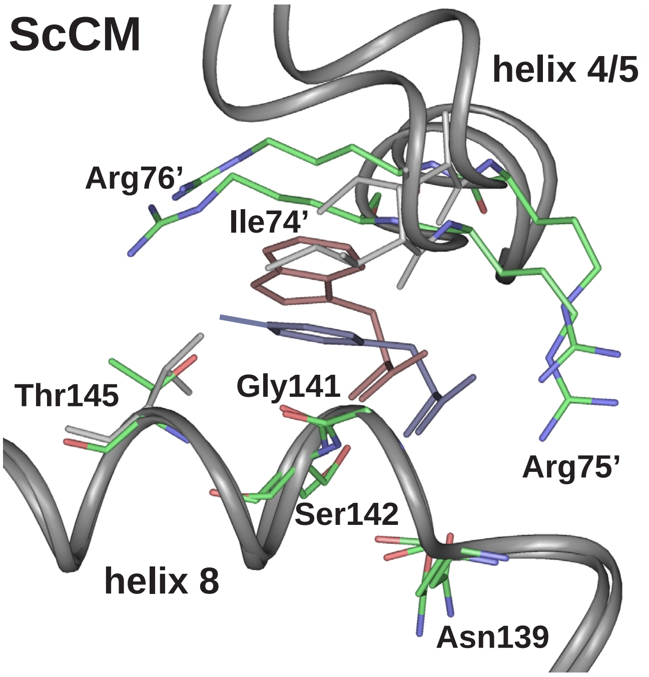

Fig. 5: Superposition of the allosteric site in the T and R states of ScCM. The polypeptide backbones of helices H4/H5 and H8 are displayed in ribbon style. The residues necessary for binding of tyrosine (blue) and tryptophan (red) are shown as sticks with atoms labelled by color (green, carbon; blue, nitrogen; red, oxygen). Apostrophes indicate the respective residue's position in an adjacent polypeptide chain. The dimer in the T state is superimposed onto the dimer in the R state using residues 1 to 214 and 224 to 254.

The feedback inhibitor tyrosine makes additional polar interactions with the side chains of Thr145^{A} in helix H8 of monomer A and Arg75^{B} and Arg76^{B} between H4 and H5 of monomer B. When tyrosine is bound, the second carboxyl oxygen is in hydrogen bond distance to the guanidinium and one amino group of Arg75^{B}, because this residue changes its conformation compared to the tryptophan bound state. The phenol ring binds at the same place as the five-membered ring of tryptophan, so that the phenolic hydroxyl group forms hydrogen bonds with both monomers, with the side chain of Thr145^{A} and with the guanidinium group of Arg76^{B}.

Due to the numerous hydrogen bonds to tyrosine, the allosteric site is narrower than in the unliganded wild-type enzyme. Therefore, tyrosine inhibits the enzyme by pulling the two subunits closer together. In the tryptophan-bound state the six-membered ring of tryptophan closely approaches main-chain as well as side-chain atoms of Ile74^{B}. Hence, the bulkier side chain of this amino acid pushes helices H4 and H5 away from helix H8 and opens the allosteric site. Thus, both effectors can initiate allosteric transitions with different results by using the same binding site. The polar contacts to Arg76^{B} and Thr145^{A} are of special importance for allosteric inhibition. For that reason phenylalanine lacking the phenolic hydroxyl group cannot inhibit yeast chorismate mutase. In fact, this amino acid was shown to produce the opposite effect. Although binding cannot be measured directly, a slight activation of wt chorismate mutase was found under enzyme assay conditions by reduction of the $S_{0.5}$ value (Schnappauf *et al*., 1998). The hydroxyl group of tyrosine therefore is necessary for strong binding and inhibition of the enzyme.

Site-directed mutagenesis experimentally confirmed the location of the allosteric site and showed the importance of Gly141^{A}, Ser142^{A}, Thr145^{A} and the arginine residues Arg75^{B} and Arg76^{B} of the other monomer (Schnappauf *et al*., 1998).

Conformations of ScCM

During T-R transition, the two monomers of yeast chorismate mutase rotate relative to each other (Sträter *et al*., 1996; Sträter *et al.*, 1997). The rotation axis is perpendicular to the dimer axis and 2.4 Å away from the center of the dimer in the direction of the allosteric sites. One monomer rotates 15° around this axis and is shifted 2.8 Å axially against the other monomer. Due to this screw motion, nearly all contacts at the dimer interface are changed. Alternatively, each monomer rotates by 8° around an axis which passes through the center of the monomers. To describe the differences between the T and R states, one can separate the monomers into catalytic and allosteric domains. The allosteric domain is composed of residues 44 to 107 (including helices H4 and H5 and adjacent loops). The catalytic domain comprises the rest of the monomer except of loop L220s, which, in fact, seems to connect both domains as a hinge. The latter domain includes the four-helix bundle which contains the active site. During transition from T to R state helix H8 moves away from the allosteric site and is shifted by 0.7 Å along the axis, accompanied by tryptophan, whose C_α atoms move 2 Å relative to the C_α atoms of tyrosine. This transition is followed by the four-helix bundle. The regulatory domain, however, moves into the opposite direction with a shift of 1.5 Å away from the allosteric site. This opposite shift is the basis for separating the monomer into these two domains.

As mentioned above, studies with a stable transition-state analogue demonstrated that binding of the substrate causes further rotations, thereby inducing transition to a super R state (Sträter *et al*., 1997). The rotation angle around the allosteric rotation axis is further increased to approximately 22° relative to the T state. This larger rotation is even achieved when tyrosine is bound to the regulatory domain. Tyrosine moves the regulatory domain toward the T state conformation, whereas the substrate simultaneously causes a super R state in the catalytic domain. Therefore, the hinge between regulatory and catalytic domain has to be flexible enough to permit such an intermediate T-super R as well as an R-super R state.

Intramolecular signal transduction in ScCM and *E. coli* ATCase

ScCM. In the dimeric yeast chorismate mutase, the regulatory sites are located at the dimer interface and involve residues from both subunits. Dimer formation therefore seems to be a prerequisite for effector binding and subsequent allosteric regulation. The amino acids tyrosine and tryptophan influence the activity of chorismate mutase by triggering allosteric transitions to the T and R state, respectively. The structural changes caused by both effectors are initiated at the effector binding site and transduced through the polypeptides toward the active sites, albeit as different processes and on different routes. While the signaling of tyrosine binding follows a linear path through the enzyme, the transition leading to activation cannot be depicted that precisely and may influence the catalytic site in multiple ways. Being positioned between the two monomers, the effectors also influence cooperativity toward the substrate. While tryptophan abolishes the positive cooperativity of substrate binding, tyrosine slightly enhances cooperativity.

In the T state, the regulatory domain of monomer B is pulled toward helix H8 of monomer A. These movements at the dimer interface bring about further rearrangements between the two monomers, changing the number and energy of the bonds between them which extend from the regulatory through the catalytic domain toward the active sites (Fig. 6). Helix H8 spans the molecule from the allosteric to the catalytic site and rotates slightly during transition to the T state (Sträter *et al.*, 1996; Sträter *et al*., 1997). Its C terminus moves away from the catalytic site while the N terminus moves in the opposite direction, thereby pulling the active-site residues Arg157 and Lys168 away from the substrate binding pocket. In addition, the C-terminal part of helix H2 moves away from the dimer interface by 1.7 Å. Helices H2, H11, and H12 are also driven away from the active site. Helices H11 from both monomers are pulled closer together along their axes by one helical turn causing a shift relative to helices H2 (Sträter *et al.*, 1996). As a result, several residues along H2 and H11 change their interaction partners. The movements in this part of the protein seem to originate from loop L220s, which connects H11 and H12. This latter helix obviously changes its conformation during R-T transition because it seems sterically hindered by helices H2 and H11 of the other monomer when pointing in the same direction as in the R state.

Thr226 is the last residue in the loop L220s and plays an important role for T state formation. It is not clear if its side chain forms a hydrogen bond with Arg224 via a water molecule or to Glu228, but one of these is necessary for formation of the T state. In addition, the first residue of this loop, Tyr212, and Asp215^B and Thr217^B, which reside in the L220s loop of the other monomer, no longer interact with Lys208 and Arg204 of helix H11. Tyr212 and Phe28 are at a special position because they are next to the dimer axis and interact with each other and the corresponding residues from the other monomer. In the T state, the Tyr212 residues move between the two phenylalanine residues (Phe28^A and Phe28^B). Besides, Asp215 and Thr217 seem to point away from the interface (Lin *et al*., 1998). Along helix H11, Tyr212, Lys208, and Arg204 change their contacts to Asp24 and Glu23 of helix H2. Asp24 and Glu23 move closer to the active site so that Asp24 no longer forms salt bridges with Tyr212 and Lys208 but forms them with Arg204. Glu23 can no longer bind to Arg204, but moves 5.3 Å into the active site and interacts with Arg157. Significant differences are evident for the active sites in T and R state structures with the side chain of the active-site residue Arg157 acting as molecular switch upon T-R transition (Fig. 7A).

Arg157 is part of the long helix H8 connecting the effector binding site to the active site, and its guanidinium group chelates one carboxyl group when the inhibitory transition state analogue is bound at the active site (Fig. 4). In the T state structure, this side chain is hydrogen bonded to Glu23, which in turn interacts with Tyr234 (Fig. 7A). Replacement of this latter residue resulted in functional enzymes that are unable to respond toward tyrosine-induced feedback inhibition. Therefore, the Tyr234 side chain is likely to be important for allosteric inhibition. In the inhibited enzyme, the Glu23 residue is forced into an unfavourable conformation for substrate binding since its carboxylate group would be only 3.2 Å away from the carboxylate group of the substrate. On the transition to the active R state, the connections between the Tyr234-Glu23-Arg157 triad are abolished. Glu23 moves 5.3 Å away from the active site and no longer interacts with Arg157 but instead with the Arg204 and Lys208 residues of helix H11 (Fig. 6C). As a consequence, Arg157 is now in a suitable conformation with effective charge for interaction with the substrate.

Applying continuum electrostatics, molecular surface/volume calculations, and molecular modeling, Nussinov and co-workers have argued that the altered binding affinity of Arg157 is of less importance for the different activities displayed by the T and R state (Lin *et al.*, 1998). They proposed the position of Glu23 to be crucial for modulating the polarity of the active-site pocket. In the T state with the Glu23 side chain looming into the cavity, the interior is of negative electrostatic potential, repelling the negatively charged substrate. Upon T-R transition, Glu23 swings out of the pocket and the polarity of the active-site cavity is altered in a positive electrostatic potential. In conclusion, the Glu23 residue was proposed to be the physical carrier of an electrostatic signal caused by the allosteric transition. This is supported by the catalytic properties of enzymes mutated in this particular position (Schnappauf *et al.*, 1998). Whereas a Glu23Asp mutant enzyme displayed increased activity combined with a loss of cooperativity, Glu23Gln and Glu23Ala enzymes showed reduced catalytic activity and replacement of Glu23 by arginine led to a nonfunctional enzyme.

Fig. 6 (opposite page): Intramolecular signaling pathway. A section of the chorismate mutase dimer is presented in the T state (top), R state (middle), or super R state (bottom). The polypeptide backbone is drawn in ribbon style. The residues which change their position during allosteric transition and thereby transduce the signal of effector binding from the allosteric to the active site are shown as stick models (green, carbon; blue, nitrogen; red, oxygen). Hydrogen bonds are indicated by black lines. The position of the catalytic site inhibitor in the T and R state is derived from a superposition with the super R state structure using residues 1 to 214 and 224 to 254. Tyrosine is coloured blue, tryptophan red and the bicyclic inhibitor green.

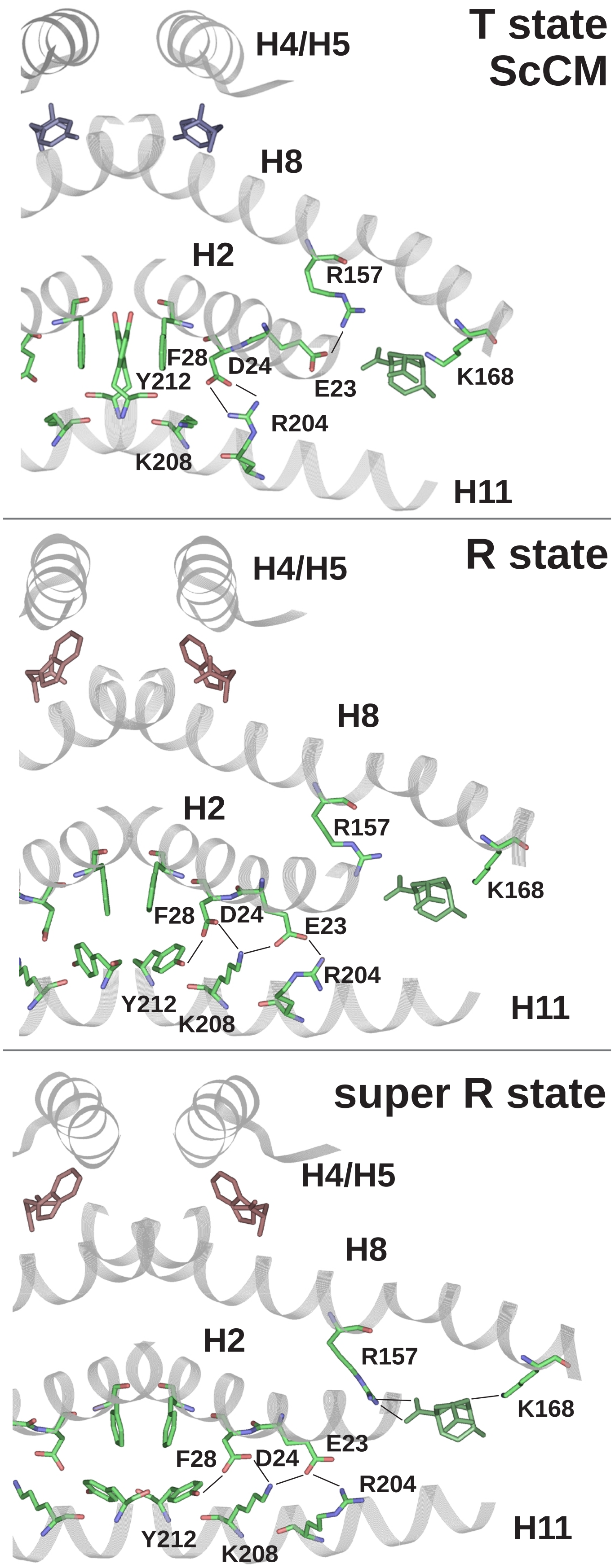
T state
ScCM
H4/H5
H8
H2
R157
F28
D24
Y212
E23
K168
R204
K208
H11
R state
H4/H5
H8
H2
R157
K168
F28
D24
E23
R204
Y212
K208
H11
super R state
H4/H5
H8
H2
R157
K168
F28
D24
E23
R204
Y212
K208
H11

The conformational changes at the dimer interface might also explain homotropic effects of the substrate. Signal transduction between the active sites of this allosteric enzyme might follow the same path along helices H2, H11, and H12 and loop L220s. While the heterotropic effects of the allosteric ligands lead to T-R transition, the homotropic effect of the substrate is the induction of the super R state in the catalytic domain.

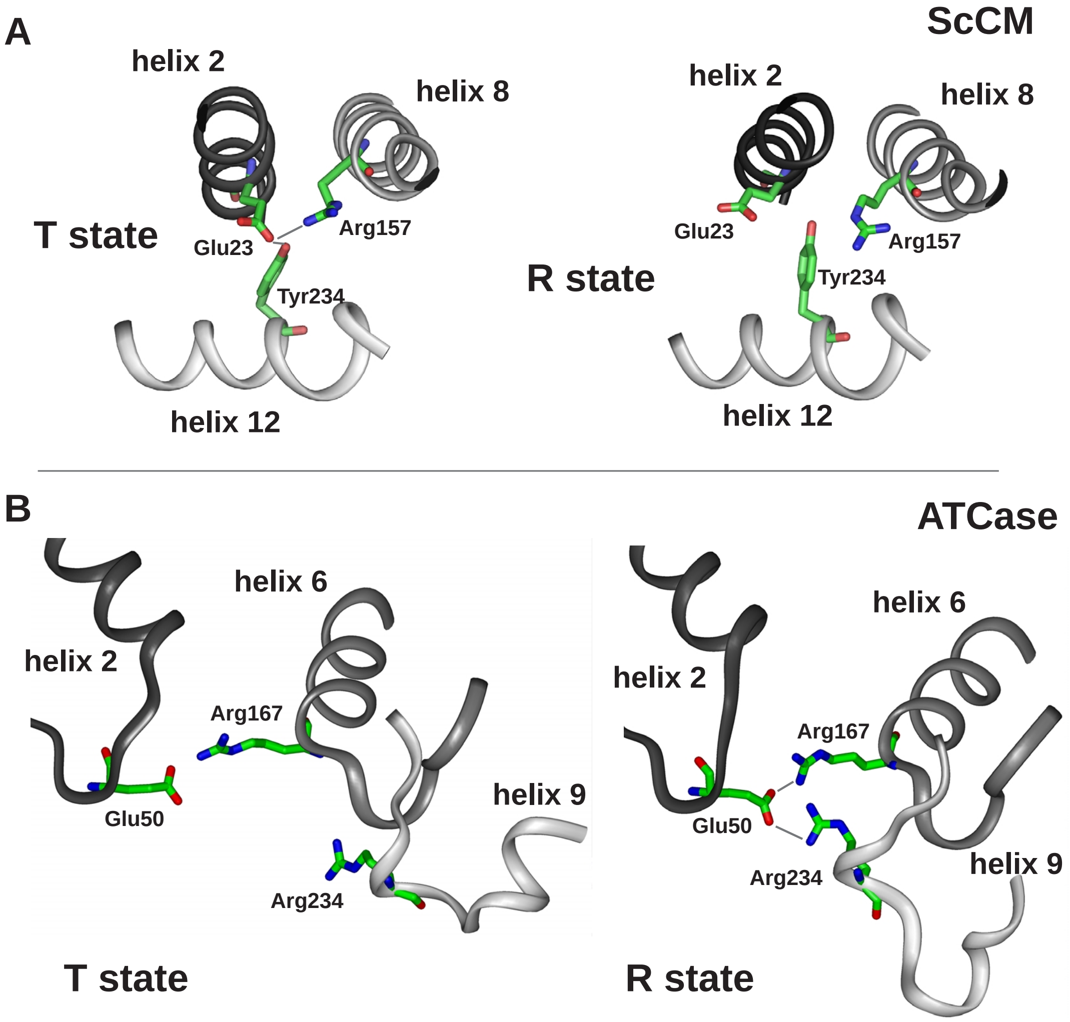
A
ScCM
helix 2
helix 8
T state
Glu23
Arg157
Tyr234
helix 12
helix 2
helix 8
R state
Glu23
Arg157
Tyr234
helix 12
B
ATCase
helix 6
helix 2
Arg167
Glu50
helix 9
Arg234
T state
helix 6
helix 2
Arg167
Glu50
Arg234
helix 9
R state

Fig. 7: Triads of residues functioning as molecular switches in intramolecular signaling. Upon T-R transition rearrangements occur between residues Glu23, Tyr234, and Arg157 of ScCM (**A**) and between residues Glu50, Arg157, and Arg234 of ATCase (**B**). α-helices and β-strands are outlined as ribbons.

ATCase. As far as ATCase is concerned, a detailed mechanism for homotropic interactions has been described and there exist diverse theories about how the allosteric ligands exert heterotropic effects. Similar to chorismate mutase, a high-affinity active site has to be formed for the R state structure.

This is mainly achieved by closure of the aspartate domain toward the cp domain, thereby forming the complete binding pocket for aspartate accompanied by shifts of the L80s and L240s loop. Plenty of interface contacts have been identified by amino acid substitutions which are important for stabilizing either the ATCase T or R state conformation. In detail, the L80s loop contains the active side residues Ser80 and Lys84 which are the two residues contributed by the adjacent C chain. It moves into the active site during T-R transition, positioning Ser80 and Lys84 for substrate binding, which is essential for cooperativity (Macol *et al.*, 1999). The end of the L80s loop is tethered by Glu86, which is salt linked to a most critical active site residue, Arg54, across the C1-C2 interface and assists in its positioning for catalysis. This ion pair interaction exists in both T and R state and therefore is also essential for forming the catalytic subunit (Baker *et al.*, 1994).

The interdomain bridging neccessary for domain closure in ATCase is partly achieved by a salt link between the active-site residue Arg167 and Glu50 (Fig. 7B). Arg105, also in the active site pocket, is free to interact with the substrate only when it is no longer bound by Glu50 in the R state (Kantrowitz & Lipscomb, 1988; Tauc *et al.*, 1994). In addition, the whole L240s loop rearranges during T-R transition and behaves as a hinge like the L220s loop of chorismate mutase. It moves toward the cp domain during domain closure so that residues Arg167, Arg229, and Glu231, which are important for aspartate binding, are rearranged. Glu233 binds Arg229 only in the R state and positions it properly for catalysis. Arg234 is also involved in interdomain bridging. It is stabilized by binding Glu231 and also contacts Glu50. Therefore the interactions between Glu233 and Arg229 and between Glu50 and Arg234 are impotant for establishing the R state confromation of the L240s loop.

As in chorismate mutase, there is a triad of residues. Instead of Tyr-Glu-Arg the ATCase triad is composed of Glu50, Arg167 and Arg234 (Fig. 7B). However, the function of the rearrangements in the environment of the triad is to initiate T-R transition instead of maintaining the T state as in chorismate mutase. In addition, interchain contacts between Tyr240 and Asp271 have to be broken for the movements of the domains. The interruption of the important intersubunit contacts at the C1-C4 interface formed by the L240s loop residues Glu239 and Lys164-Lys165 and Lys164-Lys165 and Glu239 of the other C chain, respectively, is another prerequsite for the T-R transition. In fact, all but van der Waals interactions are eliminated at this interface when the L240s loop, which provides the only contact between C chains from different trimers, is reoriented. The distinct interchain contacts formed by the L240s loop are important for stabilization of the allosteric states. When the links between the lower and upper C trimers are lost, the T state cannot be maintained (Kantrowitz & Lipscomb, 1988). By the rearrangement of one L240s loop, the L240s loops from adjacent chains all move apart, thereby separating the catalytic subunits and releasing the restrictions present in the T state. Because every change at this intersubunit interface is transmitted to the others, the T-R transition is a concerted mechanism with the whole enzyme moving toward the R state (Kantrowitz & Lipscomb, 1990). Macol *et al.* found direct evidence that the exclusive binding of one PALA molecule per enzyme is sufficient for full T-R transition of all its subunits (Macol *et al.*, 2001). This proves that transition is concerted and clearly meets the requirement of the MWC model of allostery. All C1-R4 contacts are broken, while more contacts are made between C1 and R1. In addition, bonds at the interface between allosteric and zinc domain of the R chain are lost and new bonds are formed between the C chain domains (Allewell, 1989). The L100s loop functions as another hinge between the allosteric and zinc domains. Amino acid substitutions in these regions eliminate cooperativity and heterotropic interactions. In short, the T state is stabilized by bonds at the C1-C4, C1-R4 and allosteric-zinc interfaces, the R state is stabilized by bonds at the C1-R1, C1-C2 and polar-equatorial interfaces (also see Dembowski & Kantrowitz, 1994; Stevens *et al*., 1991).

As far as the transduction of heterotropic effects is concerned, the following pathways have been proposed for ATP signaling. ATP binds to the allosteric site in a slightly different way from CTP (Lipscomb, 1994). It expands this site and thereby influences neighboring residues. ATP undergoes more interactions to the N-terminal region of the R chains than CTP does. This region is responsible for creating high- or low-affinity binding sites and, by doing so, exerts control over inhibition and activation and is supposed to mediate communication between the two binding sites within a regulatory dimer (R1-R6 N-terminal contacts) (Sakash & Kantrowitz, 1998). The next important region is the allosteric-Zn interface, which stabilizes T and R state, respectively. The contacts between helix H1‘ of the allosteric domain and residues in the Zn domain, especially Phe33r, change because helix H1‘ is shifted (Gouaux *et al*., 1990). These perturbations, and probably also those that might be caused by CTP in the allosteric-Zn interface, are propagated to the C1-R1 or C1-R4 interface (Gouaux *et al.*, 1990). Finally, residues 146r-149r form a set of interactions with 241c-245c of the L240s loop which is involved in transduction of the ATP signal but not that of CTP (De Staercke *et al*., 1995). Alternatively, it was proposed that the ATP expansion of the allosteric site is propagated through Glu68r and reorientation of helix H2‘, thereby moving Tyr77r in the hydrophobic core, which also includes Val106r. This residue could transmit the

ATP signal towards the R1-C1 and R1-C4 interfaces between R and C chains (Xi *et al*., 1994).

Separation of activation and inhibition

ScCM. Thr226, the last residue of loop L220s in ScCM, proved necessary for R-T transition since a Thr226Ile mutant is unresponsive to the allosteric effectors and shows no cooperativity but is locked in the activated state (Schmidheini *et al*., 1990). Other amino acid residues at position 226 yielded enzymes with different intermediate degrees of regulation between the wild-type and the constitutively activated enzyme (Graf *et al*., 1995). The K_M values of the mutant enzymes were reduced compared to the wild type. The shift to the R state was strongest for Ile226 or Arg226 substitutions and weaker for enzymes with Asp226, Lys226, Ala226, or Pro226 residues; Gly226 or Ser226 substitutions had the least effect on the T-R equilibrium. However, no obvious correlation of the strength of this effect with any property of the introduced residue was found. Whereas the allosteric equilibrium is shifted toward the R state for these enzymes, the catalytic constant and the affinity for tryptophan are uneffected. The role of this loop seems to be different in the structurally related chorismate mutase from *A. nidulans* (Krappmann *et al.*, 1999). Although several residues in the regulatory and catalytic site and for signal transduction are conserved, a special role for allosteric transition could not be attributed to Asp233, the corresponding residue to Thr226. Therefore, the signal of effector and maybe substrate binding seems to follow slightly different routes in the dimer interface in this otherwise very similar enzyme.

A Thr226Ile Ile225Thr double mutant which remains sensitive to tryptophan, but insensitive to tyrosine shows that the simple two-state MWC model for allosteric transitions does not explain all characteristics of yeast chorismate mutase (Schnappauf *et al.*, 1998). The additional Ile225Thr subsitution unlocks the R state and allows activation but not inhibition. A threonine residue at the end of the loop seems to form essential hydrogen bonds, which are necessary for the conformation present in the T state. By changing its conformation, L220s serves as a hinge which can affect shifting of helices H11 and H12 and thereby lead to the formation of the inactive Tyr234-Glu23-Arg157 triad structure in the active site (Fig. 7A).

A loss of sensitivity to tyrosine alone is also shown by substitutions of Tyr234 and Glu23, respectively, which interfere with the molecular switch that modulates the active site pocket (Schnappauf *et al.*, 1998). The interactions of the phenolic hydroxyl moiety of tyrosine are necessary for the low-affinity state of the catalytic site, since a missing tyrosine at position 234 does not assist in keeping Glu23 close to the active site. An involvement of Tyr234 in homotropic interaction between the active sites is supported by the fact that cooperativity is reduced or abolished in enyzmes with substitutions at position 234. Similarly, a Glu23Gln mutation shows only residual inhibition but strong activation, which emphazises the need for negative charge for inhibition at this position to change the electrostatic field in the active-site pocket. Thus, allosteric activation seems to be signaled on a pathway distinct from allosteric inhibiton and homotropic interactions between the active sites.

These findings support the path of allosteric transition as described above, because the amino acid substitutions all affect residues found to be rearranged during T-R transition. They also clearly show that activation and inhibition are functionally divided and must follow different pathways. The interactions around Thr234 and Ile225 Thr226 are a prerequisite for forming the complete T state. Their absence has no effect on the R state, however, showing that interactions between other parts of the polypeptides are important for complete R state formation. Further rearrangements in the rest of the protein during T-R transition are not affected by these substitutions, making activation possible. In fact, it seems that transition to the R state comprises only part of the rearrangements found between T and R state. Besides T and R states, the unliganded enzyme might occupy a third state which is intermediate between the T and R states. In this state the distance between H8 of one monomer and H4, H5, and L80s of the other monomer in the allosteric site is intermediate between those in the R state and T state and is changed to R or T state by the involvement of an ‘induced fit‘ promoted by effector binding. Whether a more direct pathway for the action of tryptophan might be possible, which does not require a global change of the overall enzyme structure, is an open question. Tryptophan activation might not be triggered by loop L220s. Presumably it follows either a pathway along helix H8, which contributes residues to the regulatory as well as the catalytic site, or via helix H4 which extends from the allosteric site through the whole molecule. The existence of a preexisting T-R equilibrium in which the states are formed apart from ligand binding and which is shifted toward one state or the other by binding of an effector seems to be unlikely with the results obtained so far.

ATCase. Facts supporting this theory of different ways for activation and inhibition were found for ATCase. Regions specific for transmission of the ATP signal have been identified in the Zn-allosteric interface, mainly Leu151r and Val150r, which are near the R1-C4 interface and may transmit the signal between these two interfaces (Van Vliet *et al.*, 1991; Xi *et al.*, 1994). Also, residues 145 to 149 of the R chain which contact the L240s loop in the R1-C4 interface specifically transmit the ATP signal but not the CTP signal. Amino acid substitutions around the important salt link between Lys143r and Asp236c of the L240s loop verified the importance of this region for ATP activation (Lipscomb, 1992; Lipscomb, 1994). In addition, six residues at the C terminus of the R chain were found to be involved in the ATP activation, as found with truncated proteins derived from specific deletion alleles (De Staercke *et al.*, 1995). In particular, the R1-C1 interface, the junction between the R1-C1 and R1-C4 interfaces, and the R1-C4 interface are essential for ATP signaling. Like tryptophan and tyrosine recognition in chorismate mutase, there is a discrimination between ATP and CTP in the allosteric site, which is partly dependent of the size of the base rings. In addition to expansion or reduction of the binding pocket, the orientation of the base plays a crucial role for propagation of the activation or inhibition signal (Sakash *et al*., 2000).

Comparable to Thr226 of chorismate mutase, there are several single residues in ATCase which, when substituted, lead to enzymes which are shifted toward the R state. Among them are the residues Lys143r and its binding partner Leu235c, which normally stabilize the R1-C4 interface (Newton & Kantrowitz, 1990; Schachman, 1988). Also another mutant enzyme showed normal sensitivity to ATP activation but no CTP inhibition, though CTP can bind normally (Ladjimi *et al*., 1985). Thus, this enzyme variant is in an intermediate state in which the R1-C1 interface is weakened (Cherfils *et al*., 1987). In addition, the Lys56rAla mutant enzyme is frozen in the R state and insensitive to ATP while CTP inhibits the enyzme and restores homotropic effects (Corder & Wild, 1990). Other mutant enzymes, however, are stabilized in the T state. The Glu50cAla enzyme is unable to close the C chain domains and thus does not exist in the R state conformation (Lee *et al*., 1995; Newton & Kantrowitz, 1990). A Thr82rAla enzyme is structurally fixed in an extreme T state with the T-R equilibrium shifted toward the T state (Williams *et al*., 1998). Uncoupling of activation and inhibition can be achieved by substitutions at positions 56r and 60r. CTP inhibition but only minimal ATP activation can be observed for a Lys56rAla substitution. When Lys60r is replaced by alanine, an enzyme is generated with ATP activation and minor CTP inhibition (Stevens & Lipscomb, 1990; Zhang & Kantrowitz, 1989). When transmission of CTP is disturbed, however, larger structural changes occur in the enzyme. Amino acid residues could not be defined which specifically and exclusively affect inhibition. Therefore, it seems that inhibition is caused by long-range effects on other interfaces by a more complex set of interactions and not by signal transmission along a defined path like ATP signaling. This resembles the activation mechanism by tryptophan of chorismate mutase. For both enzymes, substitution of some specific single amino acid residues can be sufficient for changing the intensity of allosteric regulation. However, other authors found that these subsitutions need not necessarily be positioned at a defined path for signal transduction but might cause global conformational changes due to changes in free energy (Aucoin *et al*., 1996; Liu *et al*., 2000).

Separation of homotropic and heterotropic effects

ATCase. Homotropic and heterotropic effects can be almost completely separated in ATCase and seem to be mediated by different allosteric transitions, which include more than two states (Stryer, 1988). In the ‘frozen‘ T or R state, the substrate has no homotropic effects but heterotropic effects are maintained (Landfear *et al*., 1978; Peterson *et al*., 1992; Stebbins *et al*., 1990). This also means that the effectors act indirectly on substrate binding rather than on the T-R equilibrium (Hsuanyu & Wedler, 1988). Also, when Glu231c is replaced by isoleucine or asparagine, the mutant enzyme shows no reduction in heterotropic effects but reduced cooperativity with respect to aspartate (Peterson *et al.*, 1992). $V_{\max}$ is changed significantly by addition of CTP or ATP due to decreased binding of active-site ligands to the R state. The substrates are not bound preferentially to the R state, resulting in reduced cooperativity. Other variants like Glu50cAla, Glu50cGln, Ser171cAla, or Arg234cSer also bind aspartate more weakly and show similar effects on heterotropic and homotropic interactions. The MWC model describes two extreme types of allosteric enzymes: the V system for which $V_{\max}$ is different in the T and R states, and a K system in which K_m is altered. The V system exhibits heterotropic effects but no cooperativity toward the substrates. No $V_{\max}$ could be determined for the T state of ATCase, however, because it is converted to the R state in the presence of the two stubstrates. Therefore it seems that ATCase is a mixed V-K system in which some substitutions might effect $V_{\max}$ more than K_m (Peterson *et al.*, 1992). Therefore, a loss of homotropic effects need not necessarily be accompanied by a change in heterotropic effects. Similarly, a Glu239cGln enzyme shows cooperativity but no heterotropic effects. This variant is devoid of C1-C4 interchain interactions so that the enzyme undergoes transition to the R state in the presence of carbamoylphosphate alone, and heterotropic effects can no longer be observed (Ladjimi & Kantrowitz, 1988).

ScCM. When residue 226 of chorismate mutase was varied, all enzymes displayed the behaviour of a true K system (Graf *et al.*, 1995). k_{cat} values were roughly the same, K_m was decreased, and there was a loss of cooperativity. Also, when Glu23 was replaced by an aspartic acid residue, k_{cat} values remained constant while the K_m value was decreased in the R state compared to the T state (Schnappauf *et al.*, 1998). In addition, cooperativity was lost, so that this is the only mutant enzyme so far in which homotropic and heterotropic effects are uncoupled. This means that although the shorter side chain of aspartic acid positioned at the molecular switch for inhibition is sufficient for formation of the inhibitory triad of residues, it is not able to maintain cooperative substrate binding. Therefore, for chorismate mutase, slightly different allosteric transitions must exist for homotropic and heterotropic effects.

Models for the allosteric mechanisms

Two additional allosteric states besides T and R were found for chorismate mutase when chorismic acid or the transition state analogue binds to the active site of the enzyme, the T-super R and the R-superR state. As explained above, the data support the existence of a super R state when chorismate mutase is liganded exclusively to chorismate. However, a crystal structure for chorismate mutase liganded solely to the transition state analogue has not been determined yet. Therefore, it remains unclear if the substrate alone can promote the transition toward the super R state and if this state maybe is the actual R state. Binding of the transition analogue to the catalytic site and additional binding of tryptophan to the allosteric site leads to additional conformational changes so that an R-super R state is formed. This result cannot be explained by the KNF model, in which it is proposed that the activator induces the same conformation as the substrate. On the other hand, the R state structure with tryptophan bound was determined with a mutant enzyme variant. This allows speculation as to whether tryptophan induces the same conformation in the wt enzyme. It might be possible that the R-super R state is the final R state and the known tryptophan-bound form is just an intermediate. However, with tyrosine bound to the allosteric site, rearrangements to an R-like structure seem necessary prior to the catalytic step since the K_m value is increased 30-fold for the T state compared to the R state. This super R state, which is very nearly T like in the allosteric sites, occurs when tyrosine is bound to the allosteric site and the transition state analogue is bound to the catalytic center. Similarly, when PALA binds to the six active sites of ATCase the elongated R state is only slightly affected when CTP is then bound to the regulatory sites. Thus, the substrate analogues in these examples dominate the allosteric transition.

As mentioned above, homotropic cooperativity in ATCase can be fully explained by a concerted transition according to the MWC two-state model. No evidence for such behavior was found for homotropic effects of the substrate for chorismate mutase.

For the ATCase system, different models were proposed for the effect of the heterotropic ligands. Originally it was thought that the nucleotides act on the same equilibrium as aspartate in that they bind preferentially to one of the two allosteric states and thereby directly alter the equilibrium (Changeux & Rubin, 1968; Howlett *et al*., 1977; Schachman, 1988). Since it was found that homotropic and heterotropic effects can be uncoupled, this model seems to be outdated (Allewell, 1989; Lipscomb, 1994). Fetler *et al.* found that while homotropic effects can be explained by the model of concerted transition, CTP seems to slightly decrease the R state population, thus partly acts concerted, and ATP does not affect the T-R equlibrium (Fetler *et al*., 1995). So CTP acts in part independently of the T-R equlibrium while ATP activation follows a different mechanism. Models that account for the experimental data more precisely are the primary-secondary-effect model, the effector-modulated transition model and the nucleotide perturbation model. It was proposed that the nucleotides affect the affinity of the active sites for aspartate in a primary effect which includes smaller structural changes originating from the allosteric site leading to the formation of the R state structure by binding of aspartate as the secondary effect when carbamoylphosphate is already bound to ATCase (Hervé *et al*., 1985; Hsuanyu & Wedler, 1988; Tauc *et al*., 1982; Xi *et al*., 1991). As described previously, binding of CTP or ATP to the R or T state causes only minor alterations in the separation of the catalytic trimers (Gouaux *et al.*, 1990; Stevens *et al*., 1990). According to the model, this can be viewed as the primary effect. In mutant enzymes, however, which exist in intermediate conformations, both effectors manage to induce the full rearrangement to the R or T state (Stevens & Lipscomb, 1990). This model is partly in agreement with the effector-modulated transition model. The nucleotides might change the stability of the interfaces as part of the primary effect thereby influencing T-R transition on aspartate binding. According to this, Liu *et al.* proposed that changes in interfaces could influence allostery by altering the global energy of ATCase (Liu *et al.*, 2000). ATP might induce a signal transduction chain via the R1-C1 interface, while CTP exerts its function via the R1-C4 interface (Xi *et al*., 1991). Other authors favour the nucleotide perturbation model (Stevens & Lipscomb, 1992). It was found that ATP increases the size of the allosteric site, which also increases the whole allosteric domain. CTP, in contrast, decreases the size of its binding site and also the allosteric domain. Discrimination between the nucleotides occurs in the regulatory chains, as was found with regulatory-chain mutants (Van Vliet *et al.*, 1991; Zhang & Kantrowitz, 1989) and hybrid enzymes (Beck *et al*., 1989). On the pathway to the active site, the signal has to be transmitted via the allosteric-Zn, R1-C1, R1-C4 and/or R1-allosteric/R6-allosteric interfaces. These effects would lead to domain movements of C and R chains which, however, would be by far smaller than those during T-R transition, namely, the separation of the catalytic trimers by less than 1 Å. A direct signal could be transmitted via allosteric-Zn and C-R interfaces, but indirect signalling is also proposed. In the R state, CTP binding might influence the R1-C1 interface and thereby decrease the trimer separation in the R state. These movements should affect the C1-C4 interface, leading to changes in the L240s loop and the active site. As a consequence, the R state is destabilized (Stevens & Lipscomb, 1992). In the T state, CTP binding stabilizes this conformation even further without affecting trimer separation due to steric hindrance, but influences residues in the active site. ATP increases trimer separation by influencing these interfaces in the opposite way, which destabilizes the T state. In the R state, this influence of ATP might well perturb (stabilize) this structure even further (Stevens & Lipscomb, 1992). It was found that in an unliganded T state, ATP or CTP binding can change the orientation of the active-site residue Arg229 and that interactions around the L240s loop are weakened (Lipscomb, 1992; Lipscomb, 1994).

The structure of unliganded ATCase is known only to 2.6 Å resolution (Ke *et al*., 1984) and no structure has been determined for unliganded chorismate mutase. High-resolution structures for both enzymes would facilitate the construction of models for the allosteric mechanism. In addition, only a mutant version of chorismate mutase was crystallized in complex with the activator tryptophan. Equilibrium dialysis and kinetic studies showed that tyrosine is unable to bind to this variant whereas tryptophan binding can be detected. This suggests that the enzyme is locked in an R-like state and that tryptophan binding has no influence on enzyme activity. The mutant enzyme structure does not answer the question whether tryptophan induces the full transition to the R state or super R state in the wt enzyme. However, it might well be that like in ATCase, the activator as single ligand is not able to shift the equilibrium fully toward the R state but that the substrate is required for forming the ultimate high-affinity high-activity super R state. It cannot be excluded that even when only tryptophan is bound the wt enzyme resembles the T state. Whether the allosteric inhibitor has a destabilizing effect on the high-affinity state of chorismate mutase is not clear either. The presence of the T-super R state, however, shows that structural changes occur at least in the allosteric domains, although the catalytic domains seem to remain in the super R state. These changes require a flexible hinge region which connects the allosteric and the regulatory domain. This flexibility might be an indirect reminder of the probable origin of both domains as a result of an evolutionary gene duplication event. The mixed states which are found in different chorismate mutase cocrystals might be consistent with the nucleotide perturbation model of transition in ATCase. According to that model, the activator tryptophan shifts the equilibrium from the T to the R state and further stabilizes the super R state induced by the substrate. Tyrosine slightly destabilzes the R-like state by formation of the T-super R state, but strongly stabilizes the T state. Also, the other models can explain some characteristics found for chorismate mutase. The further structural rearrangements occuring upon binding of the transiton state analogue might also be addressed by the primary-secondary-effect model. Effector binding might cause a primary effect, while substrate binding leads to the secondary effect, namely, the transition to the super R state. Finally, the effector-modulated transition model accounts for the broader structural changes induced by tryptophan binding to chorismate mutase. No direct signal transduction pathway has been found for this effector yet, but it seems to modulate activity by influencing the subunit interface or global energy of the protein conformation.

Lessons learned from the model systems and the dawn of a new paradigm for allostery

Regulation of gene product activity by allostery is a central dogma within the field of biochemistry, and allosteric proteins acting as molecular amplifiers are widespread in nature. Since its first description, a lot of knowledge concerning the mechanisms contributing to allosteric regulation has accumulated. Naturally, model systems have emerged in which the basic principles that constitute allostery were defined and scrutinized. The first polypeptide on which the basic principles of homotropic and heterotropic interactions were applied was hemoglobin. Although hemoglobin is not an enzyme, the availability of numerous mutants with single amino acid substitutions and the existance of a solved X-ray structure lead to its establishment as a paradigm of allostery. Among the numerous enzymatic activities, the *E. coli* ATCase system has emerged as a proper model for allosteric mechanisms. Here we summarized the knowledge and insights gained over the past ten years for another metabolic enzyme, the baker’s yeast chorismate mutase. For ScCM, a multitude of data has been determined, complemented by a variety of solved crystal structures defining different allosteric states. With respect to ATCase, ScCM offers additional advantages for general research on allostery. Its dimeric structure comes up to the smallest unit possible for allosteric transitions and cooperativity. In fact, ScCM displays the whole spectrum of allostery like cooperativity and negative or positive effects mediated by homotropic as well as heterotropic ligands. Thus, both model systems, ATCase and ScCM, have the capacity to improve and support our present-day view on allosteric mechanisms.

The most intriguing question which can be asked is whether one unifying model can account for allostery in general. Basically, three generalizing descriptions for allosteric transitions have been developed to date: MWC, KNF, and the unifying model by Eigen. Homotropic transition of the transcarbamoylase has been investigated conclusively, and this enzyme has provided direct structural evidence for a concerted allosteric transition as described by the MWC model. For the chorismate mutase, detailed analyses of the allosteric transition on substrate binding in the absence of heterotropic ligands are still missing and therefore no conclusive classification of this allosteric behavior of ScCM is possible. On the other hand, very accurate conclusions have been made concerning the principles for heterotropic effects acting on both enzymes. Here, the two state model as provided by the MWC theory proves to be insufficient. Five distinct structures were solved for the yeast chorismate mutase that represent different allosteric states. Additionally, several intermediate states have been created by modification of the Thr226 trigger. Most interestingly, the coexistence of different allosteric states for separate domains within the same molecule has been demonstrated by binding of a transition state analogue in the presence of either effector. This flexibility accounts for an induced-fit mechanism of allosteric transition. As stated above, a clear differentiation seems necessary with the MWC theory frequently applying for homotropic effects, whereas heterotropic transitions may be described appropriately by the KNF model. It is conclusively evident that to date no simplifying principle is sufficient to describe either allosteric enzyme and that further refinements will have to be made for elucidating their allosteric behavior completely.

Detailed analysis of the allosteric binding sites of ScCM and ATCase provides insights about how small ligands are discriminated on the protein surface. As it is the case for tyrosine and phenylalanine binding to ScCM, highly specific interactions and contacts contribute to the molecular recognition of the differing hydroxyl group. When different heterotropic effectors are concerned, a common mechanism for signal transduction can be deduced. Expansion and contraction, respectively, of the allosteric site is transduced by conformational changes to the distant active site. There the creation of a high-affinity cavity is essential for catalytic turnover. Both model enzymes demonstrate in an extraordinary way how allosteric signals are transmitted across a protein structure. While in ScCM allosteric signal transduction of inhibition can be followed along a distinct structural pathway, this is not possible for the positive effect of the activating ligand. The opposite is true for ATCase in which activation but not inhibition follows a defined path from the allosteric to the active site. In conclusion, it is obvious that different routes within an oligomeric enzyme transmit different allosteric responses. Additionally, different means of intra- and intermolecular signal transduction are possible in a nonexclusive manner, like long-range effects that may alter the global protein structure or defined rearrangements along distinct amino acid side chains. The uncoupling of allosteric activation and inhibition as demonstrated for both enzymes supports this view of distinct signal transduction pathways. The existence of molecular switches that enable allosteric transition is of special interest. For both enzymes, a triad of residues has been identified that contribute to the T-R transition and support one allosteric state, respectively. Loop regions that function as molecular hinges for the movements of domains relative to each other were also identified, and all these elements contribute to a general understanding of the common mechanisms for allosteric transition. The overall structure of allosteric proteins is delicately balanced in such a way that small changes can shift the quaternary structure toward tense or relaxed states. This means that transmission of heterotropic and homotropic signals does not necessarily follow distinct pathways and that substitutions supposed to act in a specific manner in a signalling path might as well affect the global protein structure in some cases.

As outlined above, the common theory of two major allosteric states that co-exist within a dynamic equilibrium in the absence of effectors is unlikely and must be refined towards a more dynamic model. In 1965, Monod *et al.* already stated that their ‘model offers only an over-simplified first approximation of real systems, and it may prove possible in some cases to introduce corrections and refinements…’. ScCM represents an excellent real system capable of almost all aspects of allostery. Especially when taken in combination with its text book counterpart *E. coli* ATCase, the knowledge gained from experiments with ScCM contributes to a refined understanding of the basic principles that underly allostery. Yeast chorismate mutase significantly differs from transcarbamoylase by the fact that regulatory and catalytic domains reside on the same polypeptide chain. A gene duplication and fusion event has been proposed as the evolutionary event underlying this assembly. Thus, ScCM is well suited as appropriate model enzyme in studying evolution of an allosteric mechanism. Furthermore, the knowledge concerning chorismate mutases in general is quite extensive, and by comparison to its numerous prokaryotic or eukaryotic counterparts, ScCM will provide further conclusions how rate acceleration of a pericyclic reaction can be achieved and regulated.

References

Allewell, N. M. (1989). *Escherichia coli* aspartate transcarbamoylase: structure, energetics, and catalytic and regulatory mechanisms. *Annu Rev Biophys Chem* **18**, 71-92.

Andrews, P. R., Smith, G. D. & Young, I. G. (1973). Transition-state stabilization and enzymic catalysis. Kinetic and molecular orbital studies of the rearrangement of chorismate to prephenate. *Biochemistry* **12**, 3492-3498.

Aucoin, J. M., Pishko, E. J., Baker, D. P. & Kantrowitz, E. R. (1996). Engineered complementation in *Escherichia coli* aspartate transcarbamoylase. Heterotropic regulation by quaternary structure stabilization. *J Biol Chem* **271**, 29865-29869.

Baker, D. P., Stebbins, J. W., DeSena, E. & Kantrowitz, E. R. (1994). Glutamic acid 86 is important for positioning the 80's loop and arginine 54 at the active site of *Escherichia coli* aspartate transcarbamoylase and for the structural stabilization of the C1-C2 interface. *J Biol Chem* **269**, 24608-24614.

Bartlett, P. A. & Johnson, C. R. (1985). An inhibitor of chorismate mutase resembling the transition-state conformation. *J Am Chem Soc* **107**, 7792-7793.

Beck, D., Kedzie, K. M. & Wild, J. R. (1989). Comparison of the aspartate transcarbamoylases from *Serratia marcescens* and *Escherichia coli*. *J Biol Chem* **264**, 16629-16637.

Beernink, P. T., Endrizzi, J. A., Alber, T. & Schachman, H. K. (1999). Assessment of the allosteric mechanism of aspartate transcarbamoylase based on the crystalline structure of the unregulated catalytic subunit. *Proc Natl Acad Sci USA* **96**, 5388-5393.

Bethell, M. R., Smith, K. E., White, J. S. & Jones, M. E. (1968). Carbamyl phosphate: an allosteric substrate for aspartate transcarbamylase of *Escherichia coli*. *Proc Natl Acad Sci USA* **60**, 1442-1449.

Blangy, D., Buc, H. & Monod, J. (1968). Kinetics of the allosteric interactions of phosphofructokinase from *Escherichia coli*. *J Mol Biol* **31**, 13-35.

Changeux, J. P. & Rubin, M. M. (1968). Allosteric interactions in aspartate transcarbamylase. 3. Interpretation of experimental data in terms of the model of Monod, Wyman, and Changeux. *Biochemistry* **7**, 553-561.

Cherfils, J., Vachette, P., Tauc, P. & Hervé, G. (1987). The pAR5 mutation and the allosteric mechanism of *Escherichia coli* aspartate carbamoyltransferase. *EMBO J* **6**, 2843-2847.

Chook, Y. M., Ke, H. & Lipscomb, W. N. (1993). Crystal structures of the monofunctional chorismate mutase from *Bacillus subtilis* and its complex with a transition state analog. *Proc Natl Acad Sci USA* **90**, 8600-8603.

Corder, T. S. & Wild, J. R. (1990). Discrimination between nucleotide effector response of aspartate transcarbamoylase due to a single site substitution in the allosteric binding site. *J Biol Chem* **264**, 7425-7430.

Cunin, R., Jacobs, A., Charlier, D., Crabeel, M., Hervé, G., Glansdorff, N. & Piérard, A. (1985). Structure-function relationship in allosteric aspartate carbamoyltransferase from *Escherichia coli*. I. Primary structure of a *pyrI* gene encoding a modified regulatory subunit. *J Mol Biol* **186**, 707-713.

De Staercke, C., Van Vliet, F., Xi, X. G., Rani, C. S., Ladjimi, M., Jacobs, A., Triniolles, F., Hervé, G. & Cunin, R. (1995). Intramolecular transmission of the ATP regulatory signal in *Escherichia coli* aspartate transcarbamylase: specific involvement of a clustered set of amino acid interactions at an interface between regulatory and catalytic subunits. *J Mol Biol* **246**, 132-143.

Dembowski, N. J. & Kantrowitz, E. R. (1994). The use of alanine scanning mutagenesis to determine the role of the N-terminus of the regulatory chain in the heterotropic mechanism of *Escherichia coli* aspartate transcarbamoylase. *Protein Eng* **7**, 673-679.

Dohi, Y., Sugita, Y. & Yoneyama, Y. (1973). The self-association and oxygen equilibrium of hemoglobin from the lamprey, *Entosphenus japonicus*. *J Biol Chem* **248**, 2354-2363.

Dutta, M. & Kantrowitz, E. R. (1998). The influence of the regulatory chain amino acids Glu-62 and Ile-12 on the heterotropic properties of *Escherichia coli* aspartate transcarbamoylase. *Biochemistry* **37**, 8653-8658.

Eberhard, J., Raesecke, H. R., Schmid, J. & Amrhein, N. (1993). Cloning and expression in yeast of a higher plant chorismate mutase. Molecular cloning, sequencing of the cDNA and characterization of the *Arabidopsis thaliana* enzyme expressed in yeast. *FEBS Lett* **334**, 233-236.

Eigen, M. (1967). Kinetics of reaction control and information transfer in enzymes and nucleic acids. In *Fast reactions and primary processes in chemical kinetics, Nobel Symposium* ***5****:333-369*. Edited by S. Claesson.

Eisenstein, E., Markby, D. W. & Schachman, H. K. (1990). Heterotropic effectors promote a global conformational change in aspartate transcarbamoylase. *Biochemistry* **29**, 3724-3731.

Endrizzi, J. A., Beernink, P. T., Alber, T. & Schachman, H. K. (2000). Binding of bisubstrate analog promotes large structural changes in the unregulated catalytic trimer of aspartate transcarbamoylase: implications for allosteric regulation induced cell migration. *Proc Natl Acad Sci USA* **97**, 5077-5082.

England, P., Leconte, C., Tauc, P. & Hervé, G. (1994). Apparent cooperativity for carbamoylphosphate in *Escherichia coli* aspartate transcarbamoylase only reflects cooperativity for aspartate. *Eur J Biochem* **222**, 775-780.

Fetler, L., Tauc, P., Hervé, G., Moody, M. F. & Vachette, P. (1995). X-ray scattering titration of the quaternry structure transition of aspartate transcarbamylase with a bisubstrate analogue: influence of nucleotide effectors. *J Mol Biol* **251**, 243-255.

Galopin, C. C., Zhang, S., Wilson, D. B. & Ganem , B. (1996). On the mechanism of chorisamte mutases: clues from wild-type *E. coli* enzyme and a site-directed mutant related to yeast chorismate mutase. *Tetrahedron Lett* **37**, 8675-8678.

Ganem, B. (1996). The mechanism of the Claisen rearrangement: déjà vu all over again. *Angew Chem Int Ed Engl* **35**, 936-945.

Gerhart, J. C. & Pardee, A. B. (1962). The enzymology of control by feedback inhibition. *J Biol Chem* **237**, 891-896.

Gouaux, J. E., Krause, K. L. & Lipscomb, W. N. (1987). The catalytic mechanism of *Escherichia coli* aspartate carbamoyltransferase: a molecular modelling study. *Biochem Biophys Res Commun* **142**, 893-897.

Gouaux, J. E., Stevens, R. C. & Lipscomb, W. N. (1990). Crystal structures of aspartate carbamoyltransferase ligated with phosphonoacetamide, malonate, and CTP or ATP at 2.8-Å resolution and neutral pH. *Biochemistry* **29**, 7702-7715.

Graf, R., Dubaquié, Y. & Braus, G. H. (1995). Modulation of the allosteric equilibrium of yeast chorismate mutase by variation of a single amino acid residue. *J Bacteriol* **177**, 1645-1648.

Griffin, J. H., Rosenbusch, J. P., Weber, K. K. & Blout, E. R. (1972). Conformational changes in aspartate trancarbamylase. I. Studies of ligand binding and of subunit interactions by circular dichroism spectroscopy. *J Biol Chem* **247**, 6482-6490.

Hack, E. S., Vorobyova, T., Sakash, J. B., West, J. M., Macol, C. P., Hervé, G., Williams, M. K. & Kantrowitz, E. R. (2000). Characterization of the aspartate transcarbamoylase from *Methanococcus jannaschii*. *J Biol Chem* **275**, 15820-15827.

Haynes, M. R., Stura, E. A., Hilvert, D. & Wilson, I. A. (1994). Routes to catalysis: structure of a catalytic antibody and comparison with its natural counterpart. *Science* **263**, 646-652.

Hervé, G., Moody, M. F., Tauc, P., Vachette, P. & Jones, P. T. (1985). Quaternary structure changes in aspartate transcarbamylase studied by X-ray solution scattering. Signal transmission following effector binding. *J Mol Biol* **185**, 189-199.

Honzatko, R. B. & Lipscomb, W. N. (1982). Interactions of phosphate ligands with *Escherichia coli* aspartate carbamoyltransferase in the crystalline state. *J Mol Biol* **160**, 265-286.

Howlett, G. J., Blackburn, M. N., Compton, J. G. & Schachman, H. K. (1977). Allosteric regulation of aspartate transcarbamoylase. Analysis of the structural and functional behavior in terms of a two-state model. *Biochemistry* **16**, 5091-5100.

Hsuanyu, Y. & Wedler, F. C. (1987). Kinetic mechanism of native *Escherichia coli* aspartate transcarbamylase. *Arch Biochem Biophys* **259**, 316-330.

Hsuanyu, Y. C. & Wedler, F. C. (1988). Effectors of *Escherichia coli* aspartate transcarbamoylase differentially perturb aspartate binding rather than the T-R transition. *J Biol Chem* **263**, 4172-4181.

Jackson, D. Y., Liang, M. N., Bartlett, P. A. & Schultz, P. G. (1992). Activation parameters and stereochemistry of an antibody-catalyzed Claisen rearrangement. *Angew Chem Int Ed Engl* **31**, 182-183.

Jin, L., Stec, B., Lipscomb, W. N. & Kantrowitz, E. R. (1999). Insights into the mechanisms of catalysis and heterotropic regulation of *Escherichia coli* aspartate transcarbamoylase based upon a structure of the enzyme complexed with the bisubstrate analogue N-phosphonacetyl- L-aspartate at 2.1 Å. *Proteins* **37**, 729-742.

Johnson, L. N., Hajdu, J., Acharya, K. R., Stuart, D. I., McLaughlin, P. J., Oikonomakos, N. G. & Barford, D. (1989). Glycogen phosphorylase b. In *Allosteric Proteins*. Edited by G. Hervé. Boca Raton, USA: CRC Press.

Kantrowitz, E. R. & Lipscomb, W. N. (1988). *Escherichia coli* aspartate transcarbamylase: the relation between structure and function. *Science* **241**, 669-674.

Kantrowitz, E. R. & Lipscomb, W. N. (1990). *Escherichia coli* aspartate transcarbamoylase: the molecular basis for a concerted allosteric transition. *Trends Biochem Sci* **15**, 53-59.

Ke, H. M., Honzatko, R. B. & Lipscomb, W. N. (1984). Structure of unligated aspartate carbamoyltransferase of *Escherichia coli* at 2.6-Å resolution. *Proc Natl Acad Sci USA* **81**, 4037-4040.

Kobe, B. & Kemp, B. E. (1999). Active site-directed protein regulation. *Nature* **402**, 373-376.

Koshland, D. E., Jr., Némethy, G. & Filmer, D. (1966). Comparison of experimental binding data and theoretical models in proteins containing subunits. *Biochemistry* **5**, 365-385.

Kradolfer, P., Zeyer, J., Miozzari, G. & Hütter, R. (1977). Dominant regulatory mutants in chorismate mutase of *Saccharomyces cerevisiae*. *FEMS Microbiol Lett* **2**, 211-216.

Krappmann, S., Helmstaedt, K., Gerstberger, T., Eckert, S., Hoffmann, B., Hoppert, M., Schnappauf, G. & Braus, G. H. (1999). The *aroC* gene of *Aspergillus nidulans* codes for a monofunctional, allosterically regulated chorismate mutase. *J Biol Chem* **274**, 22275-22282.

Krappmann, S., Lipscomb, W. N. & Braus, G. H. (2000). Coevolution of transcriptional and allosteric regulation at the chorismate metabolic branch point of *Saccharomyces cerevisiae*. *Proc Natl Acad Sci USA* **97**, 13585-13590.

Krappmann, S., Pries, R., Gellissen, G., Hiller, M. & Braus, G. H. (2000). *HARO7* encodes chorismate mutase of the methylotrophic yeast *Hansenula polymorpha* and is derepressed upon methanol utilization. *J Bacteriol* **182**, 4188-4197.

Krause, K. L., Volz, K. W. & Lipscomb, W. N. (1987). 2.5 Å structure of aspartate carbamoyltransferase complexed with the bisubstrate analog N-(phosphonacetyl)-L-aspartate. *J Mol Biol* **193**, 527-553.

Ladjimi, M. M., Ghellis, C., Feller, A., Cunin, R., Glamsdorff, N., Piérard, A. & Hervé, G. (1985). Structure-function relationship in allosteric aspartate carbamoyltransferase from *Escherichia coli*: II. Involvement of the C-terminal region of the regulatory chain in homotropic and heterotropic interactions. *J Mol Biol* **186**, 715-724.

Ladjimi, M. M. & Kantrowitz, E. R. (1988). A possible model for the concerted allosteric transition in *Escherichia coli* aspartate transcarbamylase as deduced from site-directed mutagenesis studies. *Biochemistry* **27**, 276-283.

Ladner, J. E., Reddy, P., Davis, A., Tordova, M., Howard, A. J. & Gilliland, G. L. (2000). The 1.30 A resolution structure of the *Bacillus subtilis* chorismate mutase catalytic homotrimer. *Acta Cryst* **D56**, 673-683.

Landfear, S. M., Evans, D. R. & Lipscomb, W. N. (1978). Elimination of cooperativity in aspartate transcarbamylase by nitration of a single tyrosine residue. *Proc Natl Acad Sci USA* **75**, 2654-2658.

Lee, A. Y., Karplus, B., Ganem, B. & Clardy, J. (1995). Atomic structure of the buried catalytic pocket of *Escherichia coli* chorismate mutase. *J Am Chem Soc* **117**, 3627-3628.

Lee, B. H., Ley, B. W., Kantrowitz, E. R., O'Leary, M. H. & Wedler, F. C. (1995). Domain closure in the catalytic chains of *Escherichia coli* aspartate transcarbamoylase influences the kinetic mechanism. *J Biol Chem* **270**, 15620-15627.

Lin, S. L., Xu, D., Li, A. & Nussinov, R. (1998). Electrostatics, allostery, and activity of the yeast chorismate mutase. *Proteins* **31**, 445-452.

Lin, S. L., Xu, D., Li, A., Rosen, M., Wolfson, H. J. & Nussinov, R. (1997). Investigation of the enzymatic mechanism of the yeast chorismate mutase by docking a transition state analog. *J Mol Biol* **271**, 838-845.

Lipscomb, W. N. (1992). Activity and regulation in aspartate transcarbamoylase. In *In Regulations of Proteins by Ligands*, pp. 103-143. Houston, Texas: The Robert A. Welch Foundation Conference on Chemical Research XXXVI.

Lipscomb, W. N. (1994). Aspartate transcarbamylase from *Escherichia coli*: activity and regulation. *Adv Enzymol Relat Areas Mol Biol* **68**, 67-151.

Liu, L., Wales, M. E. & Wild, J. R. (2000). Allosteric signal transmission involves synergy between discrete structural units of the regulatory subunit of aspartate transcarbamoylase. *Arch Biochem Biophys* **373**, 352-360.

Lowry, T. H. & Richardson, K. S. (1987). *Mechanism and theory in organic chemistry. chp. 10*, 3rd edn. New York, USA: Harper & Row.

MacBeath, G., Kast, P. & Hilvert, D. (1998). A small, thermostable, and monofunctional chorismate mutase from the archaeon *Methanococcus jannaschii*. *Biochemistry* **37**, 10062-10073.

Macol, C., Dutta, M., Stec, B., Tsuruta, H. & Kantrowitz, E. R. (1999). The 80s loop of the catalytic chain of *Escherichia coli* aspartate transcarbamoylase is critical for catalysis and homotropic cooperativity. *Protein Sci* **8**, 1305-1313.

Macol, C. P., Tsuruta, H., Stec, B. & Kantrowitz, E. R. (2001). Direct structural evidence for a concerted allosteric transition in *Escherichia coli* aspartate transcarbamoylase. *Nat Struct Biol* **8**, 423-426.

Mobley, E. M., Kunkel, B. N. & Keith, B. (1999). Identification, characterization and comparative analysis of a novel chorismate mutase gene in *Arabidopsis thaliana*. *Gene* **240**, 115-123.

Monod, J., Changeux, J.-P. & Jacob, F. (1963). Allosteric proteins and molecular control systems. *J Mol Biol* **6**, 306-329.

Monod, J., Wyman, J. & Changeux, J.-P. (1965). On the nature of allosteric transition: a plausible model. *J Mol Biol* **12**, 88-118.

Newton, C. J. & Kantrowitz, E. R. (1990). The regulatory subunit of *Escherichia coli* aspartate carbamoyltransferase may influence homotropic cooperativity and heterotropic interactions by a direct interaction with the loop containing residues 230-245 of the catalytic chain. *Proc Natl Acad Sci USA* **87**, 2309-2313.

Oliver, K. & Harris, D. (1995). *Schizosaccharomyces pombe* chromosome I cosmid c16E8. : Direct Submission to GenBank, Acc. No. Z98529.

Perutz, M. F. (1989). Mechanisms of cooperativity and allosteric regulation in proteins. *Q Rev Biophys* **22**, 139-237.

Peterson, C. B., Burman, D. L. & Schachman, H. K. (1992). Effects of replacement of active site residue glutamine 231 on activity and allosteric properties of aspartate transcarbamoylase. *Biochemistry* **31**, 8508-8515.

Ricard, J. & Cornish-Bowden, A. (1987). Co-operative and allosteric enzymes: 20 years on. *Eur J Biochem* **166**, 255-272.

Romero, R. M., Roberts, M. F. & Phillipson, J. D. (1995). Chorismate mutase in microorganisms and plants. *Phytochemistry* **40**, 1015-1025.

Sakash, J. B. & Kantrowitz, E. R. (1998). The N-terminus of the regulatory chain of *Escherichia coli* aspartate transcarbamoylase is important for both nucleotide binding and heterotropic effects. *Biochemistry* **37**, 281-288.

Sakash, J. B., Tsen, A. & Kantrowitz, E. R. (2000). The use of nucleotide analogs to evaluate the mechanism of the heterotropic response of *Escherichia coli* aspartate transcarbamoylase. *Protein Sci* **9**, 53-63.

Schachman, H. K. (1988). Can a simple model account for the allosteric transition of aspartate transcarbamoylase? *J Biol Chem* **263**, 18583-18586.

Schirmer, T. & Evans, P. R. (1990). Structural basis of the allosteric behaviour of phosphofructokinase. *Nature* **343**, 140-145.

Schmidheini, T., Mösch, H. U., Evans, J. N. & Braus, G. (1990). Yeast allosteric chorismate mutase is locked in the activated state by a single amino acid substitution. *Biochemistry* **29**, 3660-3668.

Schmidheini, T., Sperisen, P., Paravicini, G., Hütter, R. & Braus, G. (1989). A single point mutation results in a constitutively activated and feedback-resistant chorismate mutase of *Saccharomyces cerevisiae*. *J Bacteriol* **171**, 1245-1253.

Schnappauf, G., Krappmann, S. & Braus, G. H. (1998). Tyrosine and tryptophan act through the same binding site at the dimer interface of yeast chorismate mutase. *J Biol Chem* **273**, 17012-17017.

Schnappauf, G., Lipscomb, W. N. & Braus, G. H. (1998). Separation of inhibition and activation of the allosteric yeast chorismate mutase. *Proc Natl Acad Sci USA* **95**, 2868-2873.

Schnappauf, G., Sträter, N., Lipscomb, W. N. & Braus, G. H. (1997). A glutamate residue in the catalytic center of the yeast chorismate mutase restricts enzyme activity to acidic conditions. *Proc Natl Acad Sci USA* **94**, 8491-8496.

Segel, I. H. (1993). Multisite and allosteric enzymes. D. The symmetry model of allosteric enzymes. In *In Enyzme kinetics*, pp. 428-431. New York, USA: John Wiley & Sons Inc.

Serre, V., Guy, H., Penverne, B., Lux, M., Rotgeri, A., Evans, D. & Hervé, G. (1999). Half of *Saccharomyces cerevisiae* carbamoyl phosphate synthetase produces and channels carbamoyl phosphate to the fused aspartate transcarbamoylase domain. *J Biol Chem* **274**, 23794-23801.

Stadtman, E. R. & Ginsburg, A. (1974). The glutamine synthetase of *Escherichia coli*: structure and control. In *The Enzymes*, pp. 755-808. Edited by P. D. Boyer. New York, USA: Academic Press.

Stebbins, J. W., Robertson, D. E., Roberts, M. F., Stevens, R. C., Lipscomb, W. N. & Kantrowitz, E. R. (1992). Arginine 54 in the active site of *Escherichia coli* aspartate transcarbamoylase is critical for catalysis: a site-specific mutagenesis, NMR, and X-ray crystallographic study. *Protein Sci* **1**, 1435-1446.

Stebbins, J. W., Zhang, Y. & Kantrowitz, E. R. (1990). Importance of residues Arg 167 and Gln 231 in both the allosteric and catalytic mechanisms of *Escherichia coli* aspartate transcarbamylase. *Biochemistry* **29**, 3821-3827.

Stevens, R. C., Chook, Y. M., Cho, C. Y., Lipscomb, W. N. & Kantrowitz, E. R. (1991). *Escherichia coli* aspartate carbamoyltransferase: the probing of crystal structure analysis via site-specific mutagenesis. *Protein Eng* **4**, 391-408.

Stevens, R. C., Gouaux, J. E. & Lipscomb, W. N. (1990). Structural consequences of effector binding to the T state of aspartate carbamoyltransferase: crystal structures of the unligated and ATP- and CTP-complexed enzymes at 2.6-Å resolution. *Biochemistry* **29**, 7691-7701.

Stevens, R. C. & Lipscomb, W. N. (1990). Allosteric control of quaternary states in *E. coli* aspartate transcarbamylase. *Biochem Biophys Res Commun* **171**, 1312-1318.

Stevens, R. C. & Lipscomb, W. N. (1992). A molecular mechanism for pyrimidine and purine nucleotide control of aspartate transcarbamoylase. *Proc Natl Acad Sci USA* **89**, 5281-5285.

Stevens, R. C., Reinisch, K. M. & Lipscomb, W. N. (1991). Molecular structure of *Bacillus subtilis* aspartate transcarbamoylase at 3.0 Å resolution. *Proc Natl Acad Sci USA* **88**, 6087-6091.

Sträter, N., Håkansson, K., Schnappauf, G., Braus, G. & Lipscomb, W. N. (1996). Crystal structure of the T state of allosteric yeast chorismate mutase and comparison with the R state. *Proc Natl Acad Sci USA* **93**, 3330-3334.

Sträter, N., Schnappauf, G., Braus, G. & Lipscomb, W. N. (1997). Mechanisms of catalysis and allosteric regulation of yeast chorismate mutase from crystal structures. *Structure* **5**, 1437-1452.

Stryer, L. (1988). Control of enzymatic activity. In *In Biochemistry*, pp. 233-259. New York: W. H. Freeman and Company.

Tauc, P., Keiser, R. T., Kantrowitz, E. R. & Vachette, P. (1994). Glu-50 in the catalytic chain of *Escherichia coli* aspartate transcarbamoylase plays a crucial role in the stability of the R quaternary structure. *Protein Sci* **3**, 1998-2004.

Tauc, P., Leconte, C., Kerbiriou, D., Thiry, L. & Hervé, G. (1982). Coupling of homotropic and heterotropic interactions in *Escherichia coli* aspartate transcarbamylase. *J Mol Biol* **155**, 155-168.

Thiry, L. & Herve, G. (1978). The stimulation of *Escherichia coli* aspartate transcarbamylase activity by adenosine triphosphate. Relation with the other regulatory conformational changes; a model. *J Mol Biol* **125**, 515-534.

Van Vliet, F., Xi, X. G., De Staercke, C., de Wannemaeker, B., Jacobs, A., Cherfils, J., Ladjimi, M. M., Hervé, G. & Cunin, R. (1991). Heterotropic interactions in aspartate transcarbamoylase: turning allosteric ATP activation into inhibition as a consequence of a single tyrosine to phenylalanine mutation. *Proc Natl Acad Sci USA* **88**, 9180-9183.

Weber, K. (1968). New structural model of *E. coli* aspartate transcarbamylase and the amino-acid sequence of the regulatory polypeptide chain. *Nature* **218**, 1116-1119.

Weiss, U. & Edwards, J. M. (1980). *The biosynthesis of aromatic amino acids*. New York, USA: John Wiley & Sons Inc.

Wild, J. R., Johnson, J. L. & Loughrey, S. J. (1988). ATP-liganded form of aspartate transcarbamoylase, the logical regulatory target for allosteric control in divergent bacterial systems. *J Bacteriol* **170**, 446-448.

Wild, J. R., Loughrey-Chen, S. J. & Corder, T. S. (1989). In the presence of CTP, UTP becomes an allosteric inhibitor of aspartate transcarbamoylase. *Proc Natl Acad Sci USA* **86**, 46-50.

Wiley, D. C. & Lipscomb, W. N. (1968). Crystallographic determination of symmetry of aspartate transcarbamylase. *Nature* **218**, 1119-1121.

Williams, M. K., Stec, B. & Kantrowitz, E. R. (1998). A single mutation in the regulatory chain of *Escherichia coli* aspartate transcarbamoylase results in an extreme T-state structure. *J Mol Biol* **281**, 121-134.

Williamson, C. L. & Slocum, R. D. (1994). Molecular cloning and characterization of the *pyrB1* and *pyrB2* genes encoding aspartate transcarbamoylase in pea (*Pisum sativum* L.). *Plant Physiol* **105**, 377-384.

Xi, X. G., De Staercke, C., Van Vliet, F., Triniolles, F., Jacobs, A., Stas, P. P., Ladjimi, M. M., Simon, V., Cunin, R. & Hervé, G. (1994). The activation of *Escherichia coli* aspartate transcarbamylase by ATP. Specific involvement of helix H2' at the hydrophobic interface between the two domains of the regulatory chains. *J Mol Biol* **242**, 139-149.

Xi, X. G., van Vliet, F., Ladjimi, M. M., de Wannemaeker, B., de Staercke, C., Glansdorff, N., Pierard, A., Cunin, R. & Hervé, G. (1991). Heterotropic interactions in *Escherichia coli* aspartate transcarbamylase. Subunit interfaces involved in CTP inhibition and ATP activation. *J Mol Biol* **220**, 789-799.

Xia, T., Song, J., Zhao, G., Aldrich, H. & Jensen, R. A. (1993). The aroQ-encoded monofunctional chorismate mutase (CM-F) protein is a periplasmic enzyme in *Erwinia herbicola*. *J Bacteriol* **175**, 4729-4737.

Xue, Y. & Lipscomb, W. N. (1995). Location of the active site of allosteric chorismate mutase from *Saccharomyces cerevisiae*, and comments on the catalytic and regulatory mechanisms. *Proc Natl Acad Sci USA* **92**, 10595-10598.

Xue, Y., Lipscomb, W. N., Graf, R., Schnappauf, G. & Braus, G. (1994). The crystal structure of allosteric chorismate mutase at 2.2-Å resolution. *Proc Natl Acad Sci USA* **91**, 10814-10818.

Zhang, Y. & Kantrowitz, E. R. (1989). Lysine-60 in the regulatory chain of *Escherichia coli* aspartate transcarbamoylase is important for the discrimination between CTP and ATP. *Biochemistry* **28**, 7313-7318.

Zhang, Y. & Kantrowitz, E. R. (1991). The synergistic inhibition of *Escherichia coli* aspartate carbamoyltransferase by UTP in the presence of CTP is due to the binding of UTP to the low affinity CTP sites. *J Biol Chem* **266**, 22154-22158.

Chapter 1

A refined molecular hinge between allosteric and catalytic domain determines allosteric regulation and stability of fungal chorismate mutase

Abstract

The yeast chorismate mutase is regulated by tyrosine as feedback inhibitor and tryptophan as crosspathway activator. The monomer consists of a catalytic and a regulatory domain covalently linked by the loop L220s (212-226), which functions as a molecular hinge. Two monomers form the active dimeric enzyme stabilized by hydrophobic interactions in the vicinity of loop L220s. The role of loop L220s and its environment for enzyme regulation, dimerization, and stability was analyzed. Substitution of yeast loop L220s in place of the homologous loop from the corresponding and similarly regulated *Aspergillus* enzyme (and the reverse substitution) changed tyrosine inhibition to activation. Yeast loop L220s substituted into the *Aspergillus* enzyme resulted in a tryptophan inhibitable enzyme. Monomeric yeast chorismate mutases could be generated by substituting two hydrophobic residues in and near the hinge region. The resulting Thr212Asp-Phe28Asp enzyme was as stable as wild-type, but lost allosteric regulation and showed reduced catalytic activity. These results underline the crucial role of this molecular hinge for inhibition, activation, quaternary structure, and stability of yeast chorismate mutase.

Introduction

Chorismate mutases (CMs) catalyze the Claisen rearrangement from chorismate to prephenate in the biosynthesis of tyrosine and phenylalanine (Helmstaedt *et al*., 2001). The eukaryotic CMs from *Saccharomyces cerevisiae*, *Aspergillus nidulans*, and *Hansenula polymorpha* exhibit a very similar pattern of regulation of enzyme activity (MacBeath *et al*., 1998). They are feedback inhibited by tyrosine, one of the end products of the biosynthetic branch, and activated by tryptophan, the end product of the parallel branch (Krappmann *et al*., 2000).

X-ray structure analysis revealed that the yeast homodimeric CM contains no β-sheet structures, but 71% of the protein is formed by α-helices (Xue *et al*., 1994)). Two allosteric and two active sites occur per CM dimer. The allosteric ligands bind to a cleft in the dimer interface formed by H4 and H5 from one monomer and H8 and loop L130s from the other monomer. A twisted four-helix bundle structure is formed by helices H2, H8, H11, and H12 of each subunit at the end of which the active site is located.

Helices H2, H4, and H11 and loops L50s and L80s contribute to hydrophobic clusters that account for dimerization (Xue *et al.*, 1994). In one cluster residues Phe28, Ile31, Val211, and Tyr212 from helices H2 and H11, respectively, from both subunits are packed against each other. Residue Leu67 from helix H4 also forms a hydrophobic patch with its counterpart from the other monomer. In addition, residues from loop L50s and helix H4 from one subunit interact with loop L80s from the other subunit, leading to formation of another two hydrophobic cores. These interactions were found to be so strong that dissociation of the dimers occurred only after addition of 4 M guanidine hydrochloride upon unfolding of the monomers (Schmidheini *et al*., 1990).

Strong similarities on the primary structural level indicate conserved characteristics of the yeast enzyme with CMs from other fungi as *A. nidulans* (AnCM) and *H. polymorpha* (HpCM). Except for Asn194 of the yeast's active site, which is equivalent to Asp200 in AnCM, and Thr145 of the yeast's allosteric site, which can be aligned to Met143 in HpCM, respectively, all residues important for activity or binding of allosteric effectors are conserved among these three enzymes.

Loop L220s serves as a hinge that connects the allosteric domain with the catalytic domain within one polypeptide in the dimer interface. A constitutively activated yeast CM is known in which the last residue of this particular loop (Thr226) is substituted by an isoleucine residue. This residue locks the enzyme structure in the allosteric R state, which completely prevents inhibition or further activation (Schmidheini *et al*., 1989). The end of this loop, however, is not as strongly conserved among these homologous CMs. Sequence alignments show that the Thr residue is replaced by an aspartic acid residue in AnCM and a lysine residue in HpCM, which suggests somewhat different signaling pathways at least in this part of the homologous CMs from *A. nidulans* and *H. polymorpha*, respectively. Here, we report the construction and kinetic characterization of chimeric enzymes in which the whole loops homologous to L220s were exchanged to gain more insight in structure and function of this molecular hinge of CM. In addition, we present the generation of a stable yeast CM monomer by substituting amino acid residues in and around L220s in order to elucidate the process of dimerization and the characteristics of a single CM polypeptide.

Materials & Methods

Materials

Ethylaminosepharose was prepared following the protocol for activation of Sepharose CL-4B (Dimroth, 1986) and by coupling of the ligand, ethylamino-HCl, to the activated matrix. Protein solutions were concentrated by using stirred cells (volumes 180 ml and 10 ml) with PM-10 ultrafiltration membranes from Millipore (Eschborn, Germany). The Mini 2D SDS-polyacrylamide gel electrophoresis system and the Bradford protein assay solution for determination of protein concentrations originated from Bio-Rad (Munich, Germany). Pfu polymerase (Promega Corporation, Mannheim, Germany) was used for polymerase chain reactions. Chorismic acid as barium salt and all other chemicals were supplied by FLUKA (Neu-Ulm, Germany) or Sigma-Aldrich Chemie GmbH (Steinheim, Germany).

Yeast strains, plasmids, media and growth conditions

For overexpression of chimeric CMs, a derivative of plasmid p426MET25 (Mumberg *et al*., 1994) was used in the *S. cerevisiae* strain RH2192 (*MATα , pra1-1, prb1-1, prc1-1, cps1-3, ura3Δ5, leu2-3, 112, his*$^-$*, aro7::LEU2*), which is a derivative of the protease-deficient strain c13-ABYS-86 (Heinemeyer *et al*., 1991). For overexpression of wild-type (wt), constitutively activated, and monomeric CMs, derivatives of plasmid pME781 (Schnappauf *et al*., 1998) were used in strain RH1242 (*MATa, aro7, leu2-2*). Strain RH1671 (*MATa, ura3-251, ura3-328, ura3-375, Δaro7::URA3*) was used for integration of linear wt and monomeric *ARO7* fragments. Yeast transformation was carried out by the LiAc method (Ito *et al.*, 1983). MV minimal medium for the cultivation of yeasts was described earlier (Miozzari *et al.*, 1978). Growth rates of strains RH1671, RH2698 (*MATa, ura3-251, ura3-328, ura3-375*), and RH2699 (*MATa, ura3-251, ura3-328, ura3-375 aro7*^{m}) were determined turbidimetrically at 595 nm, and the specific growth rate is given as µ defined by $(\ln x_2-\ln x_1)/(t_2-t_1)$, where x stands for the optical density at the corresponding time t.

Sire-directed mutagenesis

A polymerase chain reaction-based method was used for site-directed mutagenesis of *ARO7* (Giebel & Spritz, 1990). The 5'- or 3'-terminal portions of the *ARO7* gene in plasmid pME1459 were replaced by a PCR-generated *Nde*I/*Xba*I or *Xba*I/*Bam*HI fragment, respectively, which encoded for one substitution each. The fragments were sequenced (Sanger *et al.*, 1977) to confirm the presence of the mutations and to rule out second-site mutations. Both mutated fragments were then combined in one plasmid to generate a double-mutant *ARO7* gene. Chimeric CM genes were constructed by overlap extension using the polymerase chain reaction (Ho *et al.*, 1989).

Purification of CMs

Yeast cells were grown at 30°C in 10-liter rotatory fermenters under aeration. Cells were harvested in mid-log phase at an OD_{546} of 4-6, washed twice with 50 mM potassium phosphate buffer, pH 7.6, and stored in 1ml of buffer/g wet cells at –20°C in the presence of protease inhibitors (0.1 mM phenylmethylsulfonyl fluoride, 0.2 mM EDTA, and 1 mM DL-dithiothreitol). For purification, 80-100 g of cells were thawed and disrupted in the one shot model of the cell disruption equipment from Constant Systems LTD. (Warwick, UK). Cell debris was sedimented by centrifugation at 17,000xg for 20 min. The enyzmes were purified as desribed previously (Schnappauf *et al.*, 1998) with the following modifications. The wt chorismate mutase was purified on an ethylamino-Sepharose column, two MonoQ columns (HR16/10 and HR5/5) using 10 mM tris-HCl, pH 7.6, followed by runs on the monoQ columns at pH 6.6. The monomeric and constitutively activated enzyme variant, respectively, were isolated in the same way with an additional gelfiltration on a Superdex 200 prepgrade column. The CM from *A. nidulans* was purified as described earlier (Krappmann *et al.*, 1999). The chimeric enzymes were purified as described for the wt enzymes with the following modifications. The ScLAn chimeric enzyme was purified on an ethylamino-

Sepharose column, a MonoQ column (HR16/10) using 10 mM Tris-HCl, pH 7.6, a smaller MonoQ column (HR5/5), and a Superdex 200 pg column followed by a last run on a MonoQ column (HR16/10) at pH 6.6. The AnLSc and AnLSc^c enyzmes were isolated using an ethylamino-Sepharose column, a MonoQ column (HR16/10) with 10 mM potassium phosphate buffer, pH 7.6, followed by a run at pH 5.8, and a last run on a Superdex 200 pg column. The eluate from the MonoQ column (HR5/5) and the gelfiltration column was collected in 1 ml fractions. Chorismate mutase was detected by SDS-polyacrylamide gel electrophoresis (Laemmli, 1970) and enzymatic activity assays. Protein concentration were determined using the Bradford assay (Bradford, 1976).

Enyzme assays and data evaluation

During purifications and for first analysis of the mutant enzyme variants, the following stop assay was performed. Reactions were carried out in a volume of 500 µl in 100 mM Tris-HCl, pH 7.6, 2 mM EDTA, 20 mM DTT and contained 10 µl of fractions and 1 µg of purified enzyme, respectively. Effector concentrations of 500 µM tryptophan and 100 µM tyrosine were used and the substrate chorismic acid was present in a concentration of 2 mM. For assays during purifications, only tryptophan was added and the substrate was present in a concentraion of 1 mM. The enzymatic reaction was started by additon of chorismic acid and stopped after 10 min and 3 min, respectively, by addition of 500 µl of 1 M HCl. After another 10 min, 4 ml of 1 M NaOH neutralized and diluted the solution. Blank absorbances were substracted from absorbances measured for enzyme activities. For substrate saturation curves, chorismate mutase activity was measured as described previously (Krappmann *et al.*, 1999). Effector concentrations were 100 µM tyrosine and 10 µM tryptophan for enzymes derived from ScCM and 50 µM tyrosine and 5 µM tryptophan for enzymes generated from AnCM, respectively. k_{cat} values were calculated using the respective molecular weight of the enzymes as calculated by the LASERGENE Biocomputing software from DNAStar (Madison, WC). pH optima were determined using a universal buffer solution with a pH range of 2.5-12 containing 30 mM citric acid, 30 mM KH_2PO_4, 30 mM H_3BO_4, 30 mM diethylbarbituric acid and different concentrations of NaOH. The tests were performed with 4 µg of purified enzyme and 2 mM chorismate concentration.

For the determination of rate constants for thermal inactivation 1 µg of purified enzyme was preincubated in the absence of effectors for different periods of time at increasing temperatures. The samples were chilled on ice, and residual activities were determined in stop assays with 2 mM chorismic acid and 2 min of catalytic turnover.

Determination of the native molecular weight

The native molecular weight of the double-mutant chorismate mutase was determined by gelfiltration on a Superdex 200-pg column using 50 mM potassium phosphate, 150 mM NaCl, pH 7.6, as elution buffer. The void volume of the column was determined with blue dextran, and a calibration plot was defined using a gel filtration chromatography standard from Bio-Rad containing thyroglobulin, bovine γ-globuline, chicken ovalbumin, equine myoglobin, and vitamin B-12. In addition, the molecular weight was estimated by native polyacrylamide gel electrophoresis using a gradient from 10-20% polyacrylamide (Andersson *et al*., 1972) and chicken egg albumin, α-lactalbumin, carbonic anhydrase, bovine serum albumin, and urease as standard.

Circular dichroism spectroscopy

The CD spectra of the wt and mutant CMs were measured in the range of 200-250 nm with a Jobin Yvon CD6 spectrometer at 0.5-nm resolution. The pathlength of the cell was 0.1 cm. The spectra were recorded as an average of three scans at 20°C with 1.33 µM of monomeric CM in 10 mM Tris-HCl, pH 7.6. Buffer baseline spectra were substracted from the protein spectra.

Sequence alignment and homology modeling studies

All sequence analyses were performed using the LASERGENE Biocomputing software. Alignments were created based on the CLUSTAL W method (Thompson *et al*., 1994) using the Network Protein Sequence analysis service (Combet *et al*., 2000). For homology modeling, the deduced primary structure of the *A. nidulans* and *H. polymorpha* CMs were aligned to the crystallographic data of yeast CMs as described in the Brookhaven protein database (Sträter *et al*., 1997) and refined by the SWISS-MODEL service (Guex & Peitsch, 1997; Peitsch, 1995). By using the WebLab Viewer software (Molecular Simulations Inc., San Diego, CA), three-dimensional structure models could be generated by calculation of secondary structures.

Results

Fungal CMs with an altered hinge connecting the catalytic and the regulatory domain

The crystal structure of yeast CM determined in complex with different ligands is an all-helical dimer composed of 256 amino acids forming 12 helices per monomer ((Sträter *et al.*, 1997), Fig. 8A). The high similarities between the deduced primary structures of CMs from *S. cerevisiae*, *A. nidulans*, and *H. polymorpha* suggest homology of the corresponding genes. Alignments of the protein sequences show more than 50% identity between all three enzymes with long conserved stretches especially in helices 2, 8, 11, and 12. Information on the three-dimensional structures of AnCM and HpCM was gained by homology modeling based on crystal structures of the yeast enzyme using SWISS-MODEL (Guex & Peitsch, 1997; Peitsch, 1995; Peitsch, 1996) (Fig. 8A). The residues that in the primary structures are homologous to residues of loop L220s of ScCM also formed corresponding loops in these structures. Therefore, the corresponding regions of the encoding genes were exchanged (Fig. 8B, C). The flexible L220s loop from the wt and the Thr226Ile loop of the mutant enzyme frozen in the activated state were introduced into the *Aspergillus* enzyme leading to chimeras AnLSc and AnLSc^c, and the corresponding loops from HpCM and AnCM were incorporated into the yeast enzyme (ScLHp and ScLAn). The ScLHp chimeric enzyme was highly unstable during purification, which suggests that this hinge region might be critical for stability and has to be well aligned to the rest of the molecule. This instability was surprising because the loop is positioned on the surface of the protein and the *Hansenula* loop has a similar size (18 aa) in comparison to the *S. cerevisiae* loop (15 aa). Thus, further analysis was only performed for the ScCM-AnCM chimeric enzymes which were stable and active.

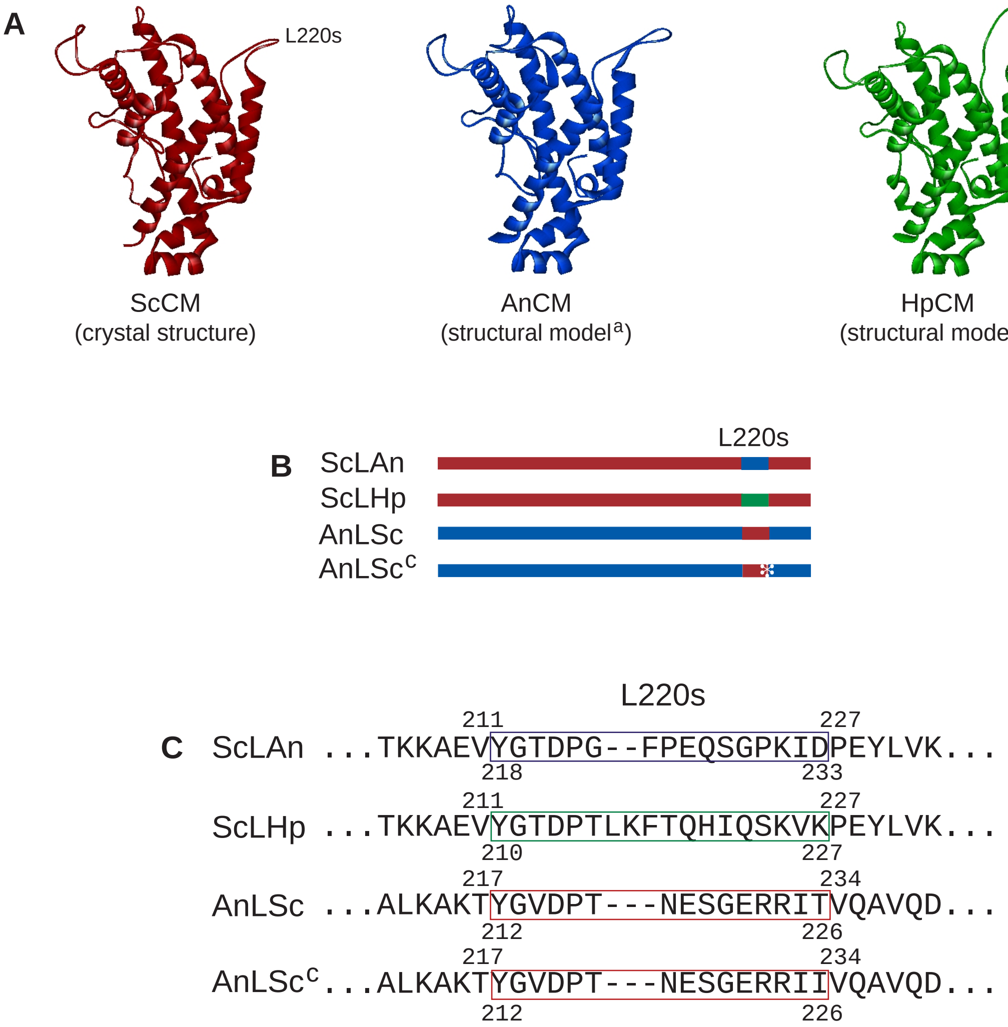
A
L220s
ScCM
(crystal structure)
AnCM
(structural model a)
HpCM
(structural model a)
B
L220s
ScLAn
ScLHp
AnLSc
AnLSc c
C
L220s
211 227
ScLAn ...TKKAEVYGTDPG--FPEQSGPKIDPEYLVK...
218 233
211 227
ScLHp ...TKKAEVYGTDPTLKFTQHIQSKVKPEYLVK...
210 227
217 234
AnLSc ...ALKAKTYGVDPT---NESGERRITVQAVQD...
212 226
217 234
AnLSc c...ALKAKTYGVDPT---NESGERRIIVQAVQD...
212 226

Fig. 8: Structural models of wild-type and chimeric CM monomers. **A**, The detailed structure of yeast chorismate mutase (ScCM) was determined by X-ray crystallography; the model of the three-dimensional structures of the *Hansenula* (HpCM) and *Aspergillus* (AnCM) enzymes were created using the SWISS-MODEL service([a]). **B**, Schematic drawings of the chimeras. Parts of the yeast enzyme are shown in red, of the *Hansenula* enzyme in green and fragments derived from the *Aspergillus* enzyme are shown in blue. The asterisk marks the Thr226Ile mutation in the loop from the constitutively activated yeast enzyme. **C**, Sequences of the loop L220s regions of the chimeras. The amino acid sequences are presented as they were aligned with the newly introduced loop sequences shown in place of the wt sequences. The loop from the yeast enzyme is marked with a red box, that from the *Hansenula* enzyme with a green box and from the *Aspergillus* enzyme with a blue one. The numbers indicate the amino acid position in the respective wt protein.

Tyrosine becomes a yeast enzyme activator instead of an inhibitor when the L220s hinge (212-226) is replaced by the loop from *Aspergillus* CM

Substrate saturation curves were measured to determine the catalytic parameters (Fig. 9; Tab. I). The sigmoid saturation curves of the wt yeast and *Aspergillus* CM were used as references. These curves are depressed under inhibition conditions and show Michaelis-Menten-like kinetics under activation conditions. Substrate affinity is reduced by tyrosine and increased by tryptophan. The Thr226Ile mutant yeast enzyme did not respond to the allosteric effectors. This variant showed all hyperbolic curves with Hill coefficients and K_m values smaller than 1 with overall high activity.

For the chimeric enzymes, substrate saturation curves were different. Introduction of the *Aspergillus* loop into the yeast enzyme led to an enzyme which had dramatically changed characteristics under activation conditions. ScLAn displayed a highly elevated K_m value of 16.5 mM for the activated enzyme in comparison to 0.6 mM of the yeast wt enzyme. Under this condition, the Hill coefficient was well below 1 indicating negative cooperativity of substrate binding, and the catalytic efficiency was reduced from 210 $s^{-1}mM^{-1}$ in ScCM to 13 $s^{-1}mM^{-1}$ in ScLAn. Tyrosine acted as activator instead of inhibitor under all chorismate concentrations in the substrate saturation assay. In the presence of this effector the catalytic efficiency was elevated because k_{cat} was increased while K_m was near the wt value.

Aspergillus CM with the yeast hinge between catalytic and regulatory region is inhibited by tryptophan

A different situation was found for the *Aspergillus*-derived chimeric enzymes (Fig. 9; Tab. I). For the tyrosine-bound and unliganded enzymes a decrease in K_m was accompanied by a loss of cooperativity; k_{cat} was increased compared to wt AnCM so that catalytic efficiency was strongly improved. For AnLSc, tyrosine proved to activate this enzyme at chorismate concentrations above 3.5 mM and only silghtly inhibited the enzyme below 3.5 mM chorismate. This effector still led to enzyme inhibition for AnLSc^c. In the presence of tryptophan, however, the opposite occurred. For both chimeras, tryptophan acted as inhibitor of enzyme activity. The curve of the tryptophan-liganded chimeras was always lower than the curves of the unliganded chimeras in the substrate saturation plot. In the presence of tryptophan, cooperativity was lost as in the wt, and K_m was slightly increased. k_{cat} was reduced to 49% for AnLSc and to 64% for AnLSc^c compared with the unliganded enzyme. The catalytic efficiency dropped to 23 and 31%, respectively, compared to the activated wt AnCM. Similar to the yeast enzyme, the loop L220s-Thr226Ile prevented a stronger regulation as it was found for the chimera with the wt L220s loop.

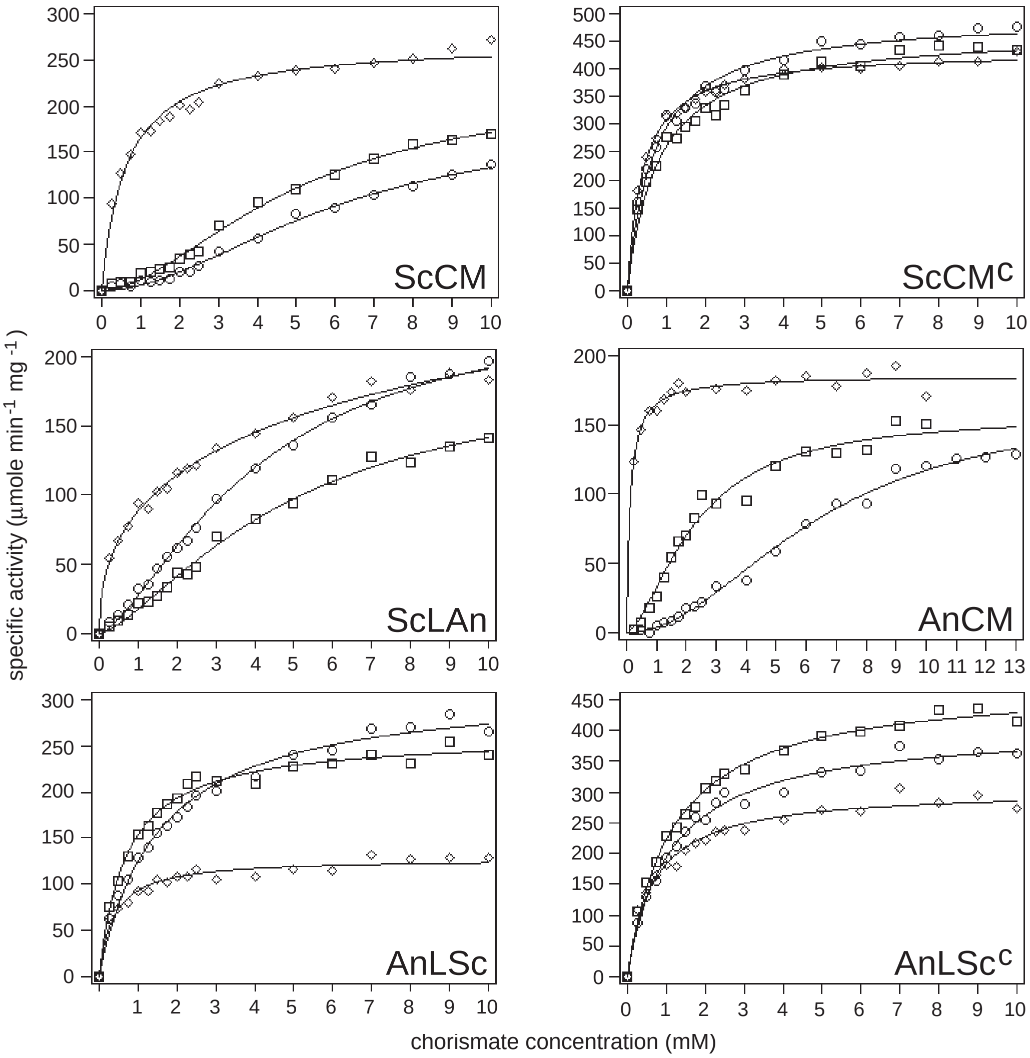

Fig. 9: Substrate-saturation plots of wild-type and chimeric CMs. The enzymes were assayed in the presence of 100 µM tyrosine for the yeast enzyme and 50 µM tyrosine for the *Aspergillus* enzyme, respectively (❍), or 10 µM tryptophan for the yeast enzyme and 5 µM tryptophan for the *Aspergillus* enzyme, respectively (✧), or were assayed unliganded (❑). The concentrations used for the chimeric enzymes depended on the origin of the protein's major part. Each point was measured at least five times and the collected data were fitted to functions describing either cooperative or Michaelis-Menten-type saturation.

Table I: Kinetic parameters of wild-type and chimeric chorismate mutases

	tyrosine-liganded[a]				unliganded				tryptophan-liganded[b]			
Protein	k_{cat} (s^{-1})	K_m, $S_{0.5}$ (mM)	n_H[c]	k_{cat}/K_m ($s^{-1}mM^{-1}$)	k_{cat} (s^{-1})	K_m, $S_{0.5}$ (mM)	n_H[c]	k_{cat}/K_m ($s^{-1}mM^{-1}$)	k_{cat} (s^{-1})	K_m, $S_{0.5}$ (mM)	n_H[c]	k_{cat}/K_m ($s^{-1}mM^{-1}$)
ScCM	91	6	2.0	15	110	5	1.9	22	134	0.6	0.8	210
ScCM[c]	246	0.7	0.8	357	232	0.8	0.8	289	214	0.4	0.9	530
ScLAn	139	5.2	1.3	27	96	4.9	1.4	19	217	16.5	0.5	13
AnCM	84	6.4	2.0	13	80	2.3	2.0	35	95	0.1	1.0	758
AnLSc[c]	161	1.5	1.0	105	133	0.7	1.0	190	65	0.4	1.0	176
AnLSc	207	1.1	1.1	189	244	1.2	1.0	213	155	0.7	0.8	233

[a] 100 µM tyrosine for the yeast-derived enzymes and 50 µM tyrosine for the *Aspergillus-derived* enzymes, respectively

[b] 10 µM tryptophan for the yeast-derived enzymes and 5 µM tryptophan for the *Aspergillus-derived* enzymes, respectively

[c] determined as the slope of the Hill plot in the region of $v=0.5V_{max}$

Two amino acid substitutions in the hydrophobic cluster including the L220s hinge are sufficient for monomerization of yeast CM

The instability of the ScLHp chimera proved the importance of an appropriate hinge region for enzyme stability. Furthermore, the C terminus of L220s is part of a dimerization domain in which hydrophobic amino acid residues establish contact between the two monomers, which prompted us to examine whether dimerization is essential for protein stability or whether an intact hinge mediates stable protein folding of a single polypeptide chain. Therefore, hydrophobic amino acid residues at positions 28 and 212 were substituted by neutral (alanine) and charged amino acid residues (aspartic acid), respectively (Fig. 10A). Single substitutions with either alanine or aspartic acid residues yielded enzymes which were impaired in inhibition and activation, but no clear results were obtained as far as their quaternary structures were concerned (data not shown). However, Tyr212Asp and Phe28Asp replacements in combination (*aro7*^{m}) were sufficient to prevent any hydrophobic interactions between chorismate mutase proteins. The purified double-mutant enzyme was electrophoresed in a native gradient polyacrylamide gel, which allowed the estimation of a molecular mass of approximately 30 kDa (data not shown). The determination of the native molecular weight by gelfiltration analysis on a calibrated Superdex 200-pg column yielded a K_d of 0.75 as calculated from the protein's elution volume (data not shown). For globular proteins this K_d value corresponds to a molecular mass of 25,449 Da. Compared to the molecular mass of one CM polypeptide of 29,746 Da, as calculated from the DNA sequence, this result confirms the monomeric state of the mutant enzyme variant.

Fig. 10 (opposite page): Structural characteristics and thermal stability of wild-type and monomeric CMs. **A**, Wt ScCM with Phe28 and Tyr212 of the dimerization region labeled yellow. **B**, CD spectra of monomeric mutant and dimeric wild-type CM. Each spectrum of the purified enzymes is an average of three independently obtained spectra, which were recorded in 10 mM Tris-HCl buffer, pH 7.6. **C**, Determination of thermal inactivation. Rate constants for thermal inactivation and half-lives of the two chorismate mutases were determined in stop assays at 30°C with 1 µg of purified enzyme, 2 mM chorismate concentration, and 2 min of catalytic turnover. One hundred percent of original activity equaled 3.2 units per mg for monomeric and 28.2 units per mg for wild-type chorismate mutase, respectively. Each value is an average of four independent measurements.

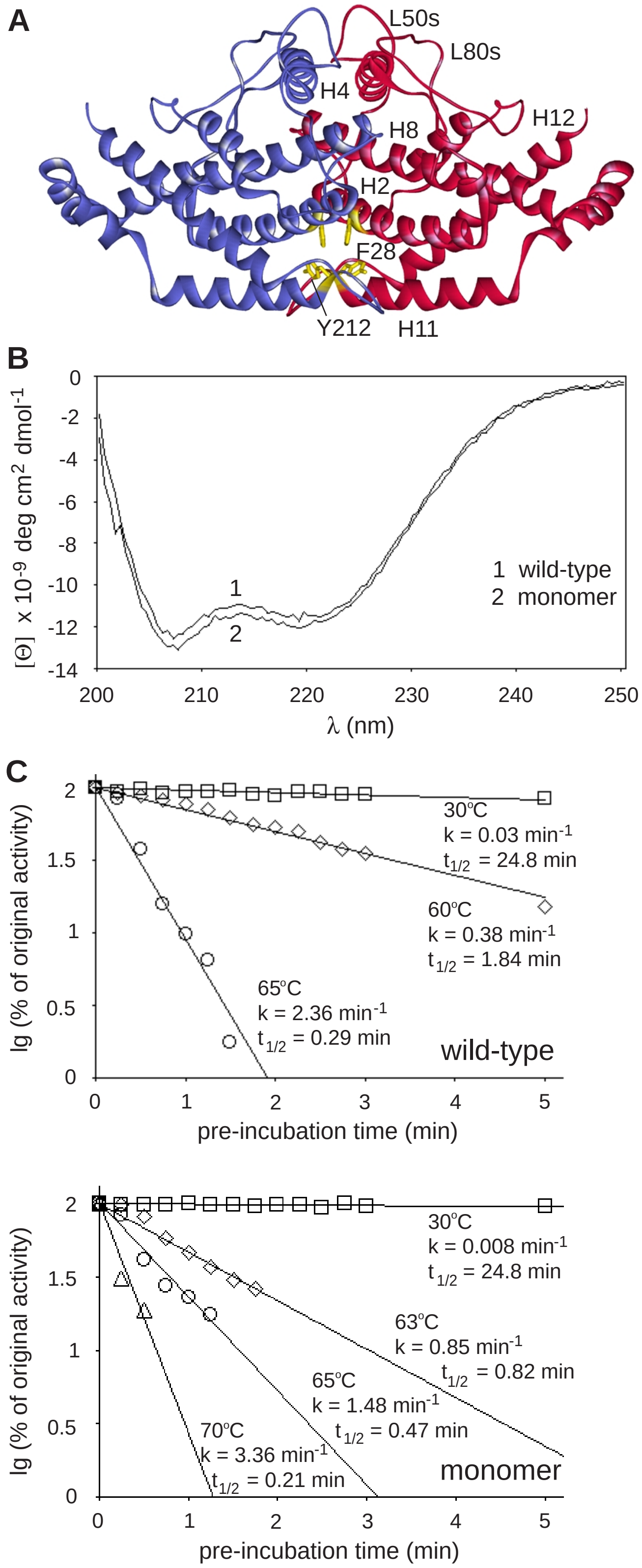
A
L50s
L80s
H4
H8
H12
H2
F28
Y212
H11
B
[Θ] x 10-9 deg cm2 dmol-1
0
-2
-4
-6
-8
-10
-12
-14
200
210
220
230
240
250
λ (nm)
1
2
1 wild-type
2 monomer
C
lg (% of original activity)
2
1.5
1
0.5
0
0
1
2
3
4
5
pre-incubation time (min)
30°C
k = 0.03 min-1
t1/2 = 24.8 min
60°C
k = 0.38 min-1
t1/2 = 1.84 min
65°C
k = 2.36 min-1
t1/2 = 0.29 min
wild-type
lg (% of original activity)
2
1.5
1
0.5
0
0
1
2
3
4
5
pre-incubation time (min)
30°C
k = 0.008 min-1
t1/2 = 24.8 min
63°C
k = 0.85 min-1
t1/2 = 0.82 min
65°C
k = 1.48 min-1
t1/2 = 0.47 min
70°C
k = 3.36 min-1
t1/2 = 0.21 min
monomer

Monomeric chorismate mutase enables growth of yeast cells in media lacking aromatic amino acids

The *aro7*^{m} gene encoding the monomeric CM was integrated at the *ARO7* locus of *S. cerevisiae* strain RH1671 by selection against a *URA3* marker (RH2699). The wt *ARO7* gene was reintegrated into the same strain to construct a control strain (RH2698). Growth rates were determined in minimal vitamins medium containing uracil or uracil plus the aromatic amino acids for comparison to the *Δaro7* strain RH1671. The growth rates of strain RH2699 (*aro7*^{m}) equaled 0.21 h^{-1} in both media. Reintegration of *ARO7* did not improve the growth rate (0.24 h^{-1} and 0.25 h^{-1}, respectively) while the *Δaro7* strain did not grow on MV+ura, but best on the medium containing aromatic amino acids (0.28 h^{-1}). Thus, compared to the strain containing the reintegrated *ARO7* gene, no growth defect under nonstarvation conditions was observed for strain RH2699 (*aro7*^{m}). A single-copy chromosomal *aro7*^{m} gene was sufficient to restore prototrophy for tyrosine and phenylalanine.

Circular dichroism curves were determined for both the monomeric and dimeric chorismate mutase (Fig. 10B). As expected, the spectrum of the wt enzyme showed a double minimum at 207 and 219 nm, which matches the minima of a typical all-helical protein. The spectrum recorded for the monomer also had two minima, and even the intensities of the minima were nearly identical. This result showed that a single CM polypeptide folds into an ordered tertiary conformation and is still all-helical. Furthermore, the monomer proved very stable in activity assays. The enzymes were preincubated at different temperatures for increasing periods of time and chilled on ice, and the residual activity was determined in stop assays at 30°C (Fig. 10C).

At temperatures above 60°C, activity decreased very rapidly. The rate constants of thermal inactivation at 65°C were 2.36 min^{-1} for the dimer and 1.48 min^{-1} for the monomer, respectively, with half lives of 0.29 min and 0.47 min respectively. These experiments show that the monomeric chorismate mutase is nearly as stable at 70°C as the wt enzyme at 65°C. Thus, monomerization did not influence the protein’s stability.

In a modulated stop assay the specific activity could be determined in dependence of the pH (Fig. 11A). The monomer has a clear optimum at pH 5.5 that is not altered by tyrosine or tryptophan. This value corresponds to that of the wt enzyme as determined (Schnappauf *et al.*, 1997), which shows that, although activity is strongly reduced, the obvious structural changes in the active site do not influence the pH dependence of the catalyzed reaction.

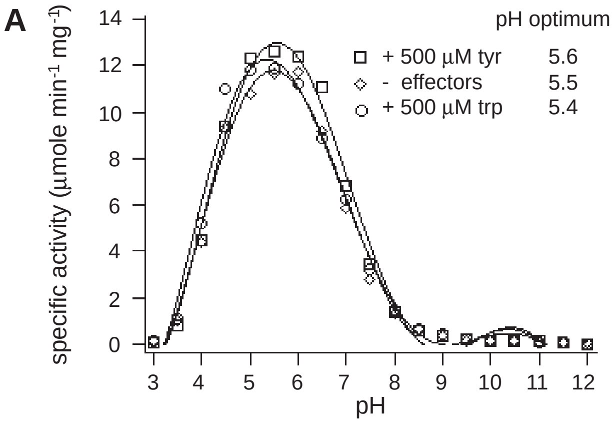

B

	specific activity (µmole min^{-1} mg^{-1})			range of modulation
	inhibited[a]	unliganded	activated[b]	
ScCM^{mon}	7.9	7.4	8.4	1.06
ScCM	12.3	26.4	96.4	7.87

[a] by 100 µM tyrosine [b] by 500 µM tryptophan

Fig. 11: Specific activity of monomeric chorismate mutase. **A**, pH optima for monomeric CM. Modified stop assays were performed with 4 µg of purified enzyme, 2 mM chorismate concentration, and 10 min of catalytic turnover. Each value is an average of four independent measurements. **B**, Specific activities under different effector conditions. Enzyme activities were determined in a stop assay with 1 µg of purified enzymes, 2 mM chorismate concentration, and 3 min of catalytic turnover. Each value is an average of four independent measurements.

Regulation of enzyme activity is lost for monomeric CM

The monomeric chorismate mutase has lost the oligomeric state of the protein and has therefore lost what is assumed to be the main prerequisite for allosteric regulation. Because the allosteric sites were formed by residues contributed from both polypeptides in the dimer interface, even the ability to bind the allosteric effectors is expected to be lost. A stop assay revealed that the range of modulation of enzyme activity under different effector conditions equaled a factor of nearly 1, whereas the wt enzyme's activity could be modulated by a factor of about 8 (Fig. 11B). Thus, essentially no regulation could be observed for the monomeric enzyme. In addition, the specific activity of the monomer was dramatically reduced. Activity dropped down to 30% compared to the unliganded wt enzyme. In fact, activity was so low that a substrate saturation plot could not be measured since standard deviations exceeded the differences of the measured activities. Thus, this monomeric yeast CM is as stable as the wt dimer, but has lost allosteric regulation. The catalytic efficiency was strongly reduced, but sufficient to complement an *aro*7 deletion under nonstarvation conditions and exhibited the same pH optimum. Indeed, a different unregulated chorismate mutase was shown earlier to be unsuitable for amino acid starvation conditions (Krappmann *et al.*, 2000).

Discussion

The eukaryotic yeast (ScCM) and the bacterial *E. coli* (EcCM) CMs seem to have one evolutionary origin (Sträter *et al.*, 1997). EcCM is a dimer composed of three helices per subunit that resembles a yeast CM monomer. It gains stability by the formation of four-helix bundles composed of helices H1, H2 and H3 of one subunit and H1‘ of the other subunit, which also form the active site cavities. Computer-modeling studies revealed that helices H8, H11, H12, and H2 of ScCM correspond to these helices of EcCM, whereas H4 and H7 of ScCM can be compared to H1‘ and H2‘ of the *E. coli* enzyme indicating an evolutionary gene duplication event (Sträter *et al.*, 1997). For stable folding of the two connected CMs additional helices and loops must have evolved, which contribute to the stability of the somewhat distorted four-helix bundle in the yeast monomer. The results presented here show the stability of this ancestral CM. The monomer generated by two amino acid substitutions can be regarded as an intermediate between a monomeric CM with two active sites and a dimeric CM with two active sites and two additional regulatory domains. The monomer is stable against heat and changes of pH and is still active.

The subsequent step in evolution might have been the generation of hydrophobic cores permitting dimerization. As described above, four regions evolved for dimerization including the formation of an additional four-helix bundle structure composed of H2, H2‘, H8, and H8‘. The stability of the artificial monomer suggests that dimerization occurs after folding of the single subunits and is not required for the correct and stable folding of the single polypeptides. Thus, for this enzyme system, formation of dimers evolved primarily for the ability to regulate enzyme activity.

After the evolutionary dimerization event, the protein’s conformation must have changed to account for possible unfavourable rearrangements around the active sites. Comparing the EcCM and ScCM active sites Xue *et al.* (1994) found that although important residues were mainly conserved, the yeast enzyme has a more exposed active site than does the bacterial counterpart (Xue *et al.*, 1994). This exposure is caused by the presence of additional helices (H9 and H10) near the active site, and it leads to a weaker binding affinity for the substrate. Nevertheless, the cooperativity of substrate binding which can be observed for the dimeric yeast enzyme seems to be sufficient for substantial activity. Perhaps, on the other hand, these rearrangements upon monomerization cause reduction of activity by reorientation of crucial residues of the active site. On the other hand, it cannot yet be excluded that the substitutions introduced at positions 28 and 212 account for the change in activity, because single subsitutions in loop L220s can strongly affect enzyme activity in some cases (Graf *et al*., 1995; Schmidheini *et al.*, 1990). However, since the pH optimum of the monomer equaled that of the unliganded wt enzyme, conformational rearrangements cannot be very pronounced. In addition to alterations in the active site, further rearrangements in the loops must have occurred during evolution in order to gain stability. These structural changes in the loops obviously contribute to stability to a different extent in a particular CM. Although all chimeric CMs investigated were dimeric enzymes, the introduction of the *Hansenula* loop into the yeast enzyme strongly reduced the protein‘s stability, which demonstrates not only the yeast L220s loop‘s function for regulation, but also its contribution to stability.

Finally, to establish an allosteric enzyme, binding sites for allosteric effectors and signaling pathways have evolved, thus destroying two of the active sites to generate two allosteric domains. The resulting binding sites are substantially identical for tyrosine as inhibitor and tryptophan as activator of the yeast wt enzyme. It is now reasonable to ask whether the consequences of effector binding can be changed along the allosteric pathway. In fact, the exchange of the molecular hinge connecting allosteric and catalytic domain presented here showed that loop L220s is one critical part for the transmission of the distinct allosteric signals. Obviously, the difference in size and probably conformation of the loops exchanged caused tertiary structural changes that promoted different rearrangements during signal transduction upon binding of the allosteric effectors. Thus, the signal of tyrosine binding can cause enzyme activation, and tryptophan binding can be a signal for enzyme inhibition. A combination of modified CMs from different organisms leads to a switch of allosteric effects. It would be interesting to identify other residue along the intramolecular signaling pathway, which when subtituted also switch between the allosteric signals. Our results presented here prove the hinge region‘s function for enzyme stability and establish discrimination between allosteric inhibition and activation. Yeast CM is therefore a model enzyme where the detailed understanding of the cooperation of various modules within the molecule allows a specific engineering of a changed regulatory behaviour of a protein.

References

Andersson, L. O., Borg, H. & Mikaelsson, M. (1972). Molecular weight estimation of proteins by electrophoresis in polyacrylamide gel of graded porosity. *FEBS Lett* **20**, 199-202.

Bradford, M. M. (1976). A rapid and sensitive method for the quantitation of microgram quantities of protein utilizing the principle of protein-dye binding. *Anal Biochem* **72**, 248-254.

Combet, C., Blanchet, C., Geourjon, C. & Deléage, G. (2000). NPS@: network protein sequence analysis. *Trends Biochem Sci* **25**, 147-150.

Dimroth, P. (1986). Preparation, characterization, and reconstitution of oxaloacetate decarboxylase from *Klebsiella aerogenes*, a sodium pump. *Methods Enzymol* **125**, 530-540.

Giebel, L. B. & Spritz, R. A. (1990). Site-directed mutagenesis using a double-stranded DNA fragment as a PCR primer. *Nucleic Acids Res* **18**, 4947.

Graf, R., Dubaquié, Y. & Braus, G. H. (1995). Modulation of the allosteric equilibrium of yeast chorismate mutase by variation of a single amino acid residue. *J Bacteriol* **177**, 1645-1648.

Guex, N. & Peitsch, M. C. (1997). SWISS-MODEL and the Swiss-PdbViewer: an environment for comparative protein modeling. *Electrophoresis* **18**, 2714-2723.

Heinemeyer, W., Kleinschmidt, J. A., Saidowsky, J., Escher, C. & Wolf, D. H. (1991). Proteinase yscE, the yeast proteasome/multicatalytic-multifunctional proteinase: mutants unravel its function in stress induced proteolysis and uncover its mecessity for cell survival. *EMBO J* **10**, 555-562.

Helmstaedt, K., Krappmann, S. & Braus, G. H. (2001). Allsoteric regulation of catalytic activity: *E. coli* ATCase versus yeast chorismate mutase. *Microbiol Mol Biol Rev* **65**, 404-421.

Ho, S. N., Hunt, H. D., Horton, R. M., Pullen, J. K. & Pease, L. R. (1989). Site-directed mutagenesis by overlap extension using the polymerase chain reaction. *Gene* **77**, 51-59.

Ito, H., Jukuda, Y., Murata, K. & Kimura, A. (1983). Transformation of intact yeast cells treated with alkali cations. *J Bacteriol* **153**, 163-168.

Krappmann, S., Helmstaedt, K., Gerstberger, T., Eckert, S., Hoffmann, B., Hoppert, M., Schnappauf, G. & Braus, G. H. (1999). The *aroC* gene of *Aspergillus nidulans* codes for a monofunctional, allosterically regulated chorismate mutase. *J Biol Chem* **274**, 22275-22282.

Krappmann, S., Lipscomb, W. N. & Braus, G. H. (2000). Coevolution of transcriptional and allosteric regulation at the chorismate metabolic branch point of *Saccharomyces cerevisiae*. *Proc Natl Acad Sci USA* **97**, 13585-13590.

Laemmli, U. K. (1970). Cleavage of structural proteins during the assembly of the head of bacteriophage T4. *Nature* **227**, 680-685.

MacBeath, G., Kast, P. & Hilvert, D. (1998). A small, thermostable, and monofunctional chorismate mutase from the archaeon *Methanococcus jannaschii*. *Biochemistry* **37**, 10062-10073.

Miozzari, G., Niederberger, P. & Hütter, R. (1978). Tryptophan biosynthesis in *Saccharomyces cerevisiae*: control of the flux through the pathway. *J Bacteriol* **134**, 48-59.

Mumberg, D., Müller, R. & Funk, M. (1994). Regulatable promoters of *Saccharomyces cerevisiae*: comparison of transcriptional activity and their use for heterologous expression. *Nucleic Acid Res* **22**, 5767-5768.

Peitsch, M. C. (1995). Protein modeling by E-mail. *Bio/Technology* **13**, 658-660.

Peitsch, M. C. (1996). ProMod and Swiss-Model: Internet-based tools for automated comparative protein modelling. *Biochem Soc Trans* **24**, 274-279.

Sanger, F., Nicklen, S. & Coulson, A. R. (1977). DNA sequencing with chain-terminating inhibitors. *Proc Natl Acad Sci U S A* **74**, 5463-5467.

Schmidheini, T., Mösch, H. U., Evans, J. N. & Braus, G. (1990). Yeast allosteric chorismate mutase is locked in the activated state by a single amino acid substitution. *Biochemistry* **29**, 3660-3668.

Schmidheini, T., Sperisen, P., Paravicini, G., Hütter, R. & Braus, G. (1989). A single point mutation results in a constitutively activated and feedback-resistant chorismate mutase of *Saccharomyces cerevisiae*. *J Bacteriol* **171**, 1245-1253.

Schnappauf, G., Krappmann, S. & Braus, G. H. (1998). Tyrosine and tryptophan act through the same binding site at the dimer interface of yeast chorismate mutase. *J Biol Chem* **273**, 17012-17017.

Schnappauf, G., Sträter, N., Lipscomb, W. N. & Braus, G. H. (1997). A glutamate residue in the catalytic center of the yeast chorismate mutase restricts enzyme activity to acidic conditions. *Proc Natl Acad Sci USA* **94**, 8491-8496.

Sträter, N., Schnappauf, G., Braus, G. & Lipscomb, W. N. (1997). Mechanisms of catalysis and allosteric regulation of yeast chorismate mutase from crystal structures. *Structure* **5**, 1437-1452.

Thompson, J. D., Higgins, D. G. & Gibson, T. J. (1994). CLUSTAL W: improving the sensitivity of progressive multiple sequence alignment through sequence weighting, position-specific gap penalties and weight matrix choice. *Nucleic Acids Res* **22**, 4673-4680.

Xue, Y., Lipscomb, W. N., Graf, R., Schnappauf, G. & Braus, G. (1994). The crystal structure of allosteric chorismate mutase at 2.2-Å resolution. *Proc Natl Acad Sci USA* **91**, 10814-10818.

Chapter 2

aro7 mutant *S. cerevisiae* strains show an osmophenotype like the wild-type

Abstract

Yeast chorismate mutase (ScCM) catalyzes the Claisen rearrangement from chorismate to prephenate in the biosynthesis of the aromatic amino acids tyrosine and phenylalanine. The encoding gene, *ARO7*, has previously been described to be identical to *OSM2*, a gene necessary for growth in hypertonic medium. In addition, a specific *aro7* allele was linked to a salt-sensitive vacuolar mutant phenotype. This study aimed to examine chorismate mutase's function in osmostress resistance. A series of *aro7* alleles including a complete deletion of the gene were constructed in different genetic backgrounds. The *ARO7* gene and the homologous gene from *Bacillus subtilis*, respectively, were introduced to test for complementation of the osmosensitive phenotype. In contrast to previous results, no osmosensitive phenotype was caused by any of the *aro7* mutations tested in this study. Strains carrying one of the *aro7* point mutations or a full deletion of *ARO7* were competent for the biogenesis of vacuoles and growth under hyperosmotic stress. Slow growth in minimal medium and medium containing a high concentration of salt was observed only in strains carrying an *aro7Δ::URA3* mutation in combination with the *ura3-251, -328, -373* allele. Thus, the previously observed deficiencies of *aro7* mutant strains may result from synthetic interactions between the *aro7* allele and *ura3-251, -328, -373* alleles or alterations in adjacent loci not recognized so far.

Introduction

Saccharomyces cerevisiae is often subject to osmotic stress in its natural habitats. The organism might suffer from a shortage of water on rotting fruit in the sun or might be exposed to the other extreme being washed away by rain. Similarly, the addition of salts or sugars disturbs the osmotic gradient across the plasma membrane decreasing the activity of free water (a_W). The result is an efflux of water from the cells (Mager & Varela, 1993). The turgor caused by the osmotic gradient is necessary for the uptake of water and expansion of the cell wall during growth (Ortega *et al*., 1989). A loss of turgor pressure makes the cells shrink resulting in a membrane bilayer which is twisted. The diminished water concentration affects the hydration of biomolecules so that protein conformation and activity are disturbed. An osmotic upshift as well as a downshift are sensed by the cell (Becker & Craig, 1994; Gustin *et al*., 1988), although the turgor change seems to be the trigger for production of the osmostress response (Tamás *et al*., 2000). Without cellular responses, growth arrest and cell death would follow (Mackenzie *et al*., 1988). However, in response to these fluctuations in environmental osmolarity, yeasts have developed mechanisms to maintain intracellular activities (for review see Hohmann, 2002).

The transcription of more than 180 genes is modulated during hyperosmotic stress to restore the optimal environment for intracellular processes (Rep *et al*., 2000). A more general stress response is mediated by the Ras-cAMP pathway which leads to the induction of target genes regulated by the transcription factors Msn2p and Msn4p which are reversibly translocated to the nucleus (for a review see Estruch, 2000). Signal transduction induces activation of protein kinase A, translocation of the activator protein into the nucleus and binding to stress responsive elements (STRE) in target promoters (Görner *et al*., 1998; Marchler *et al*., 1993). STREs are located in the promotors of genes important for the response to several different stimuli like heat shock, nitrogen starvation, or low pH. This general response leads to cross-protection for several stress factors (Estruch, 2000; Marchler *et al.*, 1993).

The high osmolarity glycerol (HOG) MAP kinase pathway in yeast is specifically activated during osmotic stress. Several parallel mitogen-activated protein kinase cascades are involved in different physiological processes in yeast as well as other organisms in response to stimuli affecting growth (Hohmann, 2002). The HOG pathway consists of the osmosensors Sln1p and Sho1p, a MAP kinase cascade including the MAP kinase Hog1p, which when phosphorylated is translocated into the nucleus to induce target gene expression via STREs (Estruch, 2000; Schüller *et al*., 1994). This osmostress induction is mediated by transcription factors like the above mentioned Msn2p/Msn4p (Estruch, 2000; Görner *et al.*, 1998), Hot1p (Rep *et al.*, 2000; Rep *et al*., 1999), Sko1p (Pascual-Ahuir *et al*., 2001; Proft & Serrano, 1999), or Msn1p (Rep *et al.*, 1999). As indicated by the name, the main cellular response under this condition is the synthesis of osmolytes for cell adaptation to external osmolarity. In yeasts, these osmolytes are polyols, mainly glycerol, which is accumulated up to molar levels (Nevoigt & Stahl, 1997; Reed *et al*., 1987). *S. cerevisiae* is a relatively osmosensitive yeast. Glycerol is produced and secreted as long as the extra- and intracellular glycerol ratio is balanced (Brown & Edgley, 1979). Therefore, the glycerol faciliator Fps1p is closed and glycerol is synthesized due to a HOG pathway-dependent 40-fold induced expression of glycerol-3-phosphate dehydrogenase activities (Blomberg *et al*., 1988). The increased synthesis and accumulation of glycerol diminishes the water activity of the cytosol so that water uptake is possible and turgor is restored (Albertyn *et al*., 1994). In addition, the intracellular cationic level is changed at least under NaCl stress. Addition of NaCl leads to a decreased K^+ concentration and an increase of intracellular Na^+ due to a weak Na^+ extrusion mechanism (Brown & Simpson, 1972). This effect can be observed even though the expression of gene *ENA1* encoding the cation extrusion ATPase is upregulated (Proft & Serrano, 1999). The total cation level is not changed in yeast when the cell is able to accumulate glycerol (Sunder *et al*., 1996).

Trehalose is a further important compound required under stress conditions because it acts as a membrane protectant and a compatible solute (Hounsa *et al*., 1998). Other cellular processes evoked in return of exposure to osmostress involve osmohomeostasis by vacuoles (Latterich & Watson, 1991). During the initial response to increased osmolarity, water leaves the vacuoles to compensate for the extrusion of water from the cytoplasm. In addition to the loss of turgor, rearrangements of the cell wall and cytoskeleton lead to growth arrest. The yeast cell wall composition undergoes modifications upon exposure to osmolytes since the expression of cell wall-related genes was found to be modulated by the HOG pathway (Alonso-Monge *et al*., 2001; Kapteyn *et al*., 2001; Rep *et al.*, 2000). In combination with that, a rapid and reversible disassembly of the actin cytoskleleton in response to osmotic stress was observed (Chowdhury *et al*., 1992; Slaninova *et al*., 2000). Also, actin gene expression is affected upon salt stress (Varela *et al*., 1992). Thus, cytoskeletal reorganisation requiring the interaction with actin-binding proteins seems to stop the delivery of cellular material for growth and to contribute to stabilization of shrinking cells and prevention of plasmolysis (Chowdhury *et al.*, 1992). Even the level and modification of unsaturated fatty acids were proposed to be a major contributor to salt tolerance (Chatterjee *et al*., 2000).

Surprisingly, the screening for genes which are modulated in expression during osmostress response yielded several genes involved in amino acid metabolism (Posas *et al*., 2000; Rep *et al.*, 2000). Also, *OSM2*, a gene necessary for growth in hypertonic medium, was isolated and shown to be identical to *ARO7*, the structural gene for yeast chorismate mutase (Ball *et al*., 1986). In addition, a mutational approach for the investigation of the vacuole's function in osmohomeostasis identified salt-sensitive vacuolar mutant strains which, too, included an *aro7/osm2* strain (Latterich & Watson, 1991). The mutant strain showed a lack of vacuoles (class C vacuolar phenotype) and a weak vacuolar sorting defect. Here, we addressed the question by which mechanism ARO7p, an enzyme involved in aromatic amino acid biosynthesis, could influence vacuolar biogenesis and osmoregulation. The growth of a strain carrying a series of different *aro7* alleles was analyzed under different osmostic conditions, and vacuolar biogenesis was studied in these strains to obtain more precise data on chorismate mutase‘s involvement in these processes.

Materials & Methods

Materials

Pfu polymerase from Promega (Madison, WI, USA) was used for polymerase chain reactions. Zymolyase was obtained from Seikagaku Corporation (Tokyo, Japan). Cell Tracker Blue CMAC and Yeast Vacuole Membrane Marker MDY-64 were purchased from MoBiTec (Göttingen, Germany). All other chemicals were supplied by Fluka/Sigma-Aldrich Chemie GmbH (Taufkirchen, Germany).

Strains, plasmids, and growth conditions

All yeast strains in this study are isogenic to the *S. cerevisiae* S288C genetic background and are listed in Table II. High-copy and low-copy vectors pME2374 and pME2375 containing a *GFP-ARO7* gene fusion (Crameri *et al*., 1996), empty vectors pME1513 and p416GAL1 (Mumberg *et al*., 1994) and control vectors pME1517 and pME2377 containing the wt *ARO7* gene were transformed into strains RH2192 and RH1347 for GFP fluorescence microscopy. An *aro7Δ::GFP-ARO7* mutation was introduced into the progenitor strain RH1671 by using a fragment from plasmid pME2373 to obtain a chromosomaly integrated *GFP-ARO7* fusion gene. *ARO7* and *aroH* which is the chorismate mutase encoding gene from *Bacillus subtilis* was reintegrated into

RH1671 by using fragments from plasmid pME2376 and pME2415. Strain *aro7Δ::kan* (RH2802) was constructed by integration of a kanamycin resistance cassette flanked by the respective untranslated regions into strain RH761 (Guldener *et al*., 1996). Prototrophy of this strain was achieved by transformation with the empty vector pRS415 containing a *LEU2* marker (Christianson *et al*., 1992; Sikorski & Hieter, 1989). Vectors pME2413 and pME2414 containing a *LEU2* marker and the wt *ARO7* gene and *aroH* encoding the chorismate mutase from *B. subtilis*, respectively, were transformed into the knock-out strain RH2802 for complementation of the putative osmosensitive phenotype.

Yeast was transformed by following a modified protocol of Elble (Elble, 1992). The knock-out strains were verified by Southern hybridization experiments (Southern, 1975) after isolation of genomic DNA according to Hoffman & Winston (1987).

Complex medium for growth of *S. cerevisiae* was YEPD (1% yeast extract, 2% peptone, 2% glucose). Minimal MV medium contained 0.14% yeast nitrogen base (without amino acids and without ammonium sulfate), 0.5% ammonium sulfate, and 2% glucose, and was buffered to pH 4.0 for liquid cultures and pH 5.5 for plates, respectively, with succinic acid and KOH as described previously (Miozzari *et al*., 1977). YNB medium was prepared essentially as described (Guthrie & Fink, 1991) with the indicated pH or concentration of osmotic agent or salt. Supplements were added according to Guthrie and Fink (Guthrie & Fink, 1991).

Growth rates were determined as described (Krappmann *et al*., 2000). The growth of cells expressing *GFP-ARO7* was assayed by spotting 10 µl of serial-diluted cell suspensions onto selective plates starting with an OD_{546} of 1 (dilutions 1:10). Transformation of *E. coli* was performed as described by Inoue *et al.* (Inoue *et al*., 1990).

Green fluorescent protein and vacuole marker fluorescence microscopy

Yeast strains harbouring plasmids encoding GFP-ScCM or with a chromosomal gene encoding GFP-ScCM were grown in the indicated media to saturation. Cells from an overnight culture in complex medium were resuspended in fresh pre-heated medium containing a final concentration of 10 µM Cell Tracker Blue CMAC. Cells were incubated under growth conditions for 45 min and resuspended again in fresh medium to continue growth for another 30 min. Cells were harvested and resuspended in 1 ml of 10 mM HEPES buffer, pH 7.4, containing 5 % glucose at a concentraion of 10^6 cells/ml. Cells were viewed *in vivo* on a Zeiss Axiovert microscope by either differential interference contrast microscopy (DIC) or fluorescence microscopy using a GFP filter set or a DAPI filter set (AHF Analysentechnik AG, Tübingen, Germany). Cells were photographed using a Xillix Microimager digital camera and the Improvision Openlab software (Improvision, Coventry, UK). The localization of the GFP-ScCM fusion in the nucleus was observed after *in vivo* staining of the cells with DAPI using the GFP and DAPI filter sets and the Openlab software for scanning through the cells in 0.2-µm steps.

For detection of the vacuolar membrane, yeast strains were cultivated in complex medium overnight. Cells from 1 ml were harvested by centrifugation and resuspended in 1 ml of 10 mM HEPES buffer, pH 7.4, containing 5% glucose at a concentration of 10^6 cells/ml. Vacuole membrane marker MDY-64 was added to a working concentration of 10 or 20 µM. Cells were incubated at room temperature for two to four minutes, pelleted by centrifugation, and resuspended in 15 µl of fresh HEPES buffer. Stained cells were visualized as described above using the GFP filter set.

Western Blot Analysis

Immunological detection of chorismate mutase proteins was performed using a polyclonal rabbit antibody raised against purified yeast chorismate mutase and a horseraddish-peroxidase conjugate as secondary antibody. Detection was carried out using the ECL method (Tesfaigzi *et al*., 1994).

Table II: *S. cerevisiae* strains used in this study

Strain	Genotype	Reference
X2180-1A	*MATa, gal2 SUC2 mal CUP1*	Miozzari *et al.* (1978)
RH2192	*MATa, aro7Δ::LEU2, pra1-1, prb1-1, prc1-1, cps1-3, ura3Δ5, leu2-3, 122, his*$^-$	Heinemeyer *et al.* (1991)
RH1347	*MATa, aro7, ura3-251, ura3-328, ura3-373*	Schmidheini (1989)
RH793	*MATa, aro7*	Kradolfer (1981)
RH1671	*MATa, ura3-251, ura3-328, ura3-373, aro7Δ::URA3*	Graf (1994)
RH2698	*MATa, ura3-251, ura3-328, ura3-373, aro7Δ::ARO7*	Helmstaedt *et al.* (2002)
RH2827	*MATa, ura3-251, ura3-328, ura3-373 aro7Δ::aroH*	this study
RH2801	*MATa, ura3-251, ura3-328, ura3-373, aro7Δ::GFP-ARO7*	this study
RH761	*MATa, leu2-2*	Paravicini (1989)
RH2802	*MATa, leu2-2, aro7Δ::kan*	this study

Results

aro7 deletions cause different growth behaviour under osmotic stress conditions

ARO7/OSM2 was proposed to be a gene necessary for amino acid biosynthesis and, in addition, for growth in hypertonic medium (Ball *et al*., 1986). For a detailed analysis of a putative second *ARO7* function during osmoregulation, an *aro7* mutant strain and two different *aro7* deletion mutant strains were analyzed for growth defects in hypertonic media in comparison to the wt (X2180-1A) and progenitor strains.

The previously observed difference in growth for the wt and an *aro7* strain might be due to either the auxotrophy for the amino acids phenylalanine and tyrosine or to a loss of function which was caused by the absence of the chorismate mutase protein. Therefore, the *aroH* gene encoding the strucurally different chorismate mutase from *Bacillus subtilis* was integrated at the *ARO7* locus (RH2827). The introduction of the homologous CM restored prototrophy for phenylalanine and tyrosine, but due to its different structure is not supposed to take over other possible cellular function from wt yeast CM. In addition, the wt *ARO7* gene was reintegrated into the *aro7Δ::URA3* strain as a control (RH2698). Similarly, *ARO7* and *aroH* were introduced into the *aro7* deletion strain RH2802 on a low-copy vector containing a *LEU2* marker gene.

Growth rates were determined to obtain precise information on the strains‘ competence to produce a cellular stress response (Tab. III). The media contained NaCl at a concentration of 1 M and 7.5 % glycerol, respectively, in order to detect possible differences in response to ionic and nonionic osmolytes. All three aromatic amino acids and, for the strains with the *ura3-251, -328, -373* background and RH793, also uracil were added to provide comparable growth conditions.

The growth rate of the wt strain in glycerol medium was reduced to 83% of that obtained for growth in normal minimal medium, and the growth rate measured in salt medium decreased to 53%. A comparison between the strains with different *ARO7* loci showed some difference in growth, especially in salt medium.

Table III: Growth behavior of *S. cerevisiae* strains under different stress conditions

	Growth rate (h^{-1}) or % of growth rate on MV medium[1]		
Strain	MV	MV + 7.5 % glycerol	MV + 1 M NaCl
wt (X2180-1A)	0.30 h^{-1}	83 %	53 %
aro7 (RH793)	0.28	82 %	54 %
aro7Δ::URA3 *ura3-251, -328, -373* (RH1671)	0.28	82 %	32 %
aro7Δ::ARO7 *ura3-251, -328, -373* (RH2698)	0.20	80 %	45 %
aro7Δ::aroH *ura3-251, -328, -373* (RH2827)	0.22	77 %	59 %
leu2-2 *[LEU2 ARS/CEN]* (RH761 [pRS415])	0.28	86 %	50 %
aro7Δ::Kan, leu2-2 *[LEU2 ARS/CEN]* (RH2802 [pRS415])	0.25	88 %	56 %
aro7Δ::Kan, leu2-2 *[ARO7 LEU2 ARS/CEN]* (RH2802 [pME2413])	0.28	79 %	54 %
aro7Δ::Kan, leu2-2 *[aroH LEU2 ARS/CEN]* (RH2802 [pME2414])	0.23	85 %	56 %

[1] Media were supplemented with phenylalanine, tyrosine, and tryptophan and for strains with the *ura3-251, -328, -373* background and for the *aro7* strain also with uracil.

While the *aro7* mutant and *aro7Δ::URA3* deletion strains showed nearly the same growth rate as the wt in supplemented minimal medium, reintroduction of the *ARO7* and *aroH* genes led to a weak growth defect even in isotonic minimal medium. Growth reduction under hyperosmotic stress resembled that of the wt for these strains with the exception of the *aro7Δ::URA3* deletion strain. For this strain, a stronger growth defect was observed than for the others with a growth rate reduction to 32% in salt medium. In addition, reintegration of the *ARO7* gene could not restore wt-like growth in salt medium, the growth rate remained at 45% of that determined for growth in normal minimal medium. Thus, the generally slower growth and the disability to restore wt like growth by introduction of the wt gene in the strains with the *ura3-251, -328, -373* background suggest some additional genetic alteration at the *ura3* locus or at any other locus produced during generation of these strains. As far as the second knock-out strain (*aro7Δ::kan*) is concerned, no real growth reduction was observed during growth in isotonic minimal medium. Growth rates fluctuated between 0.28 h^{-1} for strain RH761 and 0.25 h^{-1} for the knock-out strain, whereas introduction of *ARO7* on the low-copy plasmid restored the growth rate of 0.28 h^{-1}. Only the expression of *aroH* retarded growth to a rate of 0.23 h^{-1}, but this difference seems attributable to normal fluctuations during measurements. During growth in hypertonic medium, however, neither the latter strain nor the other two showed a stronger growth reduction than the wt strain or the progenitor strain RH761. Growth rates equaled values between 79 and 86% of those obtained under normal conditions in glycerol medium and between 50 and 56% for growth in salt medium. This result demonstrates no osmosensitive phenotype and even more suggests second-site mutations as the cause of the salt-sensitivity of the *aro7Δ::URA3 ura3-251, -328, -373* strain observed above. Thus, the generation of an *aro7Δ::kan* mutant produced a strain for which no growth defect was found when grown in hypertonic medium like observed for other *aro7* mutants before.

Aromatic amino acid auxotrophic strains are able to form vacuoles

For an *aro7* mutant strain also a defect in vacuole formation and sorting of vacuolar proteins in combination with salt-sensitivity was observed (Latterich & Watson, 1991). Therefore, the biogenesis of vacuoles was examined in the *aro7* point mutant strain, in the *aro7* deletion strains and those expressing reintroduced yeast and *Bacillus* chorismate mutase, respectively. First, the vacuolar membrane was stained with the green fluorescent marker MDY-64. Thus, the vacuoles could be detected as ring-like structures in the cells (Fig. 12A). In addition, in most cases vacuoles appeared as indentations of the cellular surface during visualization by DIC. All of the strains tested proved to form the vacuolar ring structures like those observed in the wt strain.

For comparison, yeast strains were stained using a vacuolar lumen marker (Fig. 12B). Again, all of the strains showed one, sometimes two or three blue patches within the cell indicating the presence of vacuolar organelles. Thus, a clear grouping into class A strains (formation of large vacuoles) was possible unlike classification into class C (no vacuoles) of *aro7* mutants by Latterich & Watson (1991) before.

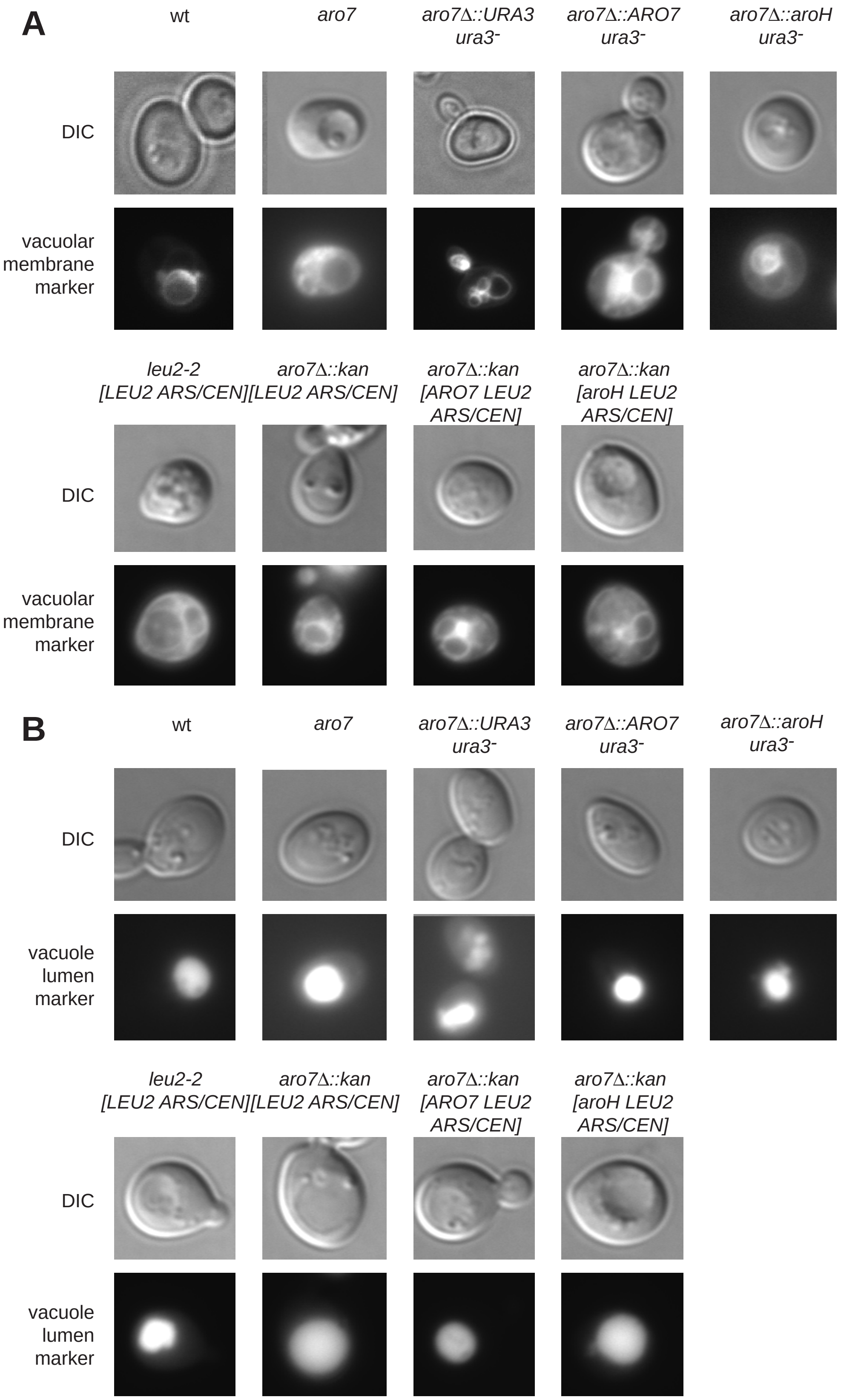
A
wt
aro7
aro7Δ::URA3 ura3⁻
aro7Δ::ARO7 ura3⁻
aro7Δ::aroH ura3⁻
DIC
vacuolar membrane marker
leu2-2 [LEU2 ARS/CEN]
aro7Δ::kan [LEU2 ARS/CEN]
aro7Δ::kan [ARO7 LEU2 ARS/CEN]
aro7Δ::kan [aroH LEU2 ARS/CEN]
DIC
vacuolar membrane marker
B
wt
aro7
aro7Δ::URA3 ura3⁻
aro7Δ::ARO7 ura3⁻
aro7Δ::aroH ura3⁻
DIC
vacuole lumen marker
leu2-2 [LEU2 ARS/CEN]
aro7Δ::kan [LEU2 ARS/CEN]
aro7Δ::kan [ARO7 LEU2 ARS/CEN]
aro7Δ::kan [aroH LEU2 ARS/CEN]
DIC
vacuole lumen marker

Yeast chorismate mutase is localized in the cytoplasm

We examined the localization of yeast chorismate mutase under different growth conditions to determine a possible association with vacuoles. The absence of specific localization signals within the amino acid sequence of chorismate mutase suggested a cytoplasmic localization.

The structural yeast *ARO7* gene was fused to GFP at its N terminus and the resulting fusion gene (GFP-ScCM) was expressed from a low-copy and high-copy vector, respectively. In addition, a copy of the GFP-ScCM encoding gene was integrated into the chromosome at the *ARO7* locus thereby replacing the authentic *ARO7* gene. Expression and function of GFP-ScCM fusion protein were tested by Western analysis, enzyme assays, and growth tests on selective media. A specific band was detected by a polyclonal anti-ScCM antibody in crude extracts of a yeast strain expressing the GFP-ScCM fusion. (Fig. 13A). While no specific band was observed in crude extracts of the *aro7* deletion strain carrying an empty vector, wt ScCM was recognized when expressed from a high-copy vector. This band which appeared at about 60 kDa, was absent in strains expressing the wt *ARO7* gene. Chorismate mutase activity of GFP-ScCM was measured in an enzyme assay *in vitro* using the same crude extracts as used for the Western analysis (Fig. 13B). As expected, no activity was found for the control strain harbouring an empty vector, whereas a slightly regulated chorismate mutase activity was measured in crude extracts with wt ScCM. Chorismate mutase activity of the GFP-ScCM fusion protein was reduced to about 25 % of wt activity. However, enzyme activity was restored to 80% of wt ScCM, when the allosteric activator tryptophan was added and repressed by the addition of the inhibitor tyrosine, demonstrating that GFP-ScCM forms a functional and regulated enzyme.

Fig. 12 (opposite page): Competence of auxotrophic yeast strains for vacuole biogenesis. **A**, Vacuoles of wt and mutant strains were labeled with the green fluorescent vacuole membrane marker MDY-64. Living cells were viewed by differential interference contrast microscopy (DIC) or by fluorescence microscopy to visualize the vacuolar membrane. **B**, The blue membrane-permeable chloromethyl coumarin derivative CMAC selectively stained the lumen of the yeast vacuole. Living cells were viewed by differential interference contrast microscopy (DIC) or by fluorescence microscopy to visualize the vacuolar lumen. wt: X2180-1A; *aro7*: RH793; *aro7Δ::URA3 ura3*$^-$: RH1671; *aro7Δ::ARO7 ura3*$^-$: RH2698; *aro7Δ::aroH ura3*$^-$: RH2827; *leu2-2* [*LEU2 ARS/CEN*]: RH761 [pRS415]; *aro7Δ::kan* [*LEU2 ARS/CEN*]: RH2802 [pRS415]; *aro7Δ::kan* [*ARO7 LEU2 ARS/CEN*]: RH2802 [pME2413]; *aro7Δ::kan* [*aroH LEU2 ARS/CEN*]: RH2802 [pME2414]. Magnification: 63x.

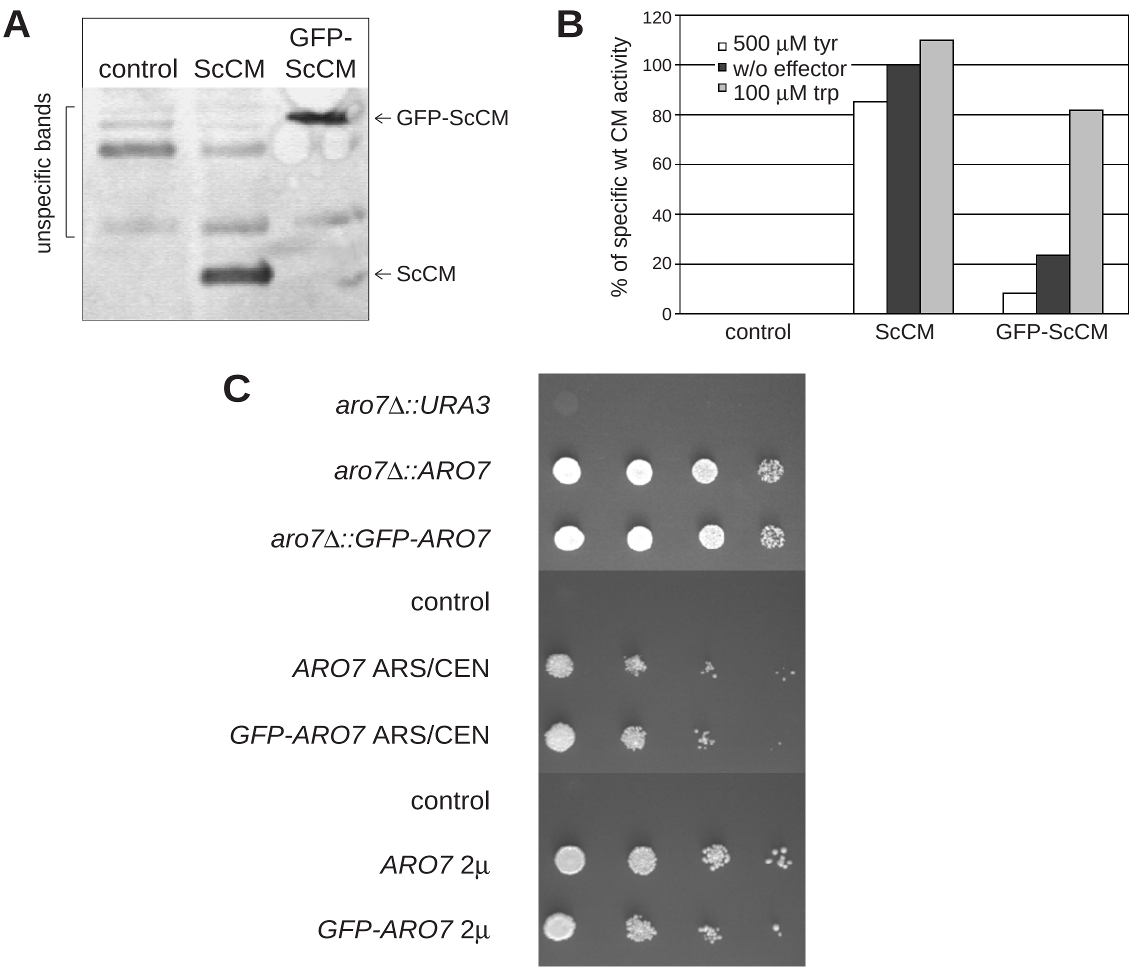

Fig. 13: A GFP-chorismate mutase fusion protein is expressed and functional in yeast. **A**, Examination of *GFP-ARO7* expression in yeast by Western analysis. A polyclonal rabbit antibody raised against wt yeast chorismate mutase binds the GFP fusion protein with high affinity. The hybridized immunoblot shows 15 µg of crude extracts of strains RH2192 [pME1513] (empty vector), RH2192 [pME1517], and RH2192 [pME2374], respectively, expressing wt and fusion protein from a 2-µm plasmid. Proteins cross-reacting with the ScCM antibody were detected using enhanced chemiluminescence. **B**, Relative enzyme activities of wt and GFP-fused chorismate mutase. The specific catalytic activities were determined in crude extracts of strains RH2192 [pME1513] (empty vector), RH2192 [pME1517] (expressing wt *ARO7*), and RH2192 [pME2374] (expressing *GFP-ARO7*), respectively. The specific activity of the wt enzyme measured without effectors was set one hundred percent. Assay conditions were 100 µg of total protein, 2 mM chorismic acid, 3 min reaction time, and 100 µM tyrosine and 500 µM tryptophan, repectively. Each value is the mean of three independent measurements. **C**, Growth test of strains expressing a *GFP-ARO7* fusion gene. Strains containing an integrated *GFP-ARO7* fusion gene (RH2801) or expressing *GFP-ARO7* from a high-copy and low-copy vector, respectively, (RH1347 [pME2374] and RH1347 [pME2375]) were grown in minimal medium and serial-diluted in water to 10^{-4} before spotting onto minimal medium plates. The optical density of each dilution was identical for all strains, starting with an OD_{546} of 1. The respective knock-out strain RH1671, strains carrying empty vectors (RH1347 [p416GAL1], RH1347 [pME1513]) and those harbouring the wt ARO7 gene (RH2698, RH1347 [pME2377], and RH1347 [pME1517]) served as controls.

In a growth assay, the *GFP-ARO7* gene fusion complemented the auxotrophy for phenylalanine and tyrosine like the wt *ARO7* gene, whereas the *aro7Δ::URA3* deletion strain and control strains carrying empty expression vectors were not able to grow (Fig. 13C). The gene copy number did not have any detectible effect on complementation, because no difference was found between growth of strains expressing wt *ARO7* or the *GFP-ARO7* fusion gene. Thus, GFP-ScCM is an active protein which is able to restore prototrophy of the cells lacking *ARO7*.

Yeast cells expressing *GFP-ARO7* from high-copy or low-copy vectors showed bright fluorescence in the cytoplasm (Fig. 14A). Fluorescence was clearly excluded from the vacuoles when compared to the visualization of vacuoles carrying a specific vacuolar marker. An overload-effect resulting from the unregulated expression of multiple gene copies could be ruled out, because strains carrying a single chromosomal *GFP-ARO7* gene showed the same localization of fluorescence in the cells (data not shown). Fluorescence was very faint compared with the strains expressing multiple gene copies, but in these cells, too, an even distribution of fluorescence without a concentration of molecules at any subcellular place could be observed.

Although GFP-ScCM localization was clearly absent from vacuoles, staining of the nucleus using DAPI revealed a localization of the protein in the nucleus in addition to the cytoplasm (Fig. 14B). Optical scanning through cells expressing GFP-ScCM in 0.2-µm steps revealed that the blue fluorescence of DAPI was always observed in the same areas of the cells as the green emission of GFP-ScCM.

Yeast cells expressing *GFP-ARO7* were grown under different osmotic stress conditions to obtain information on chorismate mutase's subcellular localization in stress response. The presence of osmolytes (1.5 M sorbitol or 1 M NaCl) or low pH of 3.0 did not alter the localization of GFP-ScCM, which is present in the cytoplasm and nucleus, and excluded from vacuoles (Fig. 14A).

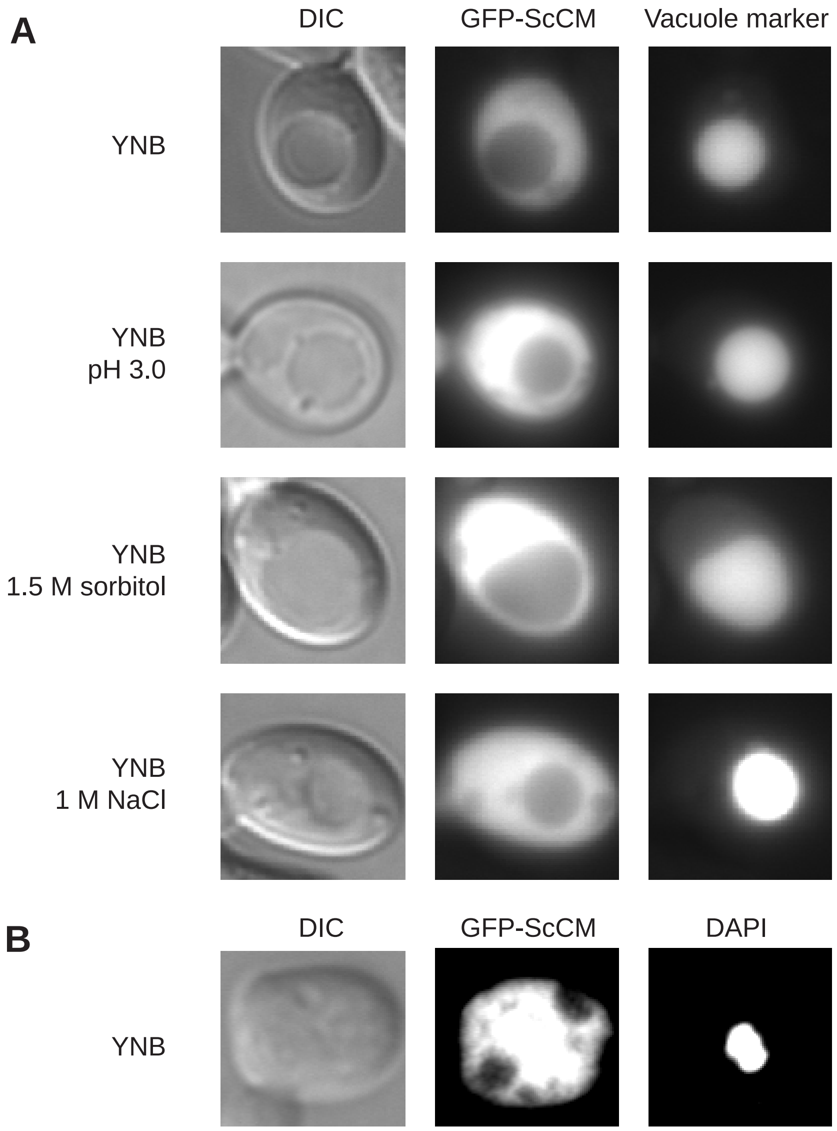
A
DIC
GFP-ScCM
Vacuole marker
YNB
YNB
pH 3.0
YNB
1.5 M sorbitol
YNB
1 M NaCl
B
DIC
GFP-ScCM
DAPI
YNB

Fig. 14: Subcellular localization of yeast GFP-ScCM. **A**, Yeast chorismate mutase is localized in the cytoplasm and the nucleus, but not in vacuoles. An *aro7Δ* strain expressing *GFP-ARO7* from a high-copy vector (RH2192 [pME2374]) was grown in the indicated media and representative cells were viewed by digital interference contrast microscopy (DIC) or by fluorescence microscopy (GFP and vacuole marker CMAC) **B**, Verification of yeast chorismate mutase localized in the nucleus. Scanning through representative cells in 0.2-µm steps showed DAPI fluorescence in the same localization as GFP fluorescence in the respective section of the cells indicating diffusion of GFP-ScCM into the nucleus. Magnification: 63x.

Discussion

In this study, the question was addressed why a chorismate-mutase deficient yeast might be osmosensitive. Therefore, an *aro7* mutant strain, two *aro7* deletion strains and control strains expressing reintroduced *ARO7* and *aroH* genes were investigated regarding localization of chorismate mutase, growth behaviour under hyperosmotic conditions, and biogenesis of vacuoles. *ARO7* was found to be involved in vacuole formation and necessary for growth in hypertonic medium before. However, a class A vacuolar morphology was determined for all strains examined in this study. We detected the vacuolar membrane as well as the vacuolar lumen by respective marker dyes in these strains indicating proper formation and function of this organelle. In fact, no *aro7* mutant investigated here showed a class B or C vacuolar phenotype. Latterich *et al.* (1991) determined only a weak sorting defect of vacuolar enzymes for this mutant and admitted that the vacuole may be vesicularized and not detectable by electron microscopy in their study.

The chorismate mutase encoding gene *ARO7* was fused to the *GFP* gene for localization of the enzyme in living yeast cells by fluorescence microscopy. In combination with this marker protein, chorismate mutase was well expressed and functional and was also supposed to form the normal dimeric structure because allosteric characteristics could be determined for the fusion protein in an enzyme assay. As expected, chorismate mutase was evenly distributed through the cytosol and was excluded from the vacuole. Any association with the vacuole, an organelle involved in osmoregulation, was not found during growth under high osmolarity or low pH either. Surprisingly, the protein colocalized with the nucleus. This observation was not expected because the dimeric fusion protein presumably had a size of 113.4 kDa and therefore, this protein being larger than 90 kDa is not supposed to migrate through nuclear pores unless a localization signal is present. When used as a control protein, yeast chorismate mutase fused to GFP and the GCN4p nuclear localization signal further accumulated in the nucleus and was no longer present in the cytoplasm (R. Pries, unpublished results). This experiment also suggested an exclusion from the nucleus of GFP-ScCM without any localization peptide, a result which, however, could not be confirmed by microscopic studies.

As far as osmosensitivity is concerned, only one *aro7* mutant (*aro7Δ::URA3 ura3-251, -328, -373*) did show retarded growth in hyperosmotic medium. An *aro7* mutant strain and another *aro7* deletion (*aro7Δ::kan*) showed growth reduction like the wt in high-osmolarity medium and thus, did not confirm the putative role of *ARO7* in osmostress resistance. The homologous *aroH* gene was used as control to investigate any additional function of the chorismate mutase enzyme apart from its amino acid biosynthetic activity. When *ARO7* and *aroH*, respectively, were reintegrated into the *aro7Δ::URA3* knock-out strain, the strain expressing *aroH* grew slightly better than the control with *ARO7* under normal conditions and did show slow growth like the wild-type in salt medium. *ARO7*, however, did neither complement the slower growth under normal conditions nor the observed osmosensitive phenotype suggesting an additional genetic alteration in this strain. Ball *et al.* (1986) found a cosegregation of the ARO^+ and OSM^+ phenotypes after transformation with a genomic fragment containing *ARO7* and concluded the identity of *ARO7* and *OSM2*, but did not prove this hypothesis by reintroduction of the isolated gene or a homologous control gene.

The fact that *aroH* complemented the growth defect in salt medium, but not that under isotonic conditions suggested that the *ura3-251, -328, -373* background impaired cell growth behaviour. Another *aro7* deletion was generated in a *leu2-2* strain with a kanamycin resistance cassette. In this genetic background, no salt sensitive phenotype was observed, again demonstrating the influence of the *ura3* marker. By the crossing of an *aro7Δ::URA3 ura3-251, -328, -373* and an *aro7Δ::kan* strain, an assignment of the genetic locus responsible for salt sensitivity could be made if the OSM^- phenotype co-segregated with the *ura3-251, -328, -373* locus or the *aro7Δ* loci.

In summary, the investigation of several chorismate-mutase deficient yeast strains and the complementation by isolated chorismate-mutase encoding genes did not confirm any osmoregulatory function of *ARO7* or the encoded protein during growth in hypertonic medium nor any role for vacuolar biogenesis like was suggested for other *aro7* mutant strains before.

References

Albertyn, J., Hohmann, S. & Prior, B. A. (1994). Characterization of the osmotic-stress response in *Saccharomyces cerevisiae*: osmotic stress and glucose repression regulate glycerol-3- phosphate dehydrogenase independently. *Curr Genet* **25**, 12-18.

Alonso-Monge, R., Real, E., Wojda, I., Bebelman, J. P., Mager, W. H. & Siderius, M. (2001). Hyperosmotic stress response and regulation of cell wall integrity in *Saccharomyces cerevisiae* share common functional aspects. *Mol Microbiol* **41**, 717-730.

Ball, S. G., Wickner, R. B., Cottarel, G., Schaus, M. & Tirtiaux, C. (1986). Molecular cloning and characterization of *ARO7-OSM2*, a single yeast gene necessary for chorismate mutase activity and growth in hypertonic medium. *Mol Gen Genet* **205**, 326-330.

Becker, J. & Craig, E. A. (1994). Heat-shock proteins as molecular chaperones. *Eur J Biochem* **219**, 11-23.

Blomberg, A., Larsson, C. & Gustafsson, L. (1988). Microcalorimetric monitoring of growth of *Saccharomyces cerevisiae*: osmotolerance in relation to physiological state. *J Bacteriol* **170**, 4562-4568.

Brown, A. D. & Edgley, M. (1979). Osmoregulation in yeast. *Basic Life Sci* **14**, 75-90.

Brown, A. D. & Simpson, J. R. (1972). Water relations of sugar-tolerant yeasts: the role of intracellular polyols. *J Gen Microbiol* **72**, 589-591.

Chatterjee, M. T., Khalawan, S. A. & Curran, B. P. (2000). Cellular lipid composition influences stress activation of the yeast general stress response element (STRE). *Microbiology* **146**, 877-884.

Chowdhury, S., Smith, K. W. & Gustin, M. C. (1992). Osmotic stress and the yeast cytoskeleton: phenotype-specific suppression of an actin mutation. *J Cell Biol* **118**, 561-571.

Christianson, T. W., Sikorski, R. S., Dante, M., Shero, J. H. & Hieter, P. (1992). Multifunctional yeast high-copy-number shuttle vectors. *Gene* **110**, 119-122.

Crameri, A., Whitehorn, E. A., Tate, E. & Stemmer, W. P. (1996). Improved green fluorescent protein by molecular evolution using DNA shuffling. *Nat Biotechnol* **14**, 315-319.

Elble, R. (1992). A simple and efficient procedure for transformation of yeasts. *Biotechniques* **13**, 18-20.

Estruch, F. (2000). Stress-controlled transcription factors, stress-induced genes and stress tolerance in budding yeast. *FEMS Microbiol Rev* **24**, 469-486.

Görner, W., Durchschlag, E., Martinez-Pastor, M. T., Estruch, F., Ammerer, G., Hamilton, B., Ruis, H. & Schüller, C. (1998). Nuclear localization of the C2H2 zinc finger protein Msn2p is regulated by stress and protein kinase A activity. *Genes Dev* **12**, 586-597.

Graf, R. (1994). Anthranilate Synthase and Chorismate Mutase: Allosteric Regulation of two Branchpoint Enzymes from the Aromatic Amino Acid Biosynthetic Pathway of the Yeast *Saccharomyces cerevisiae*. *Dissertation* **ETH No. 10724**, ETH Zürich.

Guldener, U., Heck, S., Fielder, T., Beinhauer, J. & Hegemann, J. H. (1996). A new efficient gene disruption cassette for repeated use in budding yeast. *Nucleic Acids Res* **24**, 2519-2524.

Gustin, M. C., Zhou, X. L., Martinac, B. & Kung, C. (1988). A mechanosensitive ion channel in the yeast plasma membrane. *Science* **242**, 762-765.

Guthrie, C. & Fink, G. R. (1991). Guide to yeast genetics and molecular biology. *Methods Enzymol* **194**.

Heinemeyer, W., Kleinschmidt, J. A., Saidowsky, J., Escher, C. & Wolf, D. H. (1991). Proteinase yscE, the yeast proteasome/multicatalytic-multifunctional proteinase: mutants unravel its function in stress induced proteolysis and uncover its necessity for cell survival. *Embo J* **10**, 555-562.

Helmstaedt, K., Heinrich, G., Lipscomb, W. N. & Braus, G. H. (2002). Refined molecular hinge between allosteric and catalytic domain determines allosteric regulation and stability of fungal chorismate mutase. *Proc Natl Acad Sci USA* **99**, 6631-6636.

Hohmann, S. (2002). Osmotic stress signaling and osmoadaptation in yeasts. *Microbiol Mol Biol Rev* **66**, 300-372.

Hounsa, C. G., Brandt, E. V., Thevelein, J., Hohmann, S. & Prior, B. A. (1998). Role of trehalose in survival of *Saccharomyces cerevisiae* under osmotic stress. *Microbiology* **144**, 671-680.

Inoue, H., Nojima, H. & Okayama, H. (1990). High efficiency transformation of *Escherichia coli* with plasmids. *Gene* **96**, 23-28.

Kapteyn, J. C., ter Riet, B., Vink, E., Blad, S., De Nobel, H., Van Den Ende, H. & Klis, F. M. (2001). Low external pH induces HOG1-dependent changes in the organization of the *Saccharomyces cerevisiae* cell wall. *Mol Microbiol* **39**, 469-479.

Kradolfer, P. (1981). Tryptophanstoffwechsel in *Saccharomyces cerevisiae*. *Dissertation* **ETH No. 6769**, ETH Zürich.

Krappmann, S., Lipscomb, W. N. & Braus, G. H. (2000). Coevolution of transcriptional and allosteric regulation at the chorismate metabolic branch point of *Saccharomyces cerevisiae*. *Proc Natl Acad Sci USA* **97**, 13585-13590.

Latterich, M. & Watson, M. D. (1991). Isolation and characterization of osmosensitive vacuolar mutants of *Saccharomyces cerevisiae*. *Mol Microbiol* **5**, 2417-2426.

Mackenzie, K. F., Singh, K. K. & Brown, A. D. (1988). Water stress plating hypersensitivity of yeasts: protective role of trehalose in *Saccharomyces cerevisiae*. *J Gen Microbiol* **134**, 1661-1666.

Mager, W. H. & Varela, J. C. (1993). Osmostress response of the yeast *Saccharomyces*. *Mol Microbiol* **10**, 253-258.

Marchler, G., Schüller, C., Adam, G. & Ruis, H. (1993). A *Saccharomyces cerevisiae* UAS element controlled by protein kinase A activates transcription in response to a variety of stress conditions. *Embo J* **12**, 1997-2003.

Miozzari, G., Niederberger, P. & Hütter, R. (1977). Action of tryptophan analogues in *Saccharomyces cerevisiae*. *Arch Microbiol* **115**, 307-316.

Miozzari, G., Niederberger, P. & Hütter, R. (1978). Tryptophan biosynthesis in *Saccharomyces cerevisiae:* control of the flux through the pathway. *J Bacteriol* **134**, 48-59.

Mumberg, D., Müller, R. & Funk, M. (1994). Regulatable promoters of *Saccharomyces cerevisiae*: comparison of transcriptional activity and their use for heterologous expression. *Nucleic Acids Res* **22**, 5767-5768.

Nevoigt, E. & Stahl, U. (1997). Osmoregulation and glycerol metabolism in the yeast *Saccharomyces cerevisiae*. *FEMS Microbiol Rev* **21**, 231-241.

Ortega, J. K. E., Zehr, E. G. & Keanini, R. G. (1989). *In vivo* creep and stress relaxation experiments to determine the wall extensibility and yield threshold for the sporangiophores of *Phycomyces*. *Biophys J* **56**, 465-475.

Paravicini, G. (1989). The isogenes *ARO3* and *ARO4* of *Saccharomyces cerevisiae*. *Dissertation* **ETH No. 8815**, ETH Zürich.

Pascual-Ahuir, A., Posas, F., Serrano, R. & Proft, M. (2001). Multiple levels of control regulate the yeast cAMP-response element- binding protein repressor Sko1p in response to stress. *J Biol Chem* **276**, 37373-37378.

Posas, F., Chambers, J. R., Heyman, J. A., Hoeffler, J. P., de Nadal, E. & Arino, J. (2000). The transcriptional response of yeast to saline stress. *J Biol Chem* **275**, 17249-17255.

Proft, M. & Serrano, R. (1999). Repressors and upstream repressing sequences of the stress-regulated *ENA1* gene in *Saccharomyces cerevisiae*: bZIP protein Sko1p confers HOG-dependent osmotic regulation. *Mol Cell Biol* **19**, 537-546.

Reed, R. H., Chudek, J. A., Foster, R. & Gadd, G. M. (1987). Osmotic significance of glycerol accumulation in exponentially growing yeasts. *Appl Environ Microbiol* **53**, 2119-2123.

Rep, M., Krantz, M., Thevelein, J. M. & Hohmann, S. (2000). The transcriptional response of *Saccharomyces cerevisiae* to osmotic shock. Hot1p and Msn2p/Msn4p are required for the induction of subsets of high osmolarity glycerol pathway-dependent genes. *J Biol Chem* **275**, 8290-8300.

Rep, M., Reiser, V., Gartner, U., Thevelein, J. M., Hohmann, S., Ammerer, G. & Ruis, H. (1999). Osmotic stress-induced gene expression in

Saccharomyces cerevisiae requires Msn1p and the novel nuclear factor Hot1p. *Mol Cell Biol* **19**, 5474-5485.

Schmidheini, T. (1989). Regulation of the chorismate mutase of *Saccharomyces cerevisiae*. *Dissertation* **ETH No. 9034**, ETH Zürich.

Schüller, C., Brewster, J. L., Alexander, M. R., Gustin, M. C. & Ruis, H. (1994). The HOG pathway controls osmotic regulation of transcription via the stress response element (STRE) of the *Saccharomyces cerevisiae* CTT1 gene. *Embo J* **13**, 4382-9.

Sikorski, R. S. & Hieter, P. (1989). A system of shuttle vectors and yeast host strains designed for efficient manipulation of DNA in *Saccharomyces cerevisiae*. *Genetics* **122**, 19-27.

Slaninová, I., Sesták, S., Svoboda, A. & Farkas, V. (2000). Cell wall and cytoskeleton reorganization as the response to hyperosmotic shock in *Saccharomyces cerevisiae*. *Arch Microbiol* **173**, 245-252.

Southern, E. M. (1975). Detection of specific sequences among DNA fragments separated by gel electrophoresis. *J Mol Biol* **98**, 503-517.

Sunder, S., Singh, A. J., Gill, S. & Singh, B. (1996). Regulation of intracellular level of Na+, K+ and glycerol in *Saccharomyces cerevisiae* under osmotic stress. *Mol Cell Biochem* **158**, 121-124.

Tamás, M. J., Rep, M., Thevelein, J. M. & Hohmann, S. (2000). Stimulation of the yeast high osmolarity glycerol (HOG) pathway: evidence for a signal generated by a change in turgor rather than by water stress. *FEBS Lett* **472**, 159-165.

Tesfaigzi, J., Smith-Harrison, W. & Carlson, D. M. (1994). A simple method for reusing western blots on PVDF membranes. *Biotechniques* **17**, 268-269.

Varela, J. C., van Beekvelt, C., Planta, R. J. & Mager, W. H. (1992). Osmostress-induced changes in yeast gene expression. *Mol Microbiol* **6**, 2183-2190.

Chapter 3

The chorismate mutase of *Thermus thermophilus* is a monofunctional AroH class enzyme inhibited by tyrosine

Abstract

The *aroG* gene encoding the monofunctional chorismate mutase TtCM of the thermophilic Gram-negative bacterium *Thermus thermophilus* was cloned and its gene product TtCM was characterized. The enzyme with a size of 15,812 Da was purified to homogeneity as a His-fusion protein and belongs to the rare group of AroH chorismate mutases. Whereas AroH enzymes are mainly found in the Gram-positive bacteria of the *Bacillus/Clostridia* group and the Gram-negative cyanobacteria, the first nonphotosynthetic Gram-negative organism was now shown to possess an AroH-type CM. The predicted three-dimensional structure suggests a pseudo-α/β barrel enzyme, which exists as a trimer, but also seems to form hexamers under some conditions. Analysis of the structural model revealed that an increase in hydrophilicity on the protein's surface, an improvement of hydrophobicity in cavities within the protein, and restriction of conformational freedom contribute to thermal stability of this CM. In contrast to the other characterized AroH chorismate mutase from *B. subtilis*, TtCM was found to be inhibited by tyrosine.

Introduction

Chorismate mutases (EC 5.4.99.5) catalyze the first committed reaction in the biosynthesis of the aromatic amino acids phenylalanine and tyrosine. These enzymes exist in various forms (Romero *et al*., 1995; Helmstaedt *et al*., 2001). A different number of plant isozymes of CMs were isolated, which are monofunctional and inhibited by phenylalanine, tyrosine and/or secondary metabolites as e.g., coumarate or caffeate (Romero *et al.*, 1995). Monofunctional enzymes also exist in microorganisms and are not always regulated. In addition, prokaryotes harbour bifunctional CMs which may be fused to prephenate dehydratase, prephenate dehydrogenase, and DAHP synthase activity, respectively.

Only two different polypeptide folds were identified for all chorismate mutases described so far based on crystal structure analysis (Chook *et al*., 1994; Sträter *et al*., 1997). The AroQ structural class is constituted by all CM domains of bifunctional enzymes like those of *Escherichia coli* (EcCM) and most monofunctional prokaryotic and eukaryotic CMs like those of the archaeon *Methanococcus jannaschii*, the fungi *Saccharomyces cerevisiae* (ScCM) and *Hansenula polymorpha* (HpCM) or the plant *Arabidopsis thaliana* (AtCM) (Fig. 15A). These all-helical proteins form dimers with a four-helix bundle, which contains the active sites. This fold itself does not harbour allosteric sites for regulation. However, the bifunctional P-protein of *E. coli* contains the regulatory sites in the so-called R domain (Zhang *et al*., 1998), and in the monofunctional enzyme of *S. cerevisiae* additional helices are present and allosteric domains have presumably evolved from catalytic domains after gene duplication (Sträter *et al.*, 1997).

The other class of chorismate mutases (AroH) is represented by the monofunctional CM of the Gram-positive bacterium *B. subtilis* (BsCM) (Chook *et al.*, 1994) (Fig. 15B). In the crystal structure of this enzyme, three monomers form a homotrimer with pseudo-3-fold symmetry in which most strands of the β-sheets form the core and are oriented like three sides of a prism. The helices surround the β-sheets so that the quaternary structure is termed pseudo-α/β barrel which shows some differences to a standard α/β barrel. Whereas this barrel structure is made up of three monomers, the typical α/β barrel is formed by one polypeptide chain. The number of β-strands in BsCM exceeds that of the typical barrel, and they form mixed rather than parallel β-sheets. In addition, the number of β-strands in the core does not equal that of the surrounding helices.

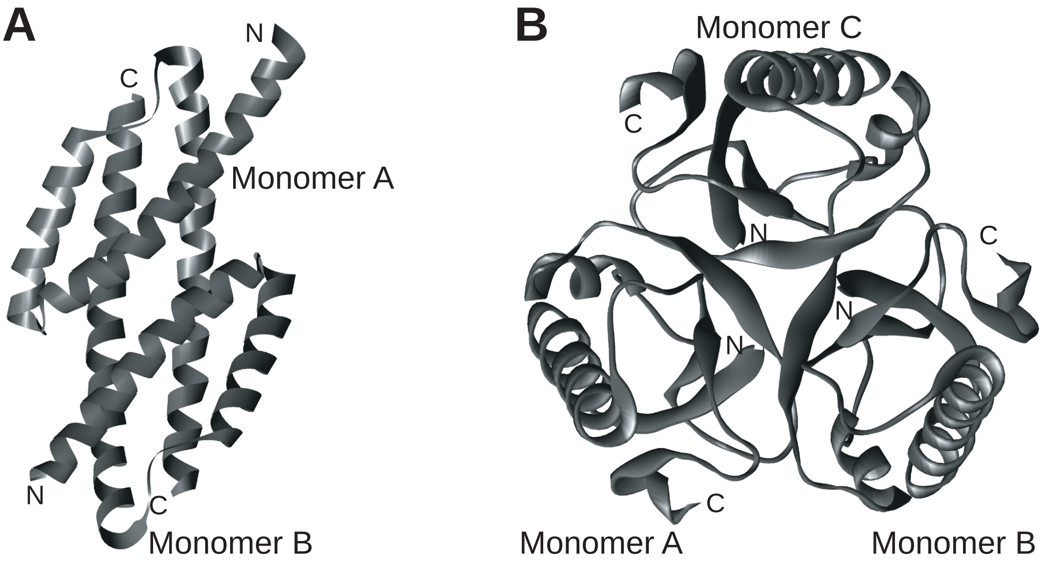

Fig. 15: Quaternary structures of *E. coli* (AroQ) and *B. subtilis* (AroH) chorismate mutase. **A**, The chorismate mutase from *E. coli* (EcCM) consists of three α-helices and forms a dimer with a four-helix bundle structure. **B**, The CM from *B. subtilis* is a homotrimeric enzyme the monomers of which consist of a mixed β-sheet packed against three α-helices. The amino- and carboxytermini of the polypeptides are indicated by N and C.

Three active site pockets are formed by residues from adjacent monomers in the clefts between the polypeptides. BLAST analysis yielded homologous AroH class sequences from Gram-positive bacteria of the *Bacillus*/*Clostridium* group like *Geobacillus stearothermophilus*, *Bacillus halodurans*, *Listeria innocua*, *Listeria monocytogenes*, *Thermoanaerobacter tengcongensis* as well as *Streptomyces coelicolor* of the *Acinetobacteria*, and from the Gram-negative cyanobacteria *Synechocystis sp.* PCC 6803 and *Nostoc sp.* PCC7120.

While many efforts have been made to gain insight into the catalysis of the rare pericyclic reaction and the structure-function relationship of enzyme regulation, little is known about the architectural features contributing to stability of these chorismate mutase folds. In recent years, an increasing number of thermostable proteins has attracted much attention to find out about the principles of protein folding and stabilization especially for industrial purposes.

Recently, a thermostable chorismate mutase from the archeon *Methanococcus jannaschii* was isolated showing that the well-known CM fold of the AroQ class can serve as scaffold for thermostable polypeptides (MacBeath *et al*., 1998). In this study, we isolated the *aroG* gene from *T. thermophilus* and characterized the encoded chorismate mutase.

T. thermophilus is an aerobic, rod-shaped, nonsporulating, gram-negative bacterium (Koyama *et al*., 1986). The optimal growth temperature equals 70°C, but *T. thermophilus* also grows at temperatures up to 85°C. In the last years, a few mutant strains were generated by mutagenesis of the wild-type strain HB27. Markers like auxotrophy for leucine, proline, tryptophan or uracil are available (Koyama *et al.*, 1986; Tamakoshi *et al.*, 1997), and stabilization of the *Staphylococcus aureu*s kanamycin nucleotidyltransferase in *Geobacillus stearothermophilus* yielded also a kanamycin resistance marker gene, which can be used in *Thermus* (Liao *et al.*, 1986). In addition, autonomously replicating plasmids as well as integration and *E. coli*-*Thermus* shuttle vectors now facilitate stable expression of proteins (de Grado *et al*., 1999; Koyama *et al*., 1990; Tamakoshi *et al.*, 1997).

In this study, an *aroG* deletion cassette was generated to establish another marker for genetic manipulation of *T. thermophilus*. Also, a *Thermus* expression vector was constructed. Furthermore, we obtained a monofunctional thermostable chorismate mutase from *T. thermophilus* which in contrast to the *M. jannaschii* enzyme belongs to the AroH class of CMs and, although similar to the unregulated *B. subtilis* enzyme, represents a tyrosine-inhibitable CM. Therefore, analysis of this enzyme showed the possibility to generate a regulated thermostable chorismate mutase and might provide information on how regulation is achieved in pseudo-α/β barrel proteins.

Materials & Methods

Materials

Pfu polymerase from Promega (Madison, WI, USA) was used for polymerase chain reactions (PCR). Chorismic acid as barium salt was purchased from Sigma (St. Louis, MO, USA). All other chemicals were obtained from Fluka/Sigma-Aldrich Chemie GmbH (Taufkirchen, Germany). Protein solutions were concentrated using Centricon-10 concentrators from Millipore (Eschborn, Germany). The Mini 2D SDS-polyacrylamide gel electrophoresis system and the Bradford protein assay solution for determination of protein concentrations originated from BIO-RAD LABORATORIES (Hercules, CA, USA). HiTrap Chelating columns (1ml) for His-Tag fusion protein purification were purchased from Amersham Biosciences Europe GmbH (Freiburg, Germany).

Strains, Plasmids, Media, and Growh Conditions

Thermus thermophilus strain HB27 (wild-type) (Oshima & Imahori, 1974) was used for cloning of *aroG* and its untranslated regions and the promoter of the *slpA* gene, which encodes the S-layer protein.

T. thermophilus strains were grown in complex medium or minimal medium (TMM) at 60–70°C. Complex medium was prepared as follows (Oshima & Imahori, 1974; Ramaley & Hixson, 1970). Three stock solutions were prepared: 1) 1 g nitrilo triacetic acid, 0.6 g $CaSO_4 \cdot 2\ H_2O$, 1 g $MgSO_4 \cdot 7\ H_2O$, 0.08 g NaCl, 1.03 g KNO_3, 6.89 g $NaNO_3$, and 1.39 g $Na_2PO_4 \cdot 2\ H_2O$ were dissolved in 980 ml of water (resulting in a turbid solution). 2) 0.257 g $FeCl_2$ were dissolved in 10 ml of water. 3) 0.5 ml H_2SO_4, 2.216 g $MnSO_4 \cdot H_20$, 0.5 g $ZnSO_4 \cdot 7\ H_2O$, 0.5 g H_3BO_3, 0.025 g $CuSO_4 \cdot 5\ H_2O$, 0.025 g $Na_2MoO_4 \cdot 2\ H_2O$, and 0.046 g $CoCl_2 \cdot 6\ H_2O$ were dissolved in 10 ml of water. Each solution was autoclaved separately and then mixed to obtain 10x Basal Salts solution. 100 ml of this solution were added to 8 g peptone, 4 g yeast extract, 2 g NaCl (20 g agar for plates) and dissolved in 850 ml of water. After adjusting the pH to 7.5 with 1 N NaOH, water was added to 1 l and the medium was autoclaved.

Minimal medium for *Thermus* was prepared according to the following protocol (Tanaka *et al*., 1981). Solution A: 5 g sucrose, 0.75 g K_2HPO4, 0.25 g KH_2PO_4, 2.5 g $(NH_3)_2SO_4$, 2 g NaCl, 5 g casamino acids (20 g agar for plates) were dissolved in 990 ml of water. The pH was adjusted to 7.0 to 7.2 with 1N NaOH, and the medium was autoclaved. Then the following stock solutions were added: 10 µl of biotin stock (10mg/ml, filter-sterilized), 200 µl of thiamin stock (5 mg/ml, filter-sterilized), 100 µl of molybdate solution (1.2 g $Na_2MoO_4 \cdot 2\ H_2O$ in 100 ml of water), 100 µl of vanadium solution (0.1 g $VOSO_4 \cdot 3\ H_2O$ in 100 ml of water), 100 µl of manganese solution (0.5 g $MnCl_2 \cdot 4\ H_2O$ in 100 ml of 0.1 N HCl), 100 µl of copper/zinc solution (0.06 g $ZnSO_4 \cdot 7\ H_2O$, 0.015 $CuSO_4 \cdot 5\ H_2O$ in 100 ml of water), 10 ml of solution B (0.125 g $MgCl_2 \cdot 6\ H_2O$, 0.025 g $CaCl_2 \cdot 2\ H_2O$ in 100 ml of water), 100 µl of solution C (6 g $FeSO_4 \cdot 7\ H_2O$, 0.8 g $CoCl_2 \cdot 6\ H_2O$, 0.02 g $NiCl_2 \cdot 6\ H_2O$, 0.02 g $NiCl_2 \cdot 6\ H_2O$ in 100 ml 0.01 N H_2SO_4).

Isolation of genomic DNA from *Thermus* sp.

Thermus strains were grown in 30 ml of selective medium overnight at 60–70°C. Cells were collected by centrifugation for 15 minutes at 3,500xg and resuspended in 12 ml of Tris-EDTA buffer (100 mM Tris-HCl, pH 8.0, 10 mM EDTA). After another centrifugation step, the pellet was resuspended in 3 ml of the same buffer and 60 mg lysozyme were added for a 20-minutes incubation at 42°C. The suspension was frozen and thawed for three times (-80°C and +60°C) and incubated with 600 µg of RNase I at 37°C for 30 min. After addition of 780 µl of 10 % sodium dodecylsulfate and 78 µl of 0.5 M EDTA (pH 8.0), another 30-minutes incubation at 37°C followed. Proteins were degraded by

300 µg of Proteinase K during incubation at 56°C for 30 min. The suspension was extracted with phenol-methylene-chloride for three times and once with chloroform. DNA was precipitated by addition of 0.1 volume of 3 M sodium acetate, pH 4.8, and 2.5 volumes of ice-cold ethanol. After washing with 70 % ethanol and drying at 65°C the DNA was resolved in 0.5 to 1 ml of Tris-EDTA buffer by gentle shaking at room temperature overnight.

Cloning of *T. thermophilus* genomic sequences

aroG of *T. thermophilus* encoding a monofuntional chorismate mutase was cloned by PCR using primers OLCW22 (5'-GGG GTA CCA TGG TCC GGG GCA TCC GCG GCG CCA TC-3') and OLCW23 (5'-GGG GTA CCC TAC TGG GCG CTT TCC AGG TCG GGC CG-3') using genomic wild-type DNA as template. These primers annealed directly 3' and 5', respectively, of the open reading frame and contained an overhang with a *Kpn*I restriction site for cloning into pBluescript II SK (pME2030). The sequence of the *aroG* locus was obtained from the Göttingen Genomics Laboratory (Göttingen, Germany; personal communication).

For construction of an *ΔaroG* deletion cassette, a 760-bp fragment of the 5' untranslated region (UTR) of *aroG* was cloned by PCR using primers OLKH50 (5'-CAG TGA AAG CTT GGT TAC GGC CTA TCC TAA GG-3') and OLCW1 (5'-CAG TGA AAG CTT GCG GTC TTC GTG AGC TAC GC-3') containing a *Hin*dIII restriction site using genomic wild-type DNA as template. A 1.5-kb fragment of the 3' UTR of *aroG* was amplified using primers OLCW3 (5'-GAG CAT GTC GAC CCA AGT GCG CGC ACG TCG-3') and OLKH46 (5'-TCA CGC GTC GAC CAA GGA CCT GGT GCG CAA G-3') introducing *Sal*I sites. *pyrE* was cloned from plasmid pINV (Tamakoshi *et al*., 1997) with primers OLKH28 (5'-CCA TCG ATA TGG ACG TCC TGG AGC TTT-3') and OLKH29 (5'-CCA TCG ATC TAG ACC TCC TCC AAG GG-3') containing *Cla*I sites. The plasmid containing the resulting knock-out cassette was named pME2417.

The *slpA* promoter was amplified using genomic wild-type DNA as template and primers OLCW9 (5'-CCC AAT TGC CCG GGG GGA GTA TAA CAG-3') containing a *Mun*I site and OLCW10 (5'-GGA ATT CAT GCC TCA CAC CTC CTT AGG G-3') containing an *Eco*RI site for cloning into the *Eco*RI site in the multiple cloning site of pMK18 (de Grado *et al.*, 1999) resulting in vector pME2418.

Purification of *Thermus* chorismate mutase

aroG encoding *Thermus* chorismate mutase was fused to an N-terminal His-tag sequence encoding six histidine residues and a thrombin cleavage site in expression vector pET15b (CN Biosciences GmbH, Schwalbach/Ts., Germany). The protein was expressed in *E. coli* strain BL21 (DE3) (F^- *ompT hsd* $S_B(r^-_B m^-_B)$ *gal dcm (DE3)*). *E. coli* was transformed according to the following protocol (Dagert & Ehrlich, 1979). 30 ml of an LB culture containing ampicillin at a concentration of 100 µg/ml were inoculated with 180 µl of an overnight culture. Cells were grown to an OD_{600} of 1, chilled on ice for 5 min with occasionally shaking. Cells were centrifuged for 5 min at 3,500xg at 4°C, the pellet was dissolved in 15 ml of ice-cold 100 mM $CaCl_2$ solution and kept on ice for 25 min. Cells were centrifuged as above and resuspended in 1.5 ml of ice-cold 100 mM $CaCl_2$ solution. 50 µl to 100 µl of these cells were mixed with DNA in an Eppendorf cup and incubated on ice for 30 min. A heat shock was performed for 2 min at 42°C, followed by an incubation step on ice for 5 min. 1 ml of LB medium was added, the cells were grown for one hour at 37°C with shaking, then plated on LB plates containing ampicillin and incubated at 37°C overnight.

For protein expression, cells were grown in 2 ml LB medium containing ampicillin over night at 37°C and diluted into 100 ml of fresh medium. Cells continued to grow until OD_{600} reached 0.6. Then TtCM expression was induced by addition of IPTG from a 100 mM stock to a final concentration of 1 mM, and incubation was continued for another three hours. The flask was placed on ice for 5 min and then cells were harvested by centrifugation at 5,000xg for 5 min at 4°C. Cells were resuspended in 25 ml of cold 50 mM Tris-HCl, pH 8.0, and centrifuged as above. The pellet was stored frozen at -20°C until purification.

Cells were resuspended in 4 ml of ice-cold *binding buffer* (5 mM imidazole, 0.5 M NaCl, 20 mM Tris-HCl, pH 7.9, adjusted to a final pH of 7.9) and disrupted in the one-shot model of the cell disruption equipment from Constant Systems LTD. (Warwick, UK) at 2 kbar. Cell debris was removed by centrifugation at 17,000xg for 20 min. The mesophilic host proteins in the crude extract were heat-inactivated by incubation at 65°C for 15 min and centrifuged as above. A HiTrap Chelating column (1ml) was charged with nickel ions by loading 0.5 ml of *charge buffer* (100 mM $NiSO_4$) and washing with water until unbound ions were removed. The column was equilibrated with *binding buffer*, loaded with the supernatant of the heat-inactivation step and unbound protein was washed from the column with *binding buffer*. Bound protein was eluted with a gradient of *elution buffer* (1 M imidazole, 0.5 M NaCl, 20 mM Tris-HCl, pH 7.9, adjusted to pH 7.9) from 0-100% over 20 column volumes. Nickel ions were removed from the column with *strip buffe*r (100 mM EDTA, 0.5 M NaCl, 20 mM Tris-HCl, pH 7.9, adjusted to pH 7.9) and reequilibrated with water. PMSF was added to the cell suspension before disruption and to the buffers at a concentration of 0.1 mM. Buffers were filter-sterilized and degased before use.

T. thermophilus chorismate mutase was detected in the collected fractions by enzyme assay and SDS-polacrylamide gel electrophoresis. Fractions were pooled, dialysed against 10 mM potassium phosphate buffer, pH 7.6, and frozen in liquid nitrogen.

Chorismate mutase assay

During purification and for investigation of allosteric effects, the following stop assay for chorismate mutase activity was performed. Reactions were carried out in a volume of 500 µl in 100 mM Tris-HCl, pH 7.6, 2 mM EDTA, 20 mM dithiothreitol, and contained 10 µl of fractions and 1 µg of purified enzyme, respectively. Chorismic acid as substrate was present in a concentration of 1 mM. The enzymatic reaction was started in a water bath at 70°C by addition of 100 µl of chorismic acid and stopped after 10 minutes by addition of 500 µl of 1 M HCl. The reaction was continued in a water bath at 30°C, because the extinction coefficient of phenylpyruvate was determined at 30°C. After another 10 min, 4 ml of 1 M NaOH neutralized and diluted the solution. Blank absorbances were substracted from the absorbances measured for enzyme activities.

For determination of the rate constants for thermal inactivation, samples containing 1 µg of purified enzyme were preincubated in a PCR block for different periods of time at increasing temperatures. The samples were chilled on ice, and residual activities were determined in a stop assay with 2 mM chorismic acid and 2 min of catalytic turnover at 70°C.

Determination of the native molecular weight

The native molecular weight of the *T. thermophilus* chorismate mutase was determined by gelfiltration on a Superdex 200-pg column using 50 mM potassium phosphate, 150 mM NaCl, pH 7.6, as elution buffer. The void volume of the column was determined with blue dextran, and a calibration plot was defined using a gel filtration chromatography standard from Bio-Rad containing thyroglobulin (M_r 670,000), bovine γ-globuline (M_r 58,000), chicken ovalbumin (M_r 44,000), equine myoglobin (M_r 17,000), and vitamin B-12 (M_r 1,350). In addition, the molecular weight was estimated by native polyacrylamide gel electrophoresis using a gradient from 10-20% polyacrylamide (Andersson *et al*., 1972) and chicken ovalbumin (M_r 44,000), bovine serum albumin (M_r 66,000 and 132,000), and urease (M_r 272,000 and 545,000) as standard.

CD spectroscopy

The CD spectrum of *T. thermophilus* chorismate mutase was measured in the range of 180-260 nm with a Jasco J-720 spectropolarimeter (Labor- und Datentechnik GmbH, Groß-Umstadt, Germany) at 1 nm resolution. The pathlength of the cell was 0.1 cm. The spectrum was recorded as an average of five scans at 20°C with 3 µM of chorismate mutase in 10 mM potassium phosphate buffer, pH 7.6. Appropriate buffer baseline spectra were substracted from the protein spectra.

Sequence alignments and homology modeling studies

All sequence analyses were performed using the LASERGENE Biocomputing software (DNASTAR, Ltd., London, UK). Alignments were also created based on the CLUSTAL W method (Thompson *et al*., 1994) using the Network Protein Sequence analysis service (Combet *et al*., 2000). For homology modeling, the deduced primary structure of *T. thermophilus* CM was aligned to the crystallographic data of *B. subtilis* CM as described in the Brookhaven protein database (2cht) and refined by the SWISS-MODEL service (Guex & Peitsch, 1997; Peitsch, 1995). By using the WebLab Viewer software (Molecular Simulations, San Diego, CA), three-dimensional structure models were generated by calculation of secondary structures. Ligand binding sites in *T. thermophilus* CM were identified applying the Binding Site Analysis module of the InsightII 2001 software (Molecular Simulations, San Diego, CA).

Results

The *aroG* gene of *T. thermophilus* is similar to genes encoding chorismate mutases of the AroH class

The chorismate mutase encoding gene *aroG* from *T. thermophilus* was cloned by PCR using genomic DNA as template. This gene‘s open reading frame consists of 369 basepaires encoding a deduced protein of 122 amino acids (Fig. 16). In the promoter region, a Pribnow box 10 bp upstream of the ORF (TAGGAT) as well as a –35 box motif (TTGCCC) were identified, which are similar to the consensus sequences of *E. coli* promoters and other characterized *Thermus* promoters (Faraldo *et al*., 1992).

A BLAST analysis of the encoded protein sequence revealed highest similarity to the group of AroH chorismate mutases which, included *B. subtilis* CM like described above. An alignment of the encoded proteins‘ sequences showed the highest identity of 49% in the residues in *T. thermophilus* chorismate mutase (TtCM) and the *G. stearothermophilus* enzyme (GsCM) whereas the identity equaled 46% between TtCM and the well-characterized *B. subtilits* chorismate mutase (BsCM) (Fig. 17A). *aroG* showed a similarity of the nucleotides of 41% to the corresponding gene from *G. stearothermophilus*.

A phylogenetic tree based on the amino acid sequences of the best characterized CMs demonstrated the high similarity of the *T. thermophilus* enzyme with the AroH class chorismate mutase from *B. subtilis* and the structural difference to other well-known CMs of the AroQ type like those of *E. coli and S. cerevisiae* (Fig. 17B). Therefore, *T. thermophilus* CM was classified into the AroH group of monofunctional chorismate mutases.

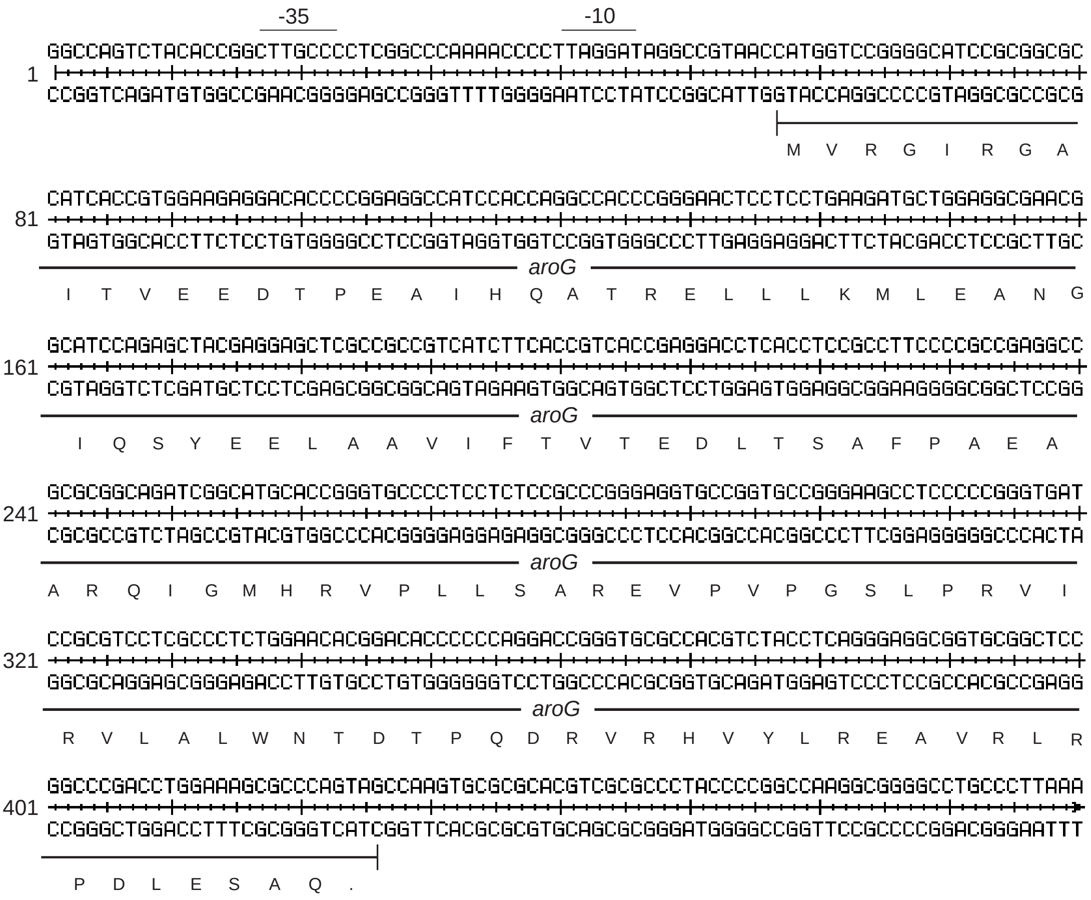
-35
-10
GGCCAGTCTACACCGGCTTGCCCCTCGGCCCAAAACCCCTTAGGATAGGCCGTAACCATGGTCCGGGGCATCCGCGGCGC
1
CCGGTCAGATGTGGCCGAACGGGGAGCCGGGTTTTGGGGAATCCTATCCGGCATTGGTACCAGGCCCCGTAGGCGCCGCG
M V R G I R G A
CATCACCGTGGAAGAGGACACCCCGGAGGCCATCCACCAGGCCACCCGGGAACTCCTCCTGAAGATGCTGGAGGCGAACG
81
GTAGTGGCACCTTCTCCTGTGGGGCCTCCGGTAGGTGGTCCGGTGGGCCCTTGAGGAGGACTTCTACGACCTCCGCTTGC
aroG
I T V E E D T P E A I H Q A T R E L L L K M L E A N G
GCATCCAGAGCTACGAGGAGCTCGCCGCCGTCATCTTCACCGTCACCGAGGACCTCACCTCCGCCTTCCCCGCCGAGGCC
161
CGTAGGTCTCGATGCTCCTCGAGCGGCGGCAGTAGAAGTGGCAGTGGCTCCTGGAGTGGAGGCGGAAGGGGCGGCTCCGG
aroG
I Q S Y E E L A A V I F T V T E D L T S A F P A E A
GCGCGGCAGATCGGCATGCACCGGGTGCCCCTCCTCTCCGCCCGGGAGGTGCCGGTGCCGGGAAGCCTCCCCCGGGTGAT
241
CGCGCCGTCTAGCCGTACGTGGCCCACGGGGAGGAGAGGCGGGCCCTCCACGGCCACGGCCCTTCGGAGGGGGCCCACTA
aroG
A R Q I G M H R V P L L S A R E V P V P G S L P R V I
CCGCGTCCTCGCCCTCTGGAACACGGACACCCCCCAGGACCGGGTGCGCCACGTCTACCTCAGGGAGGCGGTGCGGCTCC
321
GGCGCAGGAGCGGGAGACCTTGTGCCTGTGGGGGGTCCTGGCCCACGCGGTGCAGATGGAGTCCCTCCGCCACGCCGAGG
aroG
R V L A L W N T D T P Q D R V R H V Y L R E A V R L R
GGCCCGACCTGGAAAGCGCCCAGTAGCCAAGTGCGCGCACGTCGCGCCCTACCCCGGCCAAGGCGGGGCCTGCCCTTAAA
401
CCGGGCTGGACCTTTCGCGGGTCATCGGTTCACGCGCGTGCAGCGCGGGATGGGGCCGGTTCCGCCCCGGACGGGAATTT
P D L E S A Q .

Fig. 16: Nucleotide sequence and deduced amino acid sequence of the *aroG* gene from *T. thermophilus*. The open reading frame of *aroG* encoding a monofunctional chorismate mutase is shown together with the promoter region containing a typical –35 and a –10 consensus sequence.

On the protein level, residues Arg7 (Arg7 in TtCM), Phe57 (Phe57), Cys75 (Ser74), Glu78 (Glu77), Arg90 (Arg89), Tyr108 (Tyr107), and Leu115 (Leu114) constituting the active site of BsCM are highly conserved (Fig. 17A). Only residue Cys75 is substituted by a serine at position 74 in TtCM, a residue, however, which may fulfil the same function in hydrogen bond formation.

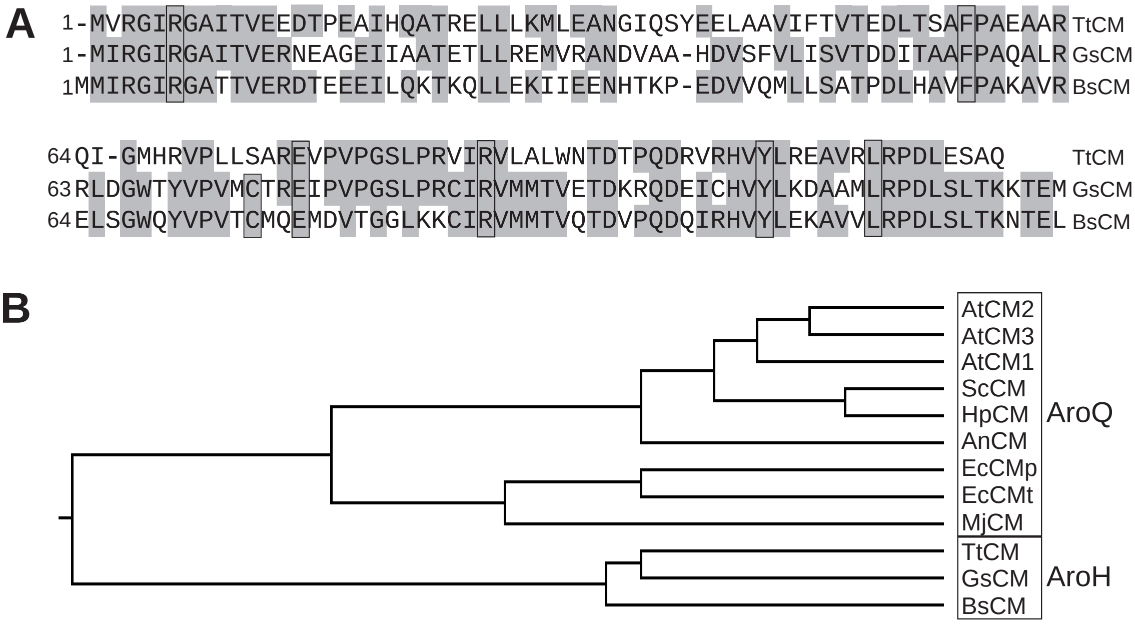
A
1-MVRGIRGAITVEEDTPEAIHQATRELLLKMLEANGIQSYEELAAVIFTVTEDLTSAFPAEAAR TtCM
1-MIRGIRGAITVERNEAGEIIAATETLLREMVRANDVAA-HDVSFVLISVTDDITAAFPAQALR GsCM
1MMIRGIRGATTVERDTEEEILQKTKQLLEKIIEENHTKP-EDVVQMLLSATPDLHAVFPAKAVR BsCM
64 QI-GMHRVPLLSAREVPVPGSLPRVIRVLALWNTDTPQDRVRHVYLREAVRLRPDLESAQ TtCM
63 RLDGWTYVPVMCTREIPVPGSLPRCIRVMMTVETDKRQDEICHVYLKDAAMLRPDLSLTKKTEM GsCM
64 ELSGWQYVPVTCMQEMDVTGGLKKCIRVMMTVQTDVPQDQIRHVYLEKAVVLRPDLSLTKNTEL BsCM
B
AtCM2
AtCM3
AtCM1
ScCM
HpCM
AnCM
EcCMp
EcCMt
MjCM
AroQ
TtCM
GsCM
BsCM
AroH

Fig. 17: The chorismate mutase of *T. thermophilus* shows similarity to *Bacillus* enzymes. **A**, The alignment shows a comparison of the deduced amino acid sequence of *T. thermophilus* chorismate mutase (TtCM) with those of *Geobacillus stearothermophilus* (GsCM) and *Bacillus subtilis* (BsCM). Identical residues are shaded grey, residues constituting the active site of BsCM are indicated by boxes. **B**, In the phylogenetic tree of different chorismate mutases, the *T. thermophilus* enzyme is positioned close to the AroH type enzyme of *Bacillus subtilis*. The *E. coli* and *Methanococcus* enzymes and the eukaryotic chorismate mutases represent the AroQ type of enzymes. Considered were chorismate mutases of *Arabidopsis thaliana* (AtCM1, AtCM2, and AtCM3), *Saccharomyces cerevisiae* (ScCM), *Hansenula polymorpha* (HpCM), *Aspergillus nidulans* (AnCM), *Escherichia coli* (EcCMp (P-protein) and EcCMt (T-protein)), *Methanococcus jannaschii* (MjCM), *Thermus thermophilus* (TtCM), *Geobacillus stearothermophilus* (GsCM), and *Bacillus subtilis* (BsCM). The tree was created with the LASERGENE Biocomputing software applying the CLUSTAL method with a gap weight of 10 and a gap length weight of 10.

The *aroG* gene of *T. themophilus* encodes a thermostable chorismate mutase

T. thermophilus TtCM was purified and characterized in order to investigate its tertiary and quaternary structure, as well as its catalytic and regulatory features. TtCM was prepared from *E. coli* according to the purification protocol described in Fig. 18A and B. The purification was based on the different thermal stabilities of TtCM and the host’s proteins and on the fusion to a 6His-tag for affinity purification. After removal of cell debris, the crude extract was heated to 65°C for 15 min during which time most of the mesophilic *E. coli* proteins denatured leading to a fourfold purification of TtCM. By affinity chromotography on a HiTrap Chelating column charged with nickel ions another 14-fold purification with a final 82% yield of recovery was acchieved. *T. thermophilus* CM was homogenous as judged by SDS/PAGE (Fig. 18B). The mobility of the purified enzyme corresponded to a molecular mass of about 16 kDa, which is similar to the size of the chorismate mutase protein containing the 6His-tag and a thrombin cleavage site (15,812 Da in comparison to 13,649 Da for TtCM only).

The stability of this thermophilic protein’s fold was examined in a thermal inactivation study. Decrease of activity caused by heat denaturation was measured in an enzyme assay after prolonged preincubation at increasing temperatures. At the optimal growth temperature of 70°C, *T. thermophilus* chorismate mutase had a half-life of over 10 minutes (Fig. 18C). No obvious difference was found at temperatures of 80°C or as high as 105°C. The rate constant of thermal inactivation equaled 0.071 min^{-1} with a half-life of 9.7 minutes at the highest temperature tested. The values obtained for this thermophilic enzyme were considerably higher than those from mesophilic chorismate mutases. For the *H. polymorpha* or *S. cerevisiae* enzymes, for instance, half-lives of 1.84 min and 2.74 min at 60°C were observed showing less thermal stability compared to the CM of the thermophile *T. thermophilus* (Helmstaedt *et al*., 2002; Krappmann *et al*., 2000).

The *T. thermophilus* chorismate mutase is an AroH class enzyme

The TtCM secondary structure was investigated by recording a circular dichroism spectrum in far UV light. This spectroscopic characterization confirmed the grouping of TtCM into the AroH class of chorismate mutases which consist of α-helices, β-sheets and about one-third of turns.

A

fraction	total protein (mg)	spec. activity (U/mg)	yield (%)	purification (x-fold)
crude extract	14.4	0.4	100	1
crude extract after heat precipitation	2.9	1.8	87	4
affinity chromatography	0.19	25	82	62

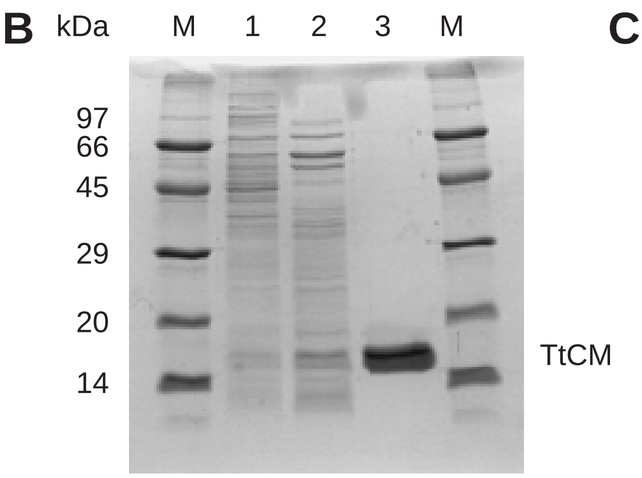

C

	k (min^{-1})	$t_{1/2}$ (min)
70ºC	0.067	10.4
80ºC	0.070	9.9
105ºC	0.071	9.7

Fig. 18: Purification steps of the chorismate mutase TtCM of *T. thermophilus*. **A**, Purification protocol for chorismate mutase. Specific activity was determined in a stop assay with 1 mM chorismate, 2 µg of protein, and 10 min of catalytic turnover. **B**, SDS-polyacrylamide gel of the purification steps. 1, Crude extract of *E. coli* BL21 (DE21) [pME2416]; 2, supernatant of heat inactivation (15 min at 65°C); 3, HiTrap Chelating column (Ni charged) pool. 5 µg of protein were applied to each lane. M, marker proteins with the indicated molecular mass in kilodaltons. **C**, Rate constants (*k*) of thermal inactivation and half-lives ($t_{1/2}$) of TtCM were determined in stop assays at 70°C with 1 µg of protein, 2 mM chorismate, and 2 min of catalytic turnover. One hundred percent of original activity equaled 148 units per mg. Each value is an average of four independent measurements with a standard deviation not exceeding 20%.

A maximum at 191 nm and a minimum between 210 and 212 nm were detected (Fig. 19). The maximum indicated α-helical structures, because a maximum at 191-193 nm can be observed in all-helical proteins whereas the maximum of β-sheet structures is recorded at a slightly higher wavelength of 195–200 nm. The minimum between 210 and 212 nm also resembled spectra of helical proteins, which show two minima at 208-210 nm and 222 nm in contrast to one minimum between 216 and 218 nm for proteins with β-sheet architecture. However, the minimum was shifted to slightly higher wavelengths and the typical second minimum at 222 nm was not recorded showing the presence of β-strands as well. The spectrum did not contain other minima or maxima typical for other secondary structures like β-turns. Thus, the structural information obatined by CD measurements suggested that the secondary structure of TtCM resembled that of AroH-type chorismate mutases.

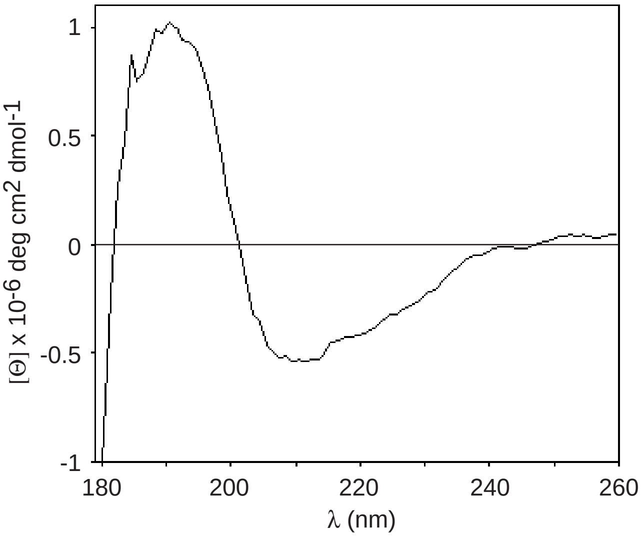

Fig. 19: Characterization of TtCM secondary structure. A circular dichroism spectrum was obtained as an average of five scans at 20°C in 10 mM potassium phosphate buffer, pH 7.6, at a protein concentration of 3 µM.

The secondary and tertiary structure of TtCM was modeled applying the SWISS-MODEL service (Guex & Peitsch, 1997; Peitsch, 1995; Peitsch, 1996). Due to the high homology between the genes encoding BsCM and TtCM, the *T. thermophilus* monomer fold could be calculated based on the three-dimensional structural data of BsCM (Fig. 20A). According to this model, the secondary structure consists of a 5-stranded mixed β-sheet containing two parallel α-helices on one side of the β-sheet and a 5-residue 3_{10} helix at the C terminus. From the topology diagram (Fig. 20B), it is obvious that the N terminus is located in the middle of the β-sheet and that one β-strand (S4) and the helices are antiparallel to the other four β-strands. In summary, the CD spectrum in combination with the modeling studies demonstrated the highly-ordered structure of an α/β-domain protein similar to AroH chorismate mutases.

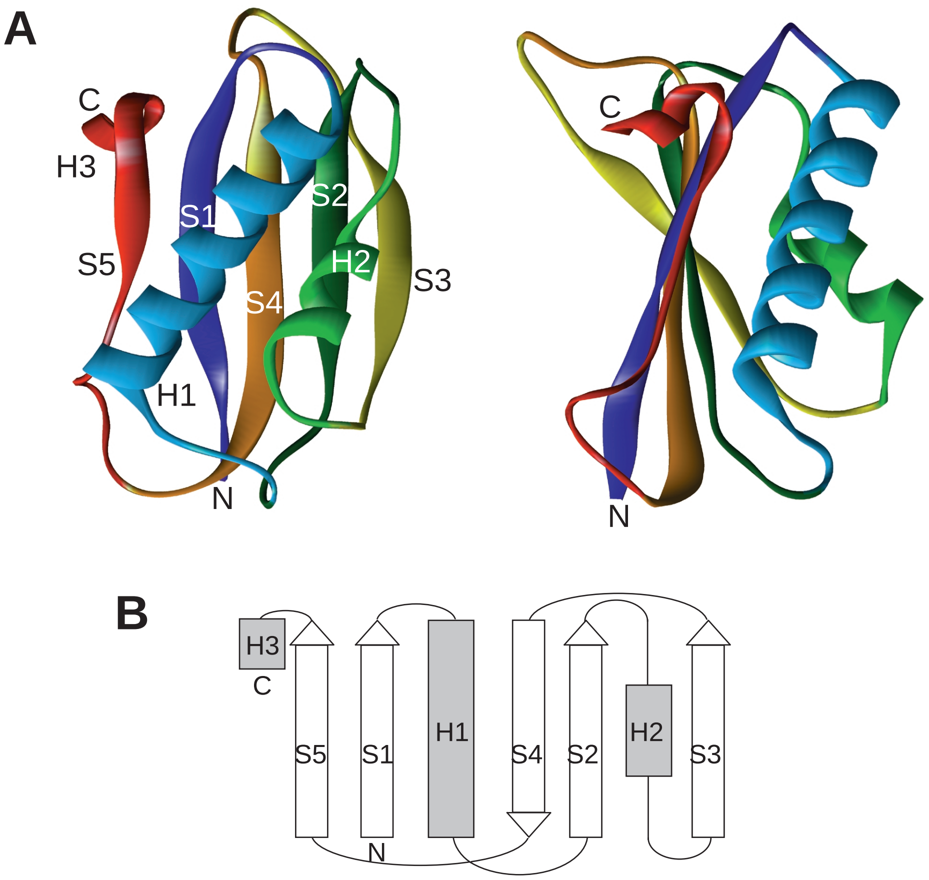

Fig. 20: The *T. thermophilus* chorismate mutase (TtCM) shares structural similarities with the *B. subtilis* enzyme. **A**, The deduced amino acid sequence of the *aroG* gene product TtCM of *T. thermophilus* was modeled on the known crystal structure of the *B. subtilis* BsCM monomer using the SWISS-MODEL service. In this model (front view and side view), the amino- and carboxytermini are labeled N and C, respectively, the strands of the β-sheet are labeled S1 to S5 and the helices H1 to H3. **B**, Topology diagram of the *T. thermophilus* chorismate mutase TtCM.

The oligomeric *T. thermophilus* chorismate mutase TtCM is feedback-inhibited by tyrosine

The reaction catalyzed by chorismate mutase is the first committed step in the biosynthesis of the amino acids tyrosine and phenylalanine. This step, therefore, is a potential point of regulation for this biosynthetic pathway. Regulation of chorismate mutase activity by prephenate or the aromatic amino acids occurs in many organisms, although by different mechanisms. Since allosteric regulation of enzymes is based on their oligomeric state, the oligomerization of TtCM was investigated.

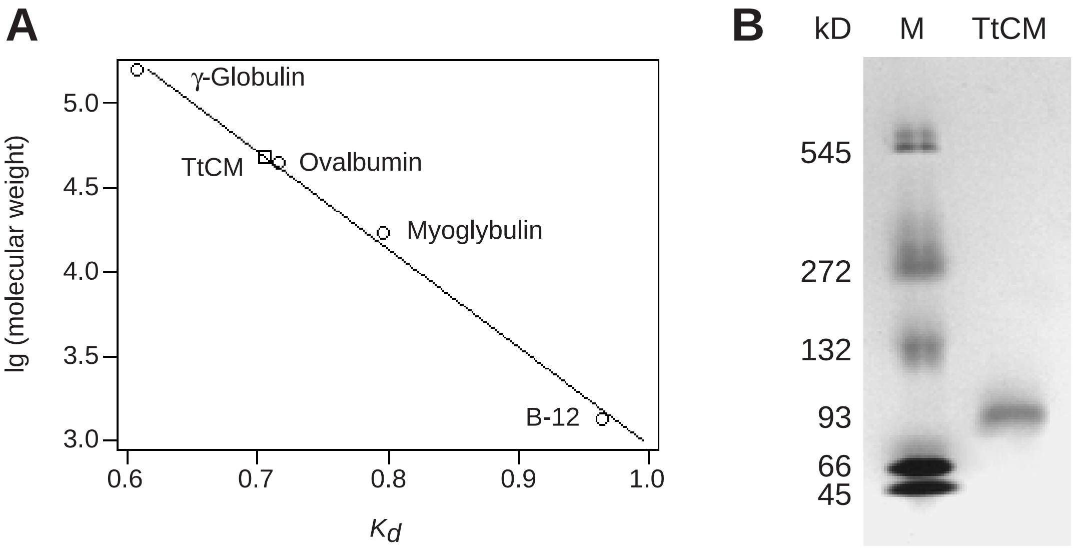

Fig. 21: Determination of the native molecular weight of TtCM. **A**, Calibration of a Superdex 200 pg column was performed using a void volume of 46.8 ml as determined by blue dextran and a total column volume of 120 ml. The K_d of native chorismate mutase containing the His-tag (□) was calculated to be 0.706. According to the calibration plot this value corresponds to a protein with an apparent molecular mass of 47,592 Da. This size equaled that of a trimeric enzyme consisting of monomers with a calculated molecular mass of 15,812. **B**, Estimation of the native molecular weight by gradient polyacrylamide gel electrophoresis using chicken ovalbumin (45 kDa), bovine serum albumin (66 and 132 kDa), and urease (272 and 545 kDa) as standard proteins yielded a size of 92,972 Da indicating the existence of a hexameric enzyme.

The apparent molecular weight of native TtCM was determined by gel filtration and native polyacrylamide gel electrophoresis. TtCM eluted from a Superdex 200-pg at a volume corresponding to a K_d of 0.706 leading to a molecular mass of 47,592 Da according to the calibration graph obtained with standard proteins (Fig. 21A). Based on the predicted molecular mass, this volume equaled well the size of a homotrimeric enzyme (47,436 Da). Estimation of the native size in a gradient polyacrylamide gel showed that TtCM might even exist as a hexamer (Fig. 21B). The migration distance in comparison to the standard proteins indicated a protein aggregate with a mass of 92,972 Da which met the 5.9-fold mass of a monomer. However, no proteins larger than a TtCM trimer were detected during gel filtration. In summary, these data suggest a trimer which under some conditions can even be part of a higher-order oligomer consisting of two trimers which result in a hexamer.

In the BsCM homologue, the active site pockets are located between adjacent monomers in a cleft, which is formed by helix H2 (containing residue Phe57), β-strand S3 (Cys75 and Glu78), and the connecting loop L60s from one subunit and parts of strands S1 (Arg7), S4 (Arg90), S5 (Tyr108), loop L80s, and H3 (Leu115) from the adjacent subunit. The conservation of the active site residues like many others as seen in the amino acid sequence alignment (Fig. 17A) also demonstrated that the quaternary structure of TtCM resembled that of the trimeric *B. subtilis* enzyme.

The influence of the aromatic amino acids on the activity of *T. thermophilus* chorismate mutase was tested in a stop assay using increasing concentrations of tyrosine, tryptophan, and phenylalanine, respectively (Fig. 22). 500 μM tyrosine inhibited TtCM activity to 40%, and a tyrosine concentration as high as 5 mM caused a reduction of activity to 5%. Neither phenylalanine, differing from tyrosine by the lack of the hydroxyl group at position four of the aromatic ring, nor tryptophan caused any alteration in enzyme activity in the concentration range used. Thus, a considerable degree of inhibition was measured at a concentration equaling the intracellular tyrosine pool of 0.5 mM (Jones & Fink, 1982).

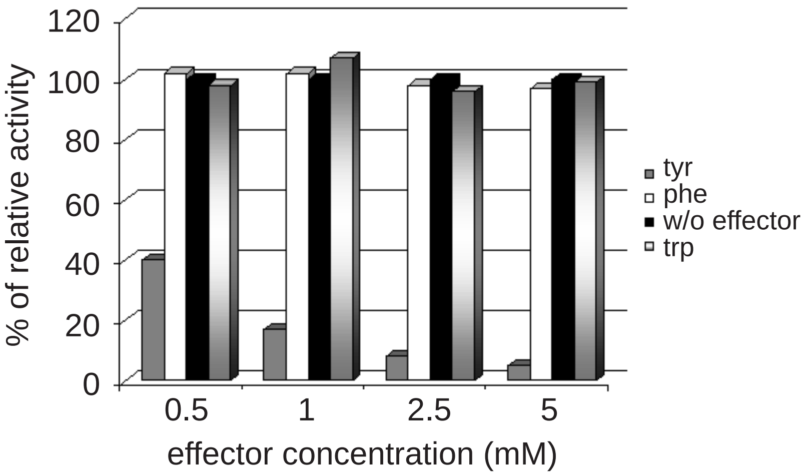

Fig. 22: Allosteric effects of aromatic amino acids on the specific activity of *T. thermophilus* chorismate mutase TtCM. Catalytic activities were determined with 1 μg of protein, 1 mM chorismate, 10 min of catalytic turnover at 70°C, and the indicated effector concentrations. One hundred percent of catalytic activity equaled 24 units per mg. Each value is the mean of four independent measurements with standard deviations not exceeding 20%.

Construction of an *aroG* disruption cassette for *T. thermophilus*

Chorismate mutases are well characterized regarding catalysis and regulation. Now the second CM of a thermophilic organism was cloned, which in contrast to the thermophilic *M. jannaschii* enzyme was grouped into the AroH class of chorismate mutases. Therefore, the question arose, which factors in both structural classes contribute to stabilization and if these factors might be identified by stabilization of the well-known mesophilic representatives of these enzymes. Our aim was to generate a chorismate-mutase deficient *T. thermophilus* strain so that in the future stabilized chorismate mutases can be selected *in vivo* by expression of the mutagenized genes in this thermophilic organism. In addition, the construction of a CM-deficient *T. thermophilus* strain together with the cloned *aroG* gene should provide another selection marker for this organism.

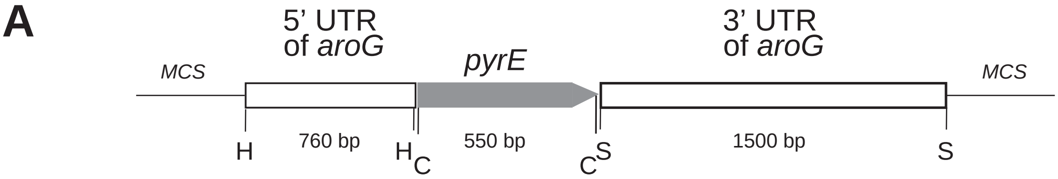

B

```
              -1                  +1
5'- . . . GTA ACC AAG CTT ATC GAT ATG GAC GTC CTG GAG CTT . . . pyrE (516 bp) . . .
          CAT TGG TTC GAA TAG CTA TAC CTG CAG GAC CTC GAA
                  -------  -------
                  HindIII   ClaI   M   D   V   L   E   L
```

```
                          +552                +370
. . . CCC TTG GAG GAG GTC TAG ATC GAT ACC GTC GAC CAA GTG CGC GCA . . . -3'
      GGG AAC CAC CAC CAG ATC TAG CTA TGG CAG CTG GTT CAC GCG CGT
                              -------     -------
       P   L   E   E   V   .   ClaI        SalI
```

Fig. 23: Construction of an *aroG* deletion cassette for *T. thermophilus*. **A**, *pyrE* from *T. thermophilus* encoding orotate phosphoribosyltransferase (EC 2.4.2.10) and the 5‘ and 3‘ untranslated regions (UTR) of *aroG* were amplified by PCR using primers which contained the indicated restriction sites in an overhang and cloned into pBluescript II SK (Primers OLKH50 and OLCW1, OLCW3 and OLKH46, OLKH28 and OLKH29). H, *Hin*dIII; C, *Cla*I; S, *Sal*I. **B**, Detailed sequence of the transitions between the untranslated regions and the *pyrE* gene. The cloned 5’ UTR fragment ends at –1 directly upstream of the *aroG* open reading frame, and the cloned 3’ UTR fragments starts directly 3’ of the *aroG* open reading frame at position +370.

The *pyrE* gene encoding the orotate phosphoribosyl-transferase (EC 2.4.2.10) was selected for construction of an *aroG* knock-out cassette because this marker was successfully used before (Tamakoshi *et al.*, 1997). This gene and fragments of the untranslated regions (UTRs) of *aroG* were cloned by PCR (Fig. 23). The 5‘ UTR fragment was 760 bp in length and the 3’ UTR was 1.5 kb long so that an altogether 2.26-kb long region of homology was obtained for homologous recombination with the *aroG* locus. The *pyrE* open reading frame of 550 bp was cloned between these regions separated from the *aroG* promoter by 12 bp containing the two restriction sites, which should allow proper transcription of the selection marker. Thus, this 2.8-kb long fragment can be used for transformation into a *∆pyrE* strain for selection of phe$^-$ tyr$^-$ ura$^+$ clones.

Construction of a *T. thermophilus* expression vector for chorismate mutases

An expression vector for *T. thermophilus* was constructed for the *in vivo* screening of stabilized chorismate mutases. The parent vector was pMK18 (de Grado *et al.*, 1999). This vector contained a *Thermus* and *E. coli* replicon, respectively, and a stabilized kanamycin resistance gene (*kat*) from *S. aureus* encoding the thermostable kanamycin nucleotidyl transferase driven by the promoter of the S-layer encoding gene *slpA*. This promoter which is also functional in *E. coli*, was also cloned for expression of other genes in this vector. It was subcloned as a *Mun*I/*Eco*RI fragment into the multiple cloning site (MCS) of pMK18, which is derived from pUC18 (Fig. 24). The restriction sites *Eco*RI and *Acc*65I downstream of this promoter were thus available for cloning of mutagenized *ARO7* or other CM encoding genes in defined orientation.

Discussion

In this study, we isolated the chorismate mutase encoding gene (*aroG*) from *T. thermophilus* and characterized the first thermostable AroH-type chorismate mutase. The *T. thermophilus* enzyme was grouped into the AroH class of CMs because of its similarity to *B. subtilis* CM, its native size, and circular dichroism spectrum. An alignment of the TtCM primary sequence to that of the AroH enzyme from *B. subtitlis* (BsCM) yielded an identity of amino acid residues of 46%. By applying homology modeling, a secondary and tertiary structure was obtained, which strongly resembled that of BsCM. This structural analysis was supported by the CD spectrum which proved the existence of a protein fold containing α-helices as well as β-strands. The existence of a trimeric quaternary structure like in BsCM was indicated by the determined native molecular weight, which in one case equaled that of a trimer, but also was found to be that of a hexamer.

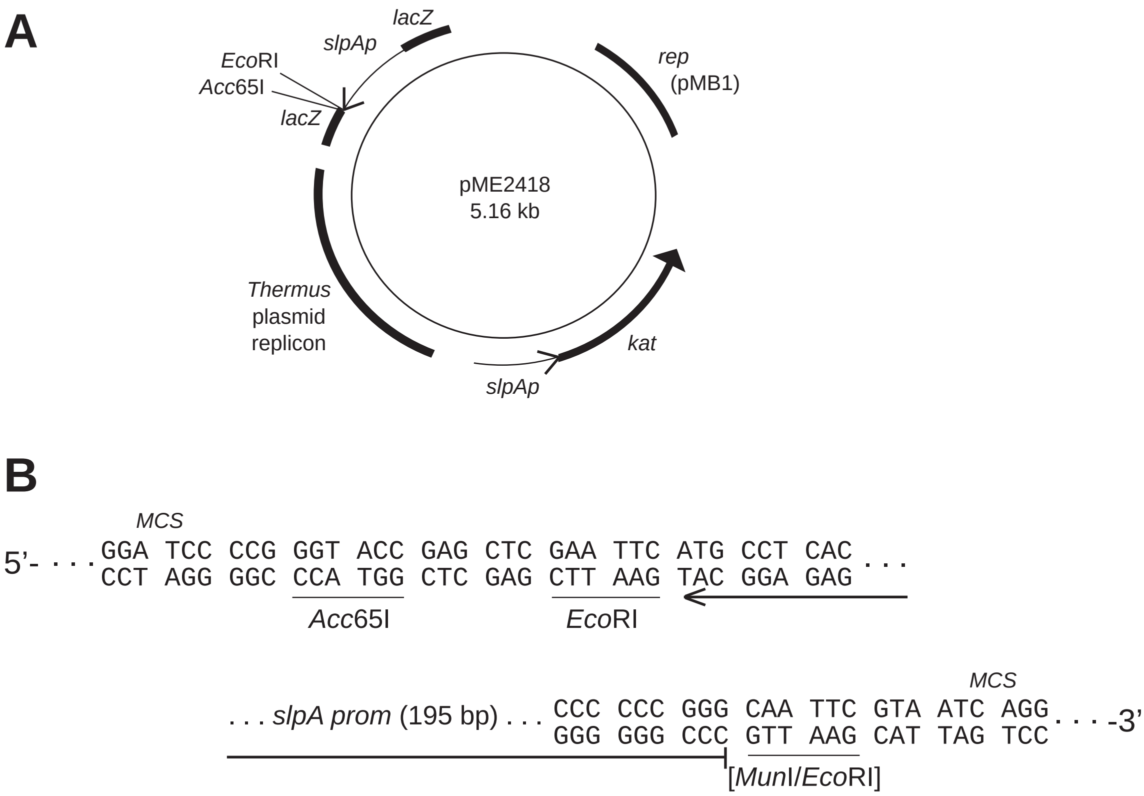
A
lacZ
slpAp
EcoRI
Acc65I
lacZ
rep
(pMB1)
pME2418
5.16 kb
Thermus
plasmid
replicon
kat
slpAp
B
MCS
5'- . . . GGA TCC CCG GGT ACC GAG CTC GAA TTC ATG CCT CAC . . .
CCT AGG GGC CCA TGG CTC GAG CTT AAG TAC GGA GAG
Acc65I
EcoRI
MCS
. . . slpA prom (195 bp) . . . CCC CCC GGG CAA TTC GTA ATC AGG . . . -3'
GGG GGG CCC GTT AAG CAT TAG TCC
[MunI/EcoRI]

Fig. 24: Construction of a *T. thermophilus* expression vector for protein stabilization *in vivo*. **A**, The promoter of *slpA* encoding S-layer protein, was integrated into the multiple cloning site (MCS) of a high-transformation efficiency vector (pMK18) containing a *Thermus* replicon of an indigenous plasmid, an *E. coli* replicon (*rep* (pMB1)), and a mutagenized kanamycin resistance gene (*kat*) from *S. aureus* driven by the *slpA* promoter. For cloning of, for instance, stabilized chorismate mutase genes in defined orientation two restriction sites are available directly downstream of the promoter (*Eco*RI) and six base pairs downstream in the MCS (*Acc*65I), which is located within the *lacZ* gene. **B**, Detailed sequence of the multiple cloning site of pME2418 containg the *slpA* promoter.

A BLAST search with the TtCM and BsCM sequence, respectively, identified other chorismate mutases which due to their amino acid similarity of over 40% can be grouped into this AroH class of enzymes. As mentioned above, these CMs were found in Gram-positive bacteria as well as in two cyanobacteria. Thus, with this TtCM an AroH representative was cloned which belongs to a third phylum of the eubacteria besides Gram-positives and cyanobacteria. AroQ enzymes, in contrast, were found in many different groups of bacteria, in archea and eukaryotes.

Another important finding obtained in this study is the tyrosine inhibition of *T. thermophilus* CM. Our results indicate that firstly, regulation of chorismate mutases is possible at high temperatures and that secondly, regulation is possible in these pseudo-α/β barrel enzymes. Comparison to real α/β barrels suggested the tyrosine binding site to be located at one end of the trimer between the loops connecting β-strands and α-helices. Active sites catalyzing many different reactions are known to reside at the carboxy end of the β-strands at one side of these barrel structures (Branden & Tooze, 1991). Thus, an allosteric binding site might also have evolved between the loops of the top of these chorismate mutases. Computer modeling studies identified a ligand binding pocket within the monomers. It was formed by residues from the carboxyterminal halves of H1 and S4, the N-terminal half of S2, from H2, and the loops connecting H1 with S2 and H2 with S3 (Fig. 20A). Cocrystalization of TtCM and tyrosine, site-directed mutagenesis and further binding studies will have to be performed to prove the presence of allosteric sites in TtCM and rule out competitive inhibition at the active sites. However, the increasing inhibition by tyrosine at concentrations of as high as 5 mM and the lack of a separate domain when compared with BsCM also indicate a competitive type of inhibition at the active site. This mode of tyrosine inhibition was proposed for inhibition of the *E. coli* T-protein and other uni-domain proteins of the TyrA familiy (Xie *et al*., 2000). In addition, the observed existence of hexamers in a native polyacrylamide gel suggested that inhibition of *T. thermophilus* chorismate mutase might occur by the formation of higher-order aggregates like it was found for the phenylalanine-inhibited *E. coli* P-protein (Baldwin *et al*., 1981) rather than through allosteric rearrangements within the trimeric enzyme. Thus, the oligomeric state of TtCM in the presence of tyrosine must further be examined to clarify the impact of tyrosine binding.

Highest homology of TtCM was found to the enzyme of *Geobacillus stearothermophilus* showing that more than one thermostable chorismate mutases of this type can be found in nature. Thus, the question arose, what makes up the differences between the mesophilic and thermophilic enzymes. Analysis of many thermophilic enzymes led to the knowledge that only little is changed in comparison to the mesophilic counterparts. The effects of substitutions most often are enhanced packing, additional salt bridges and hydrogen bonds, abbreviated loops, stabilized α-helix dipols, and restriction of conformational freedom by introduction of proline residues (Adams & Kelly, 1998; Szilagyi & Zavodszky, 2000).

The alignment between BsCM and TtCM yielded several amino acid substitutions which occur two, three, or four times. Analysis of their localization in the structural model revealed three principles of stabilization. I) Negatively charged residues (mainly Glu) in BsCM were substituted by small, uncharged ones (mainly Ala) in TtCM. Therefore, hydrophobic cores seem to be strengthened between helix H1 and β-strands S1 and S4 and between helices H1 and H2. II) Hydrophobic residues on the surface of BsCM were exchanged against neutral residues (Val to Ala substitutions) in TtCM. In addition, more negative charges were found in the periphery of the thermostable enzyme, especially by introduction of glutamate residues. Two of those form salt bridges to neighbouring residues contributing to stability on the protein's surface. Another reason for the additional charge might be to stabilize the enzyme by improving solubilization or hydration of the enzyme. III) Three additional proline residues (Pro79, Pro81, Pro85) in TtCM restrict the conformations of loop L80s. This loop is located between β-strands S3 and S4, which line the intermolecular cleft and contain active site residues.

These improvements were also found in AroQ *M. jannaschii* chorismate mutase when it was compared to mesophilic EcCMp. Hydrophobic cores were changed through nine Leu to Ile substitutions. Their side chains obviously allow a slightly different packing against neighbouring residues contributing to stability. The substitutions are focused at the points of contact between helices H1-H1', H3-H3', H3–H1/H1', and H3'–H1'/H1 thereby stabilizing the monomers as well as the dimer. Also more negative charge developed on the helices' surface by Ala to Glu subtitutions. In combination with that, Lys to Glu and Glu to Lys exchanges maintained the α-helical dipoles. Shifting of charges by Arg to Lys or Glu to Asp substitutions also seemed to contribute to dipol establishment. This effect was only observed in the all-helical *M. jannschii* CM, but not for the three helices in the pseudo α/β-barrel of TtCM. Finally, a proline (Pro47) was introduced at the C terminus of helix H2 in direct vicinity to the active site residues Asp46 in loop L40s and Glu50 in helix H2. These substitutions in MjCM increase the free energy of unfolding by 5 kcal/mol (MacBeath *et al.*, 1998). Determination of the melting temperature at which TtCM denatures will be needed to quantify the additional stability of this CM when compared to BsCM. The stabilization of the active site residues seems to be very important at high temperatures. Thus, further analysis of kinetic proterties, temperature dependence and pH optimum of the catalyzed reaction will show how efficiently this enzyme can catalyze the chorismate-prephenate rearrangement at high temperatures in comparison to its AroQ counterpart.

The *aroG* deletion cassette constructed in this study might be used for the generation of a *T. thermophilu*s knock-out strain. This strain in combination with the cloned *aroG* gene would then increase the number of marker genes available for genetic manipulations of this organisms. Furthermore, a *Thermus/E. coli* shuttle vector was developed into an expression vector by insertion of a promoter. A chorismate-mutase deficient strain together with this vector would be a suitable system for the selection of stabilized mesophilic chorismate mutases. Directed evolution of well-characterized chorismate mutases from mesophilic organsims under the selective pressure of high growth temperatures could be applied to gain further information on stabilizing factors of these enzymes. Especially, through mutagenesis of structurally well-characterized enzymes like yeast chorismate mutase, identification of features contributing to the stability of large AroQ-type chorismate mutases might be possible. In addition, more could be learned about allosteric regulation at high temperature. Similar to the stabilization of loops near the active sites observed here, loops near the allosteric sites are supposed to be restrained to some degree as well. However, the Thr226Ile variant of yeast chorismate mutase showed that locking certain loops in a defined conformation prevented regulation of activity. Thus, it will be intriguing to identify residues of such sophisticated enzymes like yeast chorismate mutase which when substituted improve stability, but do not interfere with function.

References

Adams, M. W. & Kelly, R. M. (1998). Finding and using hyperthermophilic enzymes. *Trends Biotechnol* **16**, 329-332.

Andersson, L. O., Borg, H. & Mikaelsson, M. (1972). Molecular weight estimation of proteins by electrophoresis in polyacrylamide gel of graded porosity. *FEBS Lett* **20**, 199-202.

Baldwin, G. S., McKenzie, G. H. & Davidson, B. E. (1981). The self-association of chorismate mutase/prephenate dehydratase from *Escherichia coli* K12. *Arch Biochem Biophys* **211**, 76-85.

Branden, C. & Tooze, J. (1991). Introduction to protein structure. New York and London: Garland Publisging, Inc.

Chook, Y. M., Gray, J. V., Ke, H. & Lipscomb, W. N. (1994). The monofunctional chorismate mutase from *Bacillus subtilis*. Structure determination of chorismate mutase and its complexes with a transition state analog and prephenate, and implications for the mechanism of the enzymatic reaction. *J Mol Biol* **240**, 476-500.

Combet, C., Blanchet, C., Geourjon, C. & Deléage, G. (2000). NPS@: network protein sequence analysis. *Trends Biochem Sci* **25**, 147-150.

Dagert, M. & Ehrlich, S. D. (1979). Prolonged incubation in calcium chloride improves the competence of *Escherichia coli* cells. *Gene* **6**, 23-28.

de Grado, M., Castan, P. & Berenguer, J. (1999). A high-transformation-efficiency cloning vector for *Thermus thermophilus*. *Plasmid* **42**, 241-245.

Faraldo, M. M., de Pedro, M. A. & Berenguer, J. (1992). Sequence of the S-layer gene of *Thermus thermophilus* HB8 and functionality of its promoter in *Escherichia coli*. *J Bacteriol* **174**, 7458-7462.

Guex, N. & Peitsch, M. C. (1997). SWISS-MODEL and the Swiss-PdbViewer: an environment for comparative protein modeling. *Electrophoresis* **18**, 2714-2723.

Helmstaedt, K., Heinrich, G., Lipscomb, W. N. & Braus, G. H. (2002). Refined molecular hinge between allosteric and catalytic domain determines allosteric regulation and stability of fungal chorismate mutase. *Proc Natl Acad Sci USA* **99**, 6631-6636.

Helmstaedt, K., Krappmann, S. & Braus, G. H. (2001). Allosteric regulation of catalytic activity: *Escherichia coli* aspartate transcarbamoylase versus yeast chorismate mutase. *Microbiol Mol Biol Rev* **65**, 404-421.

Jones, E. W. & Fink, G. R. (1982). Regulation of amino acid and nucleic acid biosynthesis in yeast. In *The molecular biology of the yeast Saccharomyces cerevisiae. Metabolism and gene expression.*, pp. 181-299. Edited by J. N. Strathern, E. W. Jones & J. R. Broach. Cold Spring Harbor, NY: Cold Spring Harbor Laboratory.

Koyama, Y., Arikawa, Y. & Furukawa, K. (1990). A plasmid vector for an extreme thermophile, *Thermus thermophilus*. *FEMS Microbiol Lett* **60**, 97-101.

Koyama, Y., Hoshino, T., Tomizuka, N. & Furukawa, K. (1986). Genetic transformation of the extreme thermophile *Thermus thermophilus* and of other *Thermus* spp. *J Bacteriol* **166**, 338-340.

Krappmann, S., Pries, R., Gellissen, G., Hiller, M. & Braus, G. H. (2000). *HARO7* encodes chorismate mutase of the methylotrophic yeast *Hansenula polymorpha* and is derepressed upon methanol utilization. *J Bacteriol* **182**, 4188-4197.

Liao, H., McKenzie, T. & Hageman, R. (1986). Isolation of a thermostable enzyme variant by cloning and selection in a thermophile. *Proc Natl Acad Sci USA* **83**, 576-580.

MacBeath, G., Kast, P. & Hilvert, D. (1998). A small, thermostable, and monofunctional chorismate mutase from the archaeon *Methanococcus jannaschii*. *Biochemistry* **37**, 10062-10073.

Oshima, T. & Imahori, K. (1974). Physiochemical properties of deoxyribonucleic acid from an extreme thermophile. *J Biochem (Tokyo)* **75**, 179-183.

Peitsch, M. C. (1995). Protein modeling by E-mail. *Bio/Technology* **13**, 658-660.

Peitsch, M. C. (1996). ProMod and Swiss-Model: Internet-based tools for automated comparative protein modelling. *Biochem Soc Trans* **24**, 274-279.

Ramaley, R. F. & Hixson, J. (1970). Isolation of a nonpigmented, thermophilic bacterium similar to thermophilic bacterium similar to *Thermus aquaticus*. *J Bacteriol* **103**, 526-528.

Romero, R. M., Roberts, M. F. & Phillipson, J. D. (1995). Chorismate mutase in microorganisms and plants. *Phytochemistry* **40**, 1015-1025.

Sträter, N., Schnappauf, G., Braus, G. & Lipscomb, W. N. (1997). Mechanisms of catalysis and allosteric regulation of yeast chorismate mutase from crystal structures. *Structure* **5**, 1437-1452.

Szilagyi, A. & Zavodszky, P. (2000). Structural differences between mesophilic, moderately thermophilic and extremely thermophilic protein subunits: results of a comprehensive survey. *Structure Fold Des* **8**, 493-504.

Tamakoshi, M., Uchida, M., Tanabe, K., Fukuyama, S., Yamagishi, A. & Oshima, T. (1997). A new *Thermus-Escherichia coli* shuttle integration vector system. *J Bacteriol* **179**, 4811-4814.

Tanaka, T., Kawano, N. & Oshima, T. (1981). Cloning of 3-isopropylmalate dehydrogenase gene of an extreme thermophile and partial purification of the gene product. *J Biochem (Tokyo)* **89**, 677-682.

Thompson, J. D., Higgins, D. G. & Gibson, T. J. (1994). CLUSTAL W: improving the sensitivity of progressive multiple sequence alignment through sequence weighting, position-specific gap penalties and weight matrix choice. *Nucleic Acids Res* **22**, 4673-4680.

Xie, G., Bonner, C. A. & Jensen, R. A. (2000). Cyclohexadienyl dehydrogenase from *Pseudomonas stutzeri* exemplifies a widespread type of tyrosine-pathway dehydrogenase in the TyrA protein family. *Comp Biochem Physiol C Toxicol Pharmacol* **125**, 65-83.

Zhang, S., Pohnert, G., Kongsaeree, P., Wilson, D. B., Clardy, J. & Ganem, B. (1998). Chorismate mutase-prephenate dehydratase from *Escherichia coli*. Study of catalytic and regulatory domains using genetically engineered proteins. *J Biol Chem* **273**, 6248-6253.

Conclusions

The two folding motifs of chorismate mutases

The sequencing of complete genomes steadily increases the knowledge about primary structures of chorismate mutases. Until now, two folds of CMs were identified, which by convergent evolution both have chorismate mutase activity: AroQ, represented by the four-helix bundle *E. coli* chorismate mutase (EcCM), and AroH, which according to the only available crystal structure of *B. subtilis* CM (BsCM) shows a pseudo-α/β barrel architecture.

Like the naturally occuring CMs, catalytic antibodies capable of the chorismate-to-prephenate conversion were elicited by immunization of mice with a transition state analogue (Hilvert *et al*., 1988). Solvation of the three-dimensional structure of IF7, for instance, and comparison with the *B. subtilis* CM showed that this antibody catalyzed the same concerted pericyclic mechanism as the enzymes, but is about four magnitudes less active (Haynes *et al*., 1994; Shin & Hilvert, 1994). The gene encoding this ‘abzyme‘ was functionally expressed and complemented a tyrosine and phenylalanine auxotrophy of an *S. cerevisiae* strain (Tang *et al*., 1991). Thus, the construction of artificial catalysts like this antibody also demonstrated that polypeptides with different folds can posses stucturally similar binding sites for the stabilization of transition states through convergent evolution.

In the AroQ protein fold, one polypeptide chain forms one long and two shorter α-helices which are oriented like the numeral 4. Dimerization occurs by the formation of a four-helix bundle motif containing helices H1, H2, and H3 of one monomer and H1‘ of the other monomer between which two equivalent active sites are located (Fig. 3).

The AroH enzyme from *B. subtilis* represents another structurally simple and unregulated fold of CMs. A monomer consists of three α-helices which are packed against a five-stranded mixed β-sheet. Also for this enzyme, oligomerization occurred for the formation of the three active sites which are located in the clefts between the three monomers. The monomer folding motifs are oriented like three sides of a prism so that the trimer constitutes a pseudo-α/β barrel (Fig. 15).

Here, the first thermostable enzyme representing this class of AroH chorismate mutases was isolated from the extreme thermophile *T. thermophilus* (Chapter 3). This enzyme was grouped into the AroH class, because its circular dichroism spectrum and homology modeling indicated a protein fold based on α-helices and β-strands similar to BsCM. The determination of this enzyme's native size allowed the prediction of trimerization like in the *B. subtilis* counterpart. In contrast to the latter enzyme, an aggregation of two trimers resulting in a hexamer was observed during native gradient gel electrophoresis. In addition, *T. thermophilus* TtCM is to our knowledge the first AroH enzyme inhibited by tyrosine. As known from other enzymes (Baldwin *et al*., 1981), this tyrosine inhibition may be achieved by the formation of the observed higher-order oligomers of TtCM. Thus, the observed differences between the two AroH CMs characterized so far suggest a variety among this class of chorismate mutases like it was found for the AroQ-type enzymes before. Data base searches revealed the existence of CMs homologous to these AroH chorismate mutases in other gram-positive bacteria and cyanobacteria which shows a broader distribution of this class of enzymes as expected before.

Evolution of AroQ chorismate mutases

From the AroQ group of chorismate mutases, monofunctional fungal and plant CMs were characterized which exhibit several allosteric features. In combination with the often unregulated gene expression, distinct allosteric domains evolved in these branch point enzymes (Krappmann *et al*., 1999; Krappmann *et al*., 2000; Mobley *et al*., 1999). Especially the structural features of the yeast CM (ScCM) were precisely investigated. Comparison with the *E. coli* prototype suggested that a putative gene duplication event combined the helices, which form the four-helix bundle in one polypeptide chain, allowing the development of a regulatory domain from the second catalytic domain. Dimerization and the subsequent development of allosteric sites in the interface led to the formation of the allosterically regulated yeast enzyme. Based on several crystal structures, in which ScCM was liganded to a transition-state analog and/or the allosteric effectors tyrosine and tryptophan (Sträter *et al*., 1997), a detailed model for the allosteric mechanisms was developed in this work (Introduction). It was shown that a simple two-state model of allosteric regulation did not describe neither homotropic nor heterotropic cooperativity of this chorismate mutase, because an additional super R state induced by the substrate was identified. We also proposed an unliganded intermediate between T and R state and pointed out that the allosteric effectors induce conformations different from the substrate.

A detailed intramolecular signal transduction pathway for tyrosine inhibition was known involving loops L220s in the dimer interface. The substitution of this loop by the homolgous parts of other fungal CMs proved that, although the enzymes are highly conserved, these molecular hinges evolved differently. Loop L220s was identified not only as a hinge for allosteric rearrangements during T-R transition, but proved to be a ‘hot spot‘ for the identification of the incoming signal of effector binding to the allosteric site of the different fungal chorismate mutases (Chapter 1). In combination with the site-directed mutagenesis of the yeast enzyme, we could show that regulatory components like loop L220s together with structurally important parts at the dimer interface have coevolved in this enzyme. Loop L220s and its vicinity was found to be critical also for stability and dimerization of ScCM (Chapter 1). Thus, in this work we demonstrated the multiple functions of this discrete structural element and further elucidated the structure-function relationship in yeast chorismate mutase.

Oligomerization and regulation

The protein fold of chorismate mutases diverged considerably during evolution in the different organisms. Depending on the fusion to other enzymes of amino acid biosynthesis, especially regulation of catalytic activity occurs differently.

Chorismate mutases of some organisms are not regulated at all. The mesophilic counterpart of TtCM, the *B. subtilis* enzyme, for instance, did not show regulation by aromatic amino acids or prephenate (Gray *et al*., 1990). Similarly, the first thermophilic chorismate mutase characterized, the AroQ protein from *M. jannaschii*, is unregulated (MacBeath *et al*., 1998).

In the well-characterized *E. coli* isozymes, two different types of regulation developed. In the P-protein (encoded by *pheA*), the CM domain (residues 1-109) is fused to a prephenate dehydratase domain (res. 101-285) and a regulatory domain (res. 281-386). Both activities are allosterically regulated by phenylalanine binding to the regulatory domain. Inhibition occurs via aggregation of active dimers to less active tetrameric or octameric proteins (Zhang *et al*., 1998).

The homologous CM in the *E. coli* T-protein is fused to a prephenate dehydrogenase and is encoded by *tyrA*. In this case, two allosteric sites for tyrosine binding were proposed in this dimeric enzyme although another group suggested competitive inhibition at the active sites for the TyrA protein family, because a discrete allosteric domain was not identified (Turnbull *et al*., 1991; Xie *et al*., 2000).

Like described above for yeast chorismate mutase, most characterized fungal and plant CMs exhibited several allosteric features and were reguated by amino acid binding to an allosteric domain (Krappmann *et al*., 1999; Krappmann *et al*., 2000; Mobley *et al.*, 1999).

In this work, the uni-domain AroH *T. thermophilus* CM was found to be regulated by tyrosine (Chapter 3). Thus, the possibility exists that a sophisticated allosteric signalling pathway also evolved for this monofunctional AroH chorismate mutase. A possible ligand binding pocket was identified by computer modeling studies which may serve as allosteric binding site. However, experimental evidence for allosteric regulation like in he AroQ proteins is yet to be found. On the other hand, it is more likely, that in this structurally simple protein, which is highly similar to the unregulated BsCM, competitive inhibition by tyrosine occurs at the active sites like proposed for the *E. coli* T-protein. Our data also support this type of regulation because of the increasing inhibition at very high tyrosine concentrations. With the observed hexamerization, TtCM also resembles the *E. coli* P-protein in which effector binding to the regulatory domain causes formation of higher-order aggregates with less activity. Further analysis should be done to elucidate this possible competitive inhibition causing hexamerization of thermophilic TtCM.

Thus, until now, each CM newly-discovered showed further ways of regulating a branch point enzyme and thereby the metabolic pathways it is involved.

Thermostability of chorismate mutases

Another structure-function relationship was analyzed for chorismate mutases in this work. The newly-isolated enzyme from *T. thermophilus* was compared to its mesophilic counterpart from *B. subtilis* regarding stabilizing features (Chapter 3). Similar to the structural properties of the AroQ thermophilic enzyme from *M. jannaschii*, this small stable CM followed the ’rules of protein stabilization’ like preferred amino acid exchanges for increased hydrophilicity of the exposed surface or hydrophobicity and packing of cavities within the protein (Branden & Tooze, 1991; Szilagyi & Zavodszky, 2000). In accordance with the importance of loops for stability and dimerization observed for yeast CM, also the decrease in conformational freedom by the introduction of proline residues in loop regions seemed to contribute to stabilization of thermophilic chorismate mutases.

In this context, the question arose how thermostability is compatible with regulation of enzyme activity. Whereas the rate constant of the chorismate-to-pephenate conversion was calculated to be 230-fold enhanced at 85°C compared to 30°C (MacBeath *et al.*, 1998) and thus, catalysis of this reaction is not a problem, a more difficult task will be the regulation of the catalyzed reaction at high temperatures. Wether the structural variations found in thermophilic CMs enable a controled rearrangement from one allosteric state to another, remains to be investigated. Therefore, for the observed tyrosine inhibition of *T. thermophilus* CM, a competitive mechanism might be favoured at high temperatures because less flexibility in tertiary and quaternary structure would be necessary. The stabilization of mesophilic, allosterically regulated CMs like the yeast enzyme might shed light onto the principles of allosteric transitions at high temperatures. Investigations concerning kinetics or unfolding and refolding of wild-type as well as mutagenized yeast CM will contribute to an even better understanding of chorismate mutases' structure and function.

Chorismate mutase and osmoregulation

When *ARO7* alleles were found to be involved in vacuole biogenesis and hypertonic growth (Ball *et al.*, 1986; Latterich & Watson, 1991), the question arose how these cellular processes might be interconnected with the metabolism of amino acids and other aromatic compounds. In this study, yeast strains were generated harboring a series of *aro7* alleles including a new complete deletion of the gene. However, no evidence was found that chorismate muase or the biosynthesis of phenylalanine or tyrosine was required for omotress response or generation of vacuoles (Chapter 2). Thus, a connection of these cellular events with the shikimate pathway did not seem to exist. In fact, the phenotypes described before were observed for mutagenized strains containing point mutations in *ARO7* which were not further characterized. Similarly, for the *aro7Δ::URA3* deletion strain used in this study, which was the only strain showing a weak growth defect under salt stress, neither the deletion at the *ARO7* locus nor the point mutations in the *URA3* locus were clearly mapped out. Therefore, the generation of these strains by crossings and mutagenesis supposedly accumulated further unrecognized mutations affecting their phenotype. A clear assignment to *ARO7* is, thus, impossible without further analysis of these strains' genotype. Modern genetic manipulations applied for the construction of *aro7* deletion strains and the respective control strains in this study allowed us to generate strains with a defined genotype. The examinations carried out with these yeast strains ruled out any function of chorismate mutase for osmostress resistance or vacuole biogenesis.

References

Baldwin, G. S., McKenzie, G. H. & Davidson, B. E. (1981). The self-association of chorismate mutase/prephenate dehydratase from *Escherichia coli* K12. *Arch Biochem Biophys* **211**, 76-85.

Ball, S. G., Wickner, R. B., Cottarel, G., Schaus, M. & Tirtiaux, C. (1986). Molecular cloning and characterization of *ARO7-OSM2*, a single yeast gene necessary for chorismate mutase activity and growth in hypertonic medium. *Mol Gen Genet* **205**, 326-330.

Branden, C. & Tooze, J. (1991). Introduction to protein structure. New York and London: Garland Publishing, Inc.

Gray, J. V., Eren, D. & Knowles, J. R. (1990). Monofunctional chorismate mutase from *Bacillus subtilis*: kinetic and 13C NMR studies on the interactions of the enzyme with its ligands. *Biochemistry* **29**, 8872-8878.

Haynes, M. R., Stura, E. A., Hilvert, D. & Wilson, I. A. (1994). Crystallization and preliminary structural studies of a chorismate mutase catalytic antibody complexed with a transition state analogue. *Proteins* **18**, 198-200.

Hilvert, D., Carpenter, S. H., Nared, K. D. & Auditor, M.-T. M. (1988). Catalysis of cencerted reactions by antibodies: the Claisen rearrangement. *Proc Natl Acad Sci U S A* **85**, 4953-4955.

Krappmann, S., Helmstaedt, K., Gerstberger, T., Eckert, S., Hoffmann, B., Hoppert, M., Schnappauf, G. & Braus, G. H. (1999). The *aroC* gene of

Aspergillus nidulans codes for a monofunctional, allosterically regulated chorismate mutase. *J Biol Chem* **274**, 22275-22282.

Krappmann, S., Lipscomb, W. N. & Braus, G. H. (2000). Coevolution of transcriptional and allosteric regulation at the chorismate metabolic branch point of *Saccharomyces cerevisiae*. *Proc Natl Acad Sci USA* **97**, 13585-13590.

Krappmann, S., Pries, R., Gellissen, G., Hiller, M. & Braus, G. H. (2000). *HARO7* encodes chorismate mutase of the methylotrophic yeast *Hansenula polymorpha* and is derepressed upon methanol utilization. *J Bacteriol* **182**, 4188-4197.

Latterich, M. & Watson, M. D. (1991). Isolation and characterization of osmosensitive vacuolar mutants of *Saccharomyces cerevisiae*. *Mol Microbiol* **5**, 2417-2426.

MacBeath, G., Kast, P. & Hilvert, D. (1998). A small, thermostable, and monofunctional chorismate mutase from the archaeon *Methanococcus jannaschii*. *Biochemistry* **37**, 10062-10073.

Mobley, E. M., Kunkel, B. N. & Keith, B. (1999). Identification, characterization and comparative analysis of a novel chorismate mutase gene in *Arabidopsis thaliana*. *Gene* **240**, 115-123.

Shin, J. A. & Hilvert, D. (1994). Mechanistic studies of an antibody with chorismate mutase activity. *Bioorg Med Chem Lett* **4**, 2945-2948.

Sträter, N., Schnappauf, G., Braus, G. & Lipscomb, W. N. (1997). Mechanisms of catalysis and allosteric regulation of yeast chorismate mutase from crystal structures. *Structure* **5**, 1437-1452.

Szilagyi, A. & Zavodszky, P. (2000). Structural differences between mesophilic, moderately thermophilic and extremely thermophilic protein subunits: results of a comprehensive survey. *Structure Fold Des* **8**, 493-504.

Tang, Y., Hicks, J. B. & Hilvert, D. (1991). *In vivo* catalysis of a metabolically essential reaction by an antibody. *Proc Natl Acad Sci USA* **88**, 8784-8786.

Turnbull, J., Morrison, J. F. & Cleland, W. W. (1991). Kinetic studies on chorismate mutase-prephenate dehydrogenase from *Escherichia coli*: models for the feedback inhibition of prephenate dehydrogenase by L-tyrosine. *Biochemistry* **30**, 7783-7788.

Xie, G., Bonner, C. A. & Jensen, R. A. (2000). Cyclohexadienyl dehydrogenase from *Pseudomonas stutzeri* exemplifies a widespread type of tyrosine-pathway dehydrogenase in the TyrA protein family. *Comp Biochem Physiol C Toxicol Pharmacol* **125**, 65-83.

Zhang, S., Pohnert, G., Kongsaeree, P., Wilson, D. B., Clardy, J. & Ganem, B. (1998). Chorismate mutase-prephenate dehydratase from *Escherichia coli*. Study of catalytic and regulatory domains using genetically engineered proteins. *J Biol Chem* **273**, 6248-6253.

Kerstin Helmstaedt
geb. Probst

Persönliche Daten

Geboren am 25. Mai 1973 in Bad Harzburg, deutsche Staatsangehörigkeit
Heirat am 27. November 1998 mit Andreas Helmstaedt

Schulausbildung

1979 - 1983	Grundschule Langelsheim
1983 - 1985	Orientierungsstufe Langelsheim
1985 - 1992	Ratsgymnasium Goslar

Hochschulausbildung

Okt. 1992 - Febr. 1998	Biologie-Studium (Dipl.) an der Georg-August-Universität Göttingen
Sept. 1995 - April 1996	ERASMUS-Stipendium für ein Austauschsemester am King's College, London
MÄRZ 1998 - NOV. 1998	Diplomarbeit in der Abteilung für Molekulare Mikrobiologie und Genetik am Institut für Mikrobiologie und Genetik der Georg-August-Universität Göttingen bei Prof. Dr. G. H. Braus
Seit Jan. 1999	Doktorarbeit in der Abteilung für Molekulare Mikrobiologie und Genetik am Institut für Mikrobiologie und Genetik der Georg-August-Universität Göttingen bei Prof. Dr. G. H. Braus